WRC RESEARCH REPORT NO. 91

TRANSPORT PROCESSES OF PARTICLES IN DILUTE SUSPENSIONS IN TURBULENT WATER FLOW-Phase III

Barclay G. Jones, Professor of Nuclear and
of Mechanical Engineering
Neil M. Howard, Research Assistant, Nuclear Engineering
Charles C. Meek, Research Assistant Professor of
Nuclear Engineering
James Tomkins, Research Assistant, Nuclear Engineering

University of Illinois at Urbana-Champaign

F I N A L R E P O R T

Project No. B-067-ILL

July 1, 1971 - August 31, 1974

The work upon which this publication is based was supported by funds provided by the U. S. Department of Interior as authorized under the Water Resources Research Act of 1964,

P. L. 88-379
Agreement No. 14-31-0001-3582

UNIVERSITY OF ILLINOIS
WATER RESOURCES CENTER
2535 Hydrosystems Laboratory
Urbana, Illinois 61801

December, 1974

ABSTRACT

TRANSPORT PROCESSES OF PARTICLES IN DILUTE SUSPENSIONS
IN TURBULENT WATER FLOW-PHASE III

Understanding the basic mechanisms and predicting the behavior of particles suspended in turbulent fluid flow are essential to environmental conservation and to multiphase system design. Air and water pollution, sedimentation and erosion of river beds and coastal shorelines, and atmospheric fallout are some of the areas in which particle suspensions are of key importance. Detailed experimental measurements of dilute particle suspensions have been performed which examined the effects of particle size, shape and relative density on the statistical response of such particles in a turbulent fluid. Shape was found to be of minor importance for spheres, cubes and tetrahedrons. However, size was found to be important when the particle dimension was as large or larger than the fluid turbulence structure. Relative density influenced both free fall and inertial effects. An analytical model was developed which included these latter effects. It agrees well with observed particle dispersion measurements.

Jones, Barclay G.; Howard, Neil M.; Meek, Charles C. and Tomkins, James.

TRANSPORT PROCESSES OF PARTICLES IN DILUTE SUSPENSIONS IN TURBULENT WATER FLOW-PHASE III
100 + vii pp.

December 1974, Urbana, Illinois 61801,

KEY WORDS---*turbulent transport/*dispersion/turbulent flow/*water pollution/
air pollution/*particulate transport/instrumentation/turbulence/*sedimentation

ACKNOWLEDGEMENT

Sponsorship of this research by the U. S. Department of Interior through the Office of Water Resources Research, the Water Resources Center of the University of Illinois at Urbana-Champaign, the Nuclear Engineering Program and the Mechanical Engineering Department are gratefully acknowledged-

The participation of J. Gronager, R. Helfrich and L. Lindquist in the latter stages of this project is sincerely appreciated.

TABLE OF CONTENTS

NOMENCLATURE

A_m = normalization constant for modified uniform theory

a = particle radius

a_0, a_1, a_2 = time macroscale fit constants

a_{ij} = fit coefficients for carriage calibration

a' = coefficient, Eq. (3.3-25)

c = coefficient, Eq. (3.3-24)

C_D = drag coefficient

d = particle diameter

f = frequency

f_i = particle free fall velocity

f_Q = quiescent free fall velocity

f_T = turbulent free fall velocity

$F(f)$ = normalized energy spectrum

h = functional, Eq. (3.3-23)

j = pertaining to an individual run

k = wave number

N = number of annular elements

$P(\eta)$ = radial position probability density function

$P_A(\eta)$ = probability of an acceptable run

$P_m(\eta)$ = modified uniform distribution probability density function

$P_u(\eta)$ = uniform distribution probability density function

$Q(\omega)$ = response function

r = radial position

R = pipe inside radius

R_{ij} = zero lag time velocity correlation matrix

Re = Reynolds number

$R(\tau)$ = autocorrelation function

t = time

t_j = time of run in j^{th} element

T = voltage difference

T^* = time of run

T_p = particle time constant

u = fluctuating velocity

U voltage difference

U_L = fluid velocity at pipe centerline

U_m = local mean fluid velocity

v = instantaneous velocity

V = voltage differerence

x = cartesian position

$\overline{X^2(t)}$ = dispersion function, Eq. (4.1-3)

z = axial position or separation

Greek Symbols

α = particle size parameter: $\alpha = 3\nu/a^2$

β = particle density parameter: $\beta = 3\rho/(2\rho_p+\rho)$

ζ = particle free fall parameter

η = dimensionless radial coordinate

$\overline{\eta}_r$ = dimensionless mean radius for an individual run

η_{max} = maximum dimensionless radius for acceptable runs

θ = angle

λ = spatial microscale

Λ = spatial macroscale

μ = dynamic viscosity

ν = kinematic viscosity

ξ = particle inertial parameter; time variable

ρ = density

σ = standard deviation or error

σ_r = dimensionless rms position for an individual run

τ = lag time; temporal microscale

$\mathcal{J}_E$ = Eulerian time macroscale

$\mathcal{J}_f$ = convected frame fluid time macroscale

ω = circular frequency (radians/second)

ω_o = circular frequency for zero free fall velocity particles

Subscripts and Superscripts

E = Eulerian frame of reference

f = fluid

i, j = cartesian tensor index notation, numerical index

L = Lagrangian frame

m = mean; modified uniform

max = maximum

o = zero reference condition

p = particle

Q = quiescent

r = radial direction, run

rms = root mean square

T* = particle residence time in all elements

u = uniform distribution

z = axial direction

1,2,3 = numerical index

primes = rms quantities

overbars = long time averages

< > = ensemble average

θ = azimuthal direction

1. INTRODUCTION

Predicting particle transport is a relatively complicated engineering problem which has increased significance in environmental applications and in multiphase system design. In the areas of water and air pollution, river bed erosion and sedimentation as well as atmospheric fallout the behavior of suspended particulates in turbulent fluid flows is a key importance. The studies reported here provide results which enhance scientific understanding of the basic particle transport phenomena and engineering models which provide means for predicting such transport.

1.1 Objectives and Background

Investigations completed by this project conclude a three phase study of the detailed behavior of particle transport processes in dilute suspensions in turbulent water flow. Each phase examined specific aspects of the research and represents an extension of the initial work developed by Jones (1966) and Shirazi (1967). In this portion of the report, the overall direction of these studies will be outlined. Indication of the accomplishment of the project goals will also be given. However, the detailed presentation of these accomplishments will be either given in later sections of this report or explicitly referred to in previous articles on this research.

The primary objective initiating this research was to measure directly the behavior of a suspended particle in a well documented turbulent field. From these detailed measurements of the statistical response of the particle, the associated transport processes can be evaluated. These results can be employed to develop and test analytical models of suspended particle behavior.

At the beginning of these studies only simplified models had been proposed other than the linearized, but otherwise complete, model of Chao (1964). Jones (1966) attempted to verify Chao's model, but was plagued with poor signal-to-

noise in the particle monitoring system. However, the feasibility of the research was demonstrated. Shirazi (1967) by careful use of signal filtering and controlling closely the relative density was able to obtain improved experimental results for neutrally bouyant particles and to extend the analysis to separate the "essential" and "statistical" non-linearities in the analytical formulation of the particle behavior. However, in both these studies light emitting particles were used which resulted in significant extraneous light noise and unstable light emission from the particles. Part of Phase I of this study (Jones et al., 1971) was designed to modify the particle monitoring system to remove these deficiencies.

In Phase I (Project A-019-ILL) the experimental system was improved by replacing the fluorescent light emitting material with very stable Co-60 radioactive chips as the means of particle tagging. Sodium-iodide crystals were installed as integral parts of the photomultiplier monitoring system. This system provided the necessary stability and improvement in signal-to-noise for accurate determination of particle position. In addition, commercial differential amplifiers with sharp low pass filters were added to the data procurement which further improved the signal-to-noise level. To insure proper lock-in of the particle monitoring system a signal feedback system was incorporated which improved the percentage of successful data runs. Jones, et al. (1971) and Meek (1972) have discussed these improvements and their results in detail.

To enable the detailed fluid turbulence structure to be experimentally determined in the test section, a replacement section which provided anemometer probe access parts along its length was added. Additional inlet flow section modifications were installed to improve the rate of reaching fully developed flow in the test section. These modifications enabled complete examination of the fluid

turbulence field in which the particle trajectory was measured. The data show that the stationary, fully developed condition was obtained throughout the test section. Details of these observations are given by Meek (1972) and Howard (1974).

The analytical development carried out in Phase I of the research was primarily to examine the nature of the drag law to be used over a wide range of particle parameterization. This resulted in a linearized drag law which was shown to be applicable for ranges of particle Reynolds Number up to about 400 which includes the large variety of engineering applications. This work is reported in detail by Jones, Ostensen and Meek (1973).

Phase II (Project B-042-ILL) made direct use of these improved facilities to obtain particle trajectory data. The primary objective was to study free fall effects for a variety of constant size spherical particles. These data were reported by Meek (1972) and Jones, et al. (1972). In addition a comparison of the effect of varying particle shapes (cubes, tetrahedrons and spheres) was conducted, showing no significant influence between particles with similar volumetric displacements and free fall velocities. This result is of prime significance as it allows a complete study of the problem with ideal spherical particles for which analytical relations can readily be formulated. Detailed presentation of results for this study are given by Jones, et al. (1972).

In addition, a significant goal of the Phase II project was to carefully examine and document the Eulerian fluid field turbulent structure in the test section. Meek (1972) presented detailed measurements of the axial fluid velocity component through mean velocity, intensity, skewness and flatness profiles across the pipe radius. He further analyzed the autocorrelations and spectrum at several radial and axial locations, showing the fully developed and stationary nature to the test section flow. Radial separation spatial scales were also determined. Burchill's (1970) data were used to provide intensities and scales for each of the

radial, azimuthal and axial components of the Eulerian velocity components. These fluid measurements were presented in the Phase II report by Jones, et al. (1972) and form the basis for input to analytical prediction models for particle transport.

The other major goal of the B-042-ILL project was to develop an engineering model to describe particle dispersion and related behavior. Meek (1972) developed both a complete theory and a simplified theory model for this behavior. In the former, all linearized terms were included in the governing relations. This led to a rather cumbersome engineering model. However, he was able to show that the predicted results agreed closely with the measured particle behavior, verifying the correctness of the model. The simplified theory, for a wide range of particle parameterization, gave identical results and provided a readily useable engineering model for predicting such particle behavior. Details of this model have been presented by Meek and Jones (1973) as well as Meek (1972) and Jones, et al (1972). Extensions of this theory to include nonhomogeneous and anisotropic flow field structure were left to the third phase of the study, which has just been completed and is the principle material presented in later chapters.

The final part of the research project, Phase III (B-067-ILL), has just concluded and the results are presented by Howard (1974) and in this report. The research encompassed both experimental and analytical aspects and had the following goals:

Experimental

1. To examine particles of similar size with both negative and positive buoyancy at the same free fall Reynolds number;

2. To vary particle size and determine its relation with turbulence scales in affecting particle response;

3. To simulate sand like particles to study particle inertial effects on particle response;

4. To determine two-point lateral and longitudinal fluid velocity correlations from which the convected frame structure of the turbulent field is evaluated;

and Analytical

5. To improve the theory to more correctly include effects of both particle size and relative density;

6. To examine the interrelationships of the Eulerian-Lagrangian reference frames through comparison of observed particle-fluid turbulence with analytical results suggested in the literature.

All of these objectives have been accomplished in this study with the exception of 6. This objective requires somewhat more accurate data than was experimentally procured. Although it is of high scientific interest, its direct importance to the engineering models developed in this study is of minor significance.

1.2 Review of Previous Analytical Work

The initial development of the theory of particle behavior in a quiescent fluid is generally attributed to Basset (1961), Boussinesque (1903), and Oseen (1927) in their formulation of the governing equations for suspended spherical particles. Tchen (1947) succeeded in extending the governing equation to the case of an unsteady velocity field. Subsequent contributions to the explicit nature of some of the terms in the equation by Lumley (1957) and Corrsin and Lumley (1956) have brought the problem to its present theoretical description.

The solution of the complete equations of motion has not yet been achieved. Lumley (1957) described the nature of the nonlinearities and the difficulty of solution of the complete equations of motion. Several authors have found solutions to simplified versions of the equation. Soo (1956) obtained a relation for the particle autocorrelation function in the Lagrangian frame for a highly restrictive case of the governing equation where only Stokes drag and gravity were assumed to be the important forces on the particle. Friedlander (1957) solved a similar but still incomplete version of the equation by including pressure gradient effects. He found a relation for the rms relative velocity between the particle and the fluid. The most complete solutions to the problem to date have been presented by

Hinze (1959) and by Chao (1964). They solved linearized forms of the governing equation with transform techniques and included effects of particle acceleration, apparent mass, and pressure gradients in the fluid. Shirazi (1967) used a conditional averaging technique to calculate relationships between statistical properties of the particle and the fluid under the assumption that the particle velocity and fluid velocity are uncorrelated. Peskin (1971) has solved the simplified version of the governing equation like Soo and Friedlander, but his solution does not require the restrictive side condition that the particle follow the fluid element as stipulated in the solutions by Hinze and by Chao. Meek (1972) retained the influence of finite free fall due to an external field, such as gravity. He was able to accommodate the resulting crossing trajectories effects within the restriction that the response time of the particle is short compared to the characteristic Lagrangian time scale of the fluid turbulence. His solutions provide the general analytical consistency and interrelation between the various competing phenomena. Ahmadi and Goldschmidt (1970) used three different numerical techniques to solve the governing equations of motion for the turbulent transport coefficient of a spherical particle moving in a turbulent field. They concluded that the particle diffusivity increases with increasing particle size up to the size microscale of the turbulence from whence, for larger particles, the diffusivity decreases. A relative density increase of the particle reduced the diffusivity for all but very small particles.

The theory of suspended particle dispersion is intimately involved with the dispersion and diffusion mechanisms of the underlying turbulent fluid field. Taylor's (1921) original paper considered the diffusion of fluid particles in homogeneous flow as being made up of many continuous random movements. The movements were related to each other in time by a correlation coefficient between

the Lagrangian frame velocities at different times. Only Batchelor (1957) has extended the theory into the realm of free turbulent shear flows where turbulent scales are spatially variable. The confined turbulent flow in a pipe is a situation where spatial variation of turbulent scales is also encountered. The effect of the radial nonhomogeneity of pipe flow on particle dispersion is developed in detail by Howard (1974) and is presented in detail in Chapter 3.

1.3 Review of Previous Experimental Investigations

Experimental investigations of single particle motion under a wide variety of flow conditions is extensively reported by Torobin and Gauvin (1959-61). Most of the experimental work before 1940 deals with the flow field around the sphere and the variation of the drag coefficient at different Reynolds numbers. Later experiments by Batchelor, Binnie and Phillips (1955) and Binnie and Phillips (1958) were performed with discrete spheres in a two inch diameter horizontal pipe to determine their mean velocity by a transit time technique. Kada and Hanratty (1960) measured the effect of solid particle loadings on turbulent diffusion in a pipe and found that the effect of solid particle loadings depended upon the concentration and free fall velocity of the solid particles. Concentrations above a threshold level increased the fluid's diffusion coefficient as did an increase in particle free fall velocity, presumably through the generation of increased turbulent energy in the fluid. Recent experiments on dilute suspensions have been done by Kennedy (1965), Snyder (1969), Meek (1972) and Howard (1974). Kennedy used light sensing photomultiplier tubes to detect light reflected from particles as they traversed fixed planes at selected axial locations in his vertical square duct using windtunnel grid generated turbulence. Timing techniques were used to infer particle velocities. Snyder in a similar windtunnel study used photographic techniques and graphical analysis to determine particle

positions and from which particle dispersion was inferred. Meek used a modified version of Jones' (1966) system to obtain a continuous analog track of the particle position as it moved in a vertical pipe flow. The system used by Howard was virtually identical to the one used by Meek. Howard extended the range of particle parameterization to include detailed examination of free fall effects, particle size effects and inertial effects. These are discussed in Chapters 2 and 4 and in Appendix B.

1.4 Outline of Report Coverage

This report includes an overall review of the three phase research study of the title problem. In Chapter 2 a comprehensive discussion is given of suspended particle behavior as it is understood from previous experimental studies and from work completed in this study. The detailed sets of data from this study are presented in Appendix B to provide ready access to the reader. Complete analytical model development, including a brief review of the isotropic and homogeneous model theory, is presented in Chapter 3. Also included are the extensions into nonhomogeneous fluid fields as well as the effects of anisotropy in the fluid field. Chapter 4 provides a comparison between analytical predictions and experimental observations.* In Chapter 5 research conclusions are presented with suggested areas in which future work would be useful. The three Appendices (A, B and C) present: pertinent fluid turbulence data; particle trajectory data; and data processing techniques, respectively. These are included to provide easy access of the data to the reader. Many detailed accounts of the experiments and the analyses are specifically referred to in the literature and are omitted when they are considered non-essential to the presentation.

---

*This discussion indicates the applicability of the model for several engineering problem areas.

2. GENERAL DISCUSSION OF PARTICLE MOTION BEHAVIOR

2.1 Parameters Which Effect Particle Motion

In the development of theoretical models to predict particle motion, it is essential that the phenomena be sufficiently understood to insure that the model development incorporates these features. Although the analyses and experiments were performed simultaneously, they are presented separately so as to enable a complete picture of each aspect to be developed. The experimental observations are discussed in this chapter to enable the assumptions and justifications employed in the analytical model development of chapter three to be more readily accepted. In this chapter only selected experimental results are presented. Additional data tabulation is included in several Appendices and in the referenced literature.

Those parameters effecting the motion of particles in a turbulent fluid flow can generally be classified in two groups: (1) physical parameters of the particle itself and (2) characteristics of the flow field. Physical properties of the particle include its size, shape, density and roughness and its related acceleration and spin. For simplification of analytical treatment, we and other investigators have assumed a smooth, non-spinning spherical particle. However, we (Jones et al. 1972) have investigated experimentally the effects of particle shape. Torobin and Gauvin (1959-61) discuss the effects of surface roughness as well as other physical particle characteristics. The primary characteristics of the flow field effecting particle motion are its Reynolds number and the intensities and scales of the turbulence. The variation of the flow field--whether its turbulence is homogeneous or isotropic--will also affect particle motion. Both groups of parameters act together to govern particle motion. By examining each of the parameters separately, we sought to discover its

individual importance and determine a rational explanation for the mechanism of its effect.

2.2 Particle Size

Qualitatively we expect that very large particles would not respond to the constantly occurring random velocity fluctuations characteristic of fluid turbulence. Conversely, we would expect very small particles to follow closely each change in its neighborhood fluid velocity.

Here we have implicitly made a comparison between the particle size and the eddy size of the fluid velocity turbulent fluctuations. The physical size of these fluid velocity fluctuations is known as its turbulent scale. This can be determined as either a measure of the fluid turbulence physical domain (spatial scale) or a measure of how persistent this structure is (temporal scale). To evaluate the effect of particle size on its motion in a turbulent field we would expect the fluid spatial scale to be the important factor. If the particle is large with respect to the fluid spatial scale, then the fluid velocity fluctuations (or "eddies") merely tickle the surface of the particle. Thus, the perturbing effect of these eddies is averaged over the large particle surface and particle motion is unaffected. For an extremely small particle we would expect the particle to be completely dominated by each surrounding individual fluctuating fluid element and for a neutrally buoyant small particle to behave similarly to a fluid element.

2.3 Particle Density

Acting in conjunction with the effect of particle size is the effect of particle density. A very dense particle has a relatively large inertial mass and a very light particle has a relatively small enertial mass. Since the inertial mass associated with a suspended particle is composed of not only its own mass

but that of an additional mass of a fractional amount of the displaced fluid, the low density particle does not have its inertial mass reduced to an insignificant level. In Chapter three this associated surrounding fluid mass will be shown to limit the particle inertial effect to non-zero values. It is expected, however, that relatively high density particles will behave more sluggishly than relatively low density particles of the same size.

For particles with densities different than the surrounding fluid the effect of gravitational and external body forces can be important. Only when the particle's motion relative to the surrounding fluid is small, providing an associated Reynolds Number in the non-separated, Stokes' flow regime, can the gravitational influence on the particle's turbulent motion be ignored. This is most readily examined through the particle's free fall velocity. A particle with either a relatively high or low density has a large free fall velocity (unless it is extremely small). Such a particle moves rapidly through the fluid turbulence pattern which appears frozen to the particle as it passes through eddy after eddy. The relatively high density particles are essentially unaffected by the fluid velocity. A neutrally buoyant particle with zero free fall velocity, on the other hand, tends to become trapped in a single eddy (if the particle is small enough) and is strongly affected by the fluid turbulence.

One can immediately see that size and density influence particle motion simultaneously and that at extremes either may become dominant or negligible. Another important parameter which acts at the same time as particle density and size is the state of the fluid flow field.

2.4 Fluid Flow Field

The characteristics of the fluid flow field strongly influence particle motion. If the flow is stagnant, then the fluid forces from velocity fluctuations and mean velocity (bulk motion) are zero. The particle is solely under the influence of external forces and its frictional drag with the fluid. The particle trajectory

is essentially linear when governed by an external force such as gravity. Particle size and density are important as they contribute to the frictional drag force exerted on the particle by the viscous fluid. If the flow is laminar then we again expect the particle trajectory to be linear, governed by the fluid velocity, external forces and friction. If we move in a frame where the fluid velocity is zero, then the laminar flow case reduces to the stagnant case. This reference frame is called the Lagrangian frame of motion. Now if we consider a flow field in which fully developed turbulence exists, then the particle trajectory is a random path. The mean motion is still governed by the external force, bulk fluid motion and friction between the particle and its surrounding fluid. However, in addition to this mean motion there is superimposed a particle motion as a result of particle's response to the random fluid velocity fluctuations. The trajectory of the particle is no longer linear but an irregular random path deviating in a dispersive sense from the mean fluid motion.

In the quiescent and laminar flow situations the fluid velocity field is well known. It is unchanging in time. For the case of turbulent flow, the instantaneous velocity fluctuates about some mean quantity which is assumed to be unchanging in time. This type of turbulent flow is called stationary. If at all spatial points within the flow field the mean velocity and the structure of the velocity fluctuations are the same, then the flow is said to be homogeneous. If the scales and intensity of the turbulence are the same along different orthogonal coordinate axes, then the flow is called isotropic. Due to the random nature of the turbulent flow field, it is best described by using statistical quantities. A quantitative development of statistical particle motion in a homogeneous, isotropic and stationary turbulent flow field is developed later in Chapter three.

2.5 Discussion of Principal Experimental Results

We have qualitatively presented above a discussion of those parameters effecting particle motion. Throughout this discussion it has become apparent that the various parameters influencing particle motion act in conjunction to govern particle motion. It has also been noted that there are extremes where the effect of one parameter dominates all others.

The phenomena of particle motion in a quiescent or laminar flow field is essentially a one-dimensional problem. However, due to the fact that fluid turbulence is a three-dimensional phenomena, we observe, for suspended particles, motion in all three coordinate directions. If we couple these three dimensional turbulence effects with the effects due to variations of particle parameters, we obtain a complex particle-fluid motion problem.

It is observed that some particle parameters dominate the motion in the axial direction and other particle parameters dominate motion in the lateral directions. To illustrate this point we consider two sets of experimental results: (1) An experiment performed with particle size being held constant (at 5mm diameter) while parameterizing on particle-fluid relative density and (2) An experiment utilizing relatively constant density particles of different sizes (2mm through 6.5mm diameters). All particles were tested in the same turbulent flow field. This turbulent field was the stationary and both moderately homogeneous and isotropic "core" region of a vertically oriented pipe flow. Cylindrical coordinates were used to characterize the fluid motion and the particle trajectories: axial (z), radial (r) and azimuthal (θ). The quantity by which particle motion between the two experiments is compared is the particle velocity autocorrelation function. This is a statistical quantity characteristic of turbulence structure which measures the degree to which the particle velocity at the present time is

similar to the particle velocity at previous times. The particle autocorrelation function is mathematically defined for the axial (z) direction as

$$R_{p,z}(\tau) = \frac{\overline{u_{p,z}(t)\ u_{p,z}(t+\tau)}}{\overline{u^2_{p,z}(t)}} \qquad (2.5\text{-}1)$$

where the overbar is a long time stochastic average and τ = delay time. The quantity $u_{p,z}(t)$ is a time series of the particle axial velocity component viewed from a reference frame in which the mean particle velocity is zero. (This reference frame is similar to the Lagrangian frame of the fluid but differs slightly since the mean particle velocity and mean fluid velocity are unequal unless the particle is small and neutrally buoyant, thus behaving as a small fluid element.) We shall employ this particle velocity autocorrelation function as a statistical measure of the behavior.

Figure 2.5-1 shows the axial particle autocorrelation function for the varying particle density experiments (FFP-Series) described earlier. We note as the particle density tends toward the fluid density, that the autocorrelation function tends toward that of the fluid. Since, the size of the particles is constant, the effect of that parameter is suppressed. The fluid field is the same for all particles so effects from variations in fluid turbulence are also removed.

Figure 2.5-2 shows the radial particle autocorrelation function for the FFP experiments. No effects of the varying particle density are observed. However, the spatial scale for lateral turbulent velocity fluctuations is much less than the corresponding axial space scale estimates by Howard (1974) and measurements by Sabot, Renault, and Compte-Bellot (1973) indicate that the lateral spatial microscale of the fluid turbulence may be 2 to 5 times smaller than the axial spatial microscale of the turbulence. Thus, even

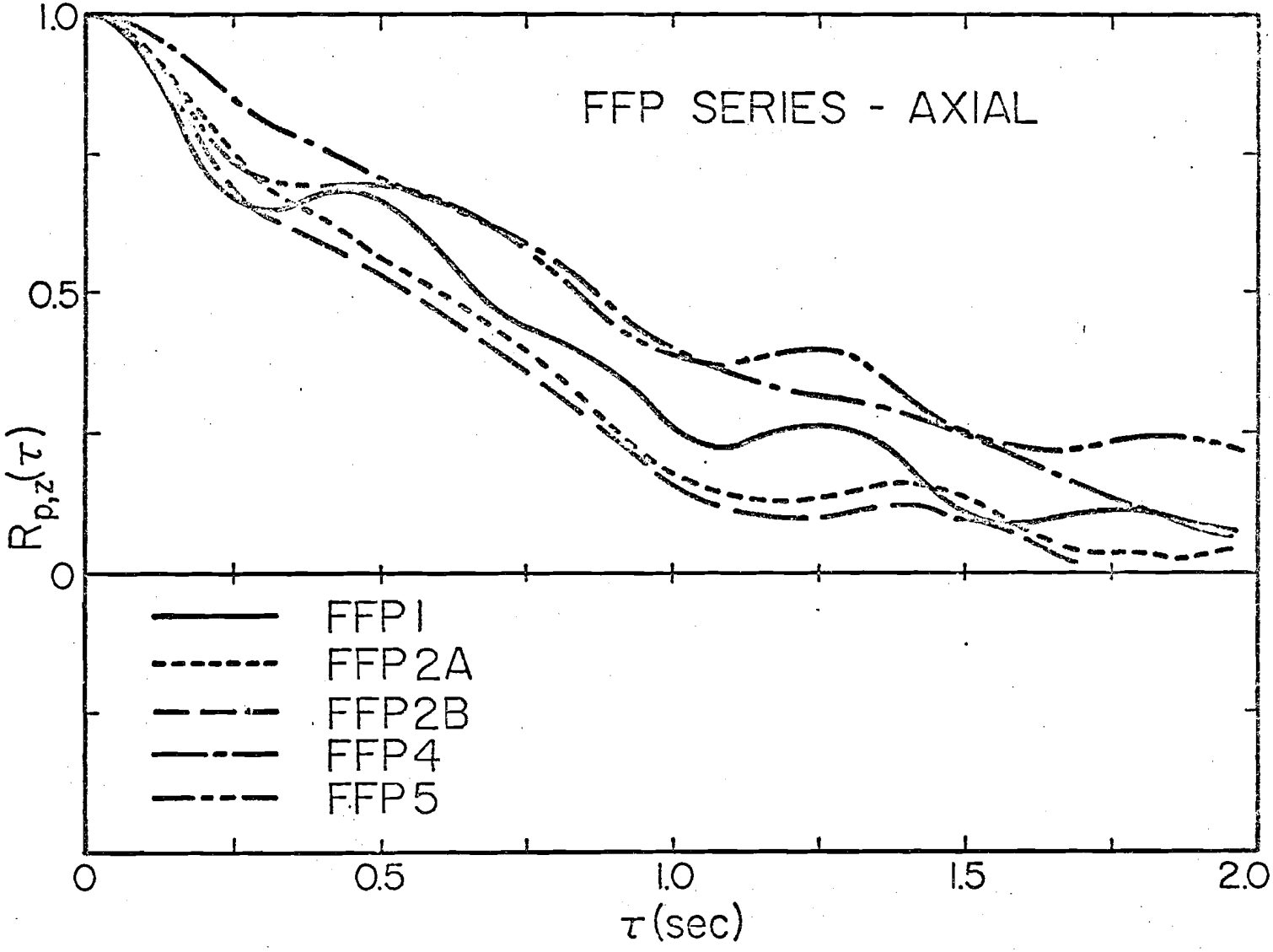

Fig. 2.5-1 Axial Particle Autocorrelations for the FFP Series.

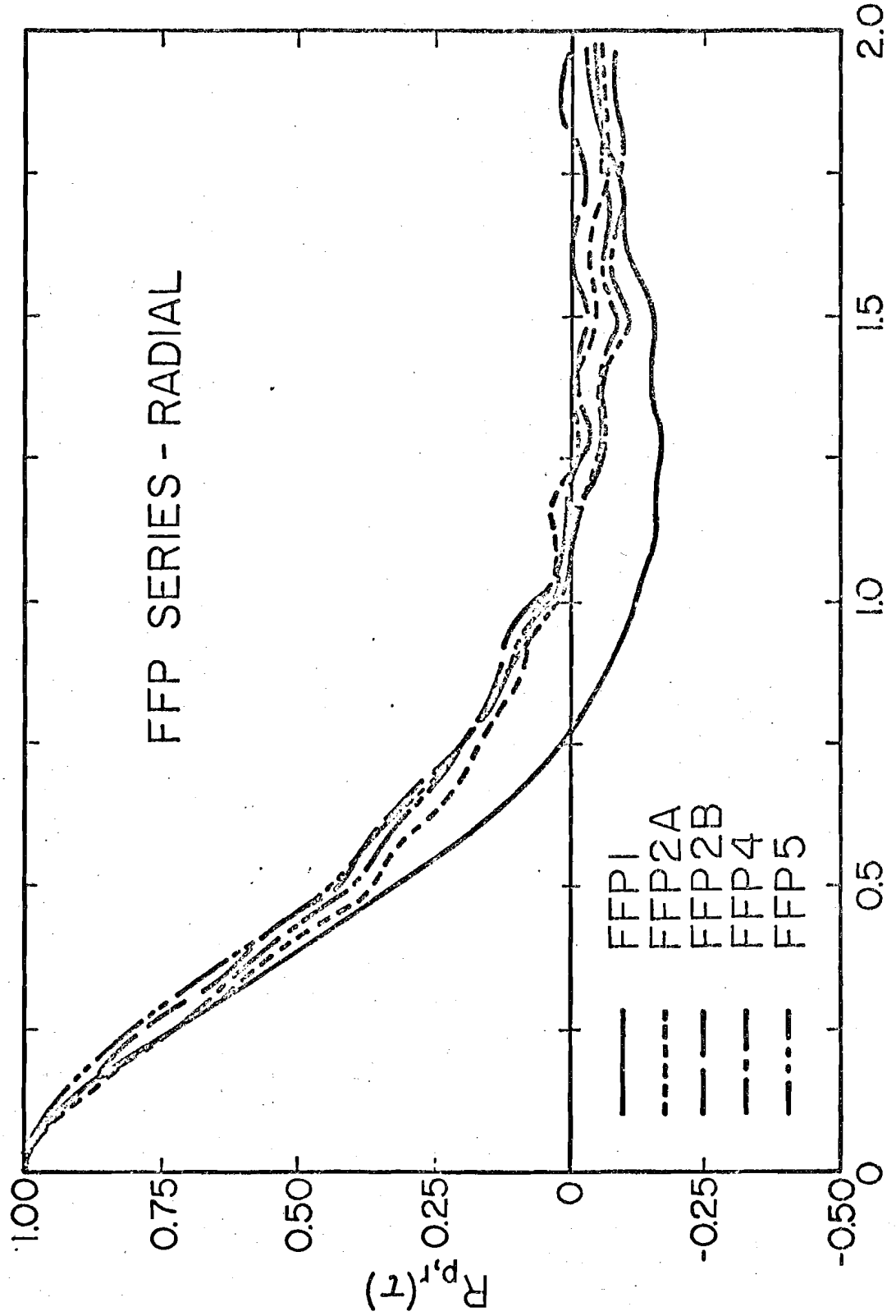

Fig. 2.5-2 Radial Particle Autocorrelations for the FFP Series.

though the particles have different densities, their relatively large size with respect to the size of the lateral turbulent scale dominates their motion. The conclusion is that in the lateral direction the response of the particle is limited by its size.

To be able to visualize the effect of particle size we examine the results of the second experimental series (SP-Series) where different size particles were tested in the turbulent flow system. Figure 2.5-3 shows the axial autocorrelation function for various size particles with relatively similar densities. Here we observe for particles of similar density that the axial response is the same regardless of particle sizes used in this experiment. These particles are all smaller than the axial turbulent spatial microscale which is estimated by Howard (1974) to be about 1.7 cm. Thus, there should be negligible effect of size because the particles are all small enough to respond well to the axial component of the turbulence structure. We conclude for particles of sufficiently small size, that density will govern their response to the axial turbulence structure.

For the lateral turbulence structure we observe some change in particle response for smaller particles as the particle size approaches the spatial microscale of the lateral component of the fluid turbulence. Indeed, this is verified by Fig. 2.5-4. As the particle size is reduced, the particle autocorrelation falls off much faster indicating (by its rapid drop off and, smaller area underneath the curve) that the particle is able to respond to the higher frequency fluctuations in the lateral turbulence structure. In addition the ratios of the rms fluctuating velocities in the radial-to-axial and azimuthal-to-axial both increased as the particle size decreased from 6.5 cm. diameter to 3 cm. and 2 cm. diameter with approximately constant free fall Reynolds number for all particles.

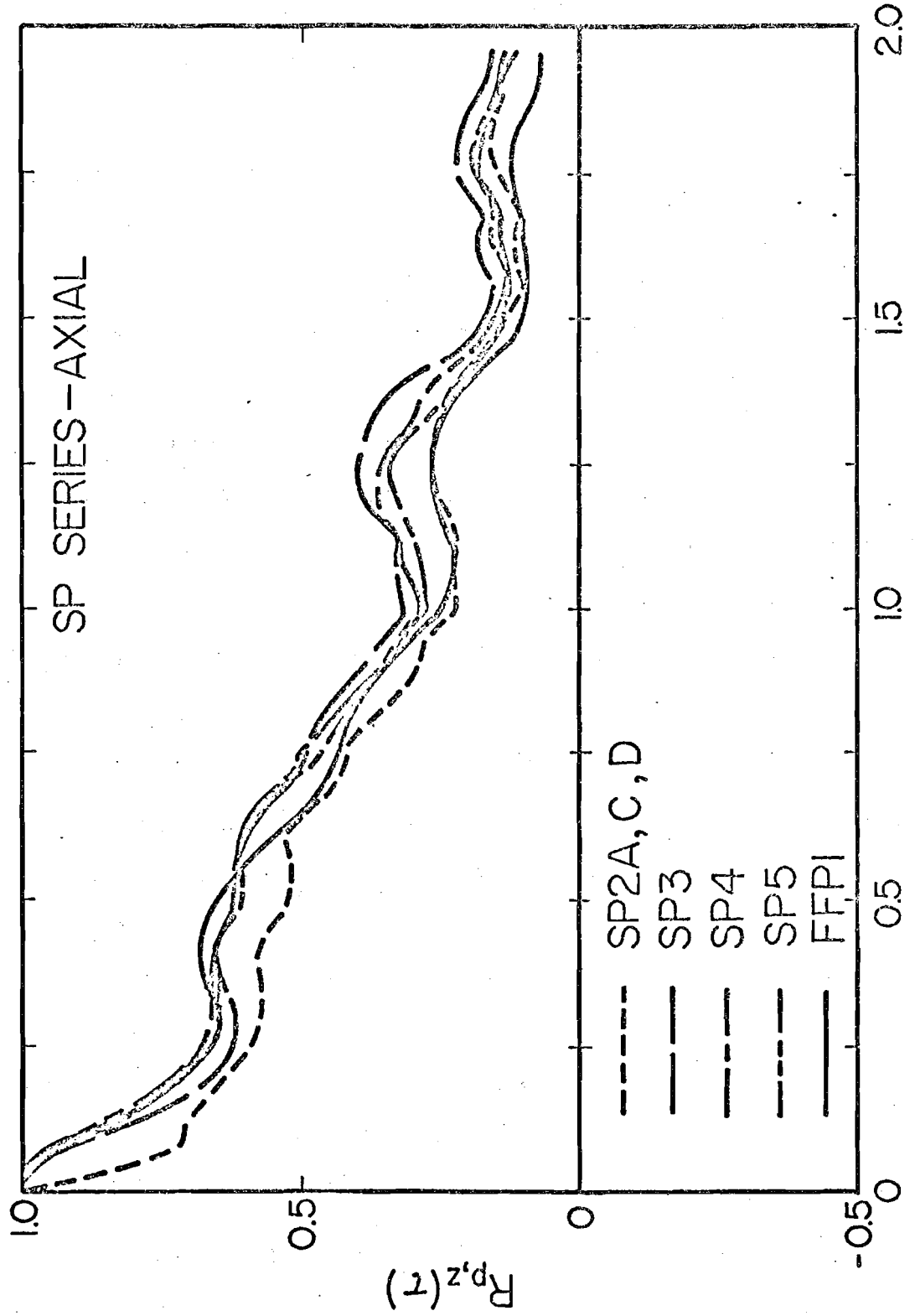

Fig. 2.5-3 Axial Particle Autocorrelations for the SP Series.

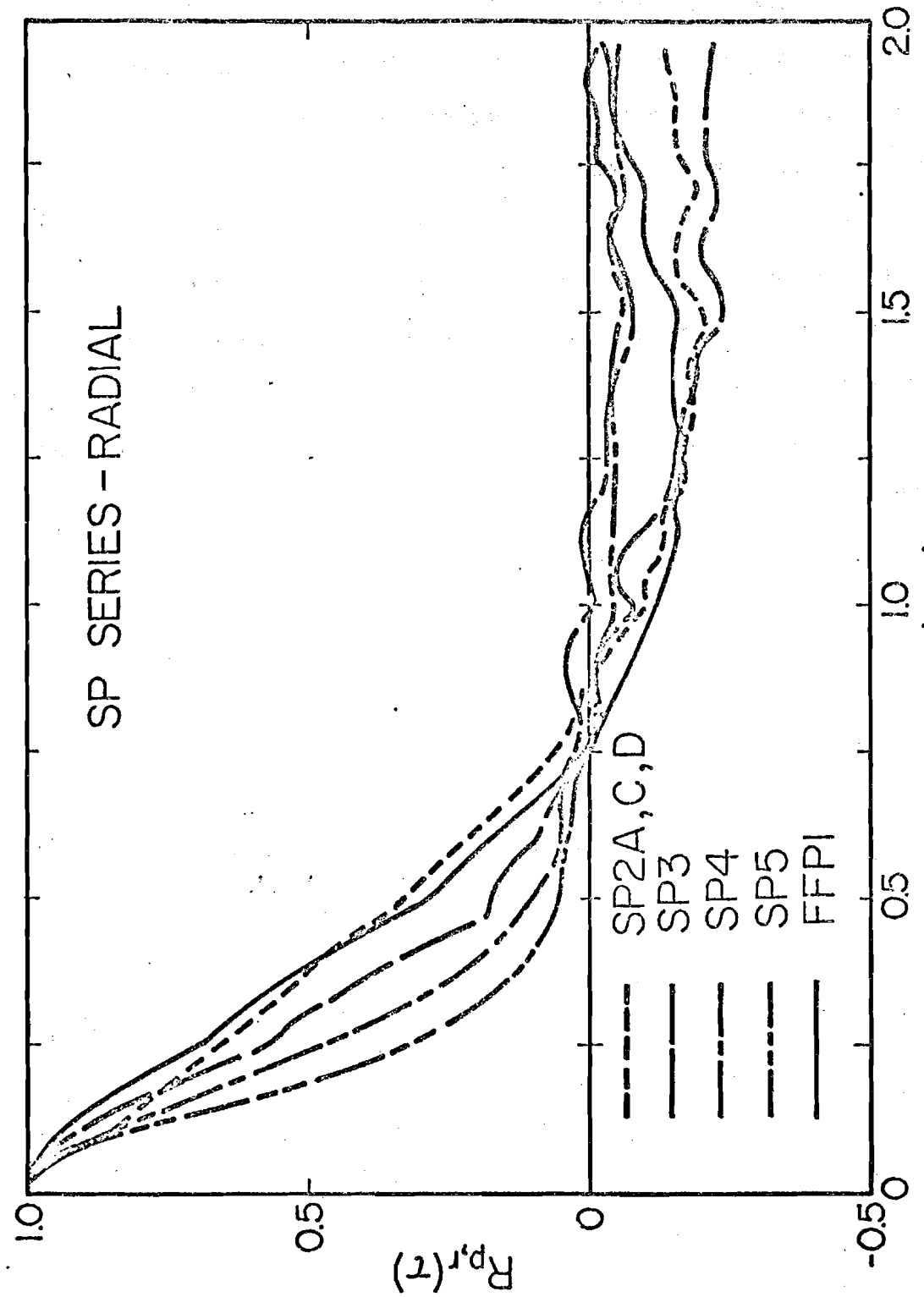

Fig. 2.5-4 Radial Particle Autocorrelations for the SP Series.

From the experiments conducted it was shown that particle motion is effected by particle size and density. Furthermore, these two effects occur simultaneously and one or the other may become dominant depending upon the size of the turbulent scale to which the particle responds.

For detailed results from the experimental program the reader is referred to the theses of Meek (1972) and Howard (1974) in which tabular and graphical presentations of the data are presented. For convenience, however, several of these data are presented in Appendices: A - "Fluid Measurements" and B - "Particle Measurements". In addition the Appendix C - "Data Processing Techniques" includes detailed discussion of the numerical procedures employed to extract these data.

3. ANALYTICAL MODEL DEVELOPMENT FOR PARTICLE MOTION

3.1 Introduction

As explained in chapter one a basic goal of these extended, in depth studies of individual particle motion in a turbulent fluid flow has been to develop a mathematical model of such motion. Particular emphasis has been placed upon the development of a model that is detailed enough to well represent the underlying physics inherent in the process while at the same time being capable of providing straightforward engineering calculations. To this end initial analytical effort was directed toward an understanding of non-Stokesian effects (Jones, et al. 1971) of importance in typical two phase flows which confront engineers in the field. Use of expansion technique coupled with Chao's (1964) earlier work furnished a basis from which non-Stokesian behavior could be predicted and accounted for. The next topic pursued (Jones, et al. 1972) was that of particle dispersion in a homogeneous, isotropic turbulent fluid. Extending the ideas of Wardell & Koefod-Hansen (1962) to include particle motion and combining the results with the earlier non-Stokesian work readily calculable expressions detailing the dispersion of non-Stokesian particles was developed. Predictions of this homogeneous theory compared favorably with experiments performed both in air and in water. The most recent analytical effort has been directed toward an understanding of inhomogeneous and anisotropic effects. Such effects are specific to the two-phase system under consideration-pipe flow in the present case. However, the present effort will emphasize development of a generalized phenomenalogical formalism applicable to typical engineering situations. Rapid prediction of engineering accuracy will be the guiding feature in its derivation. Consistent agreement with experimentally observed results, summarized in chapter two, has been applied throughout these developments. Indeed, the direction of analytical development and experimental program was designed to provide maximum understanding of the physical phenomena.

3.2 Homogeneous Flow

In the earlier study done on non-Stokesian particle motion in homogeneous turbulence (Jones, et al. 1972) it was found that the basic physics describing the phenomena could best be understood if consideration was initially directed toward the spatial-wavenumber domain rather than the more natural time-frequency realm. Since a somewhat similar description will be employed in analyzing inhomogeneous behavior a brief review of the previous work will prove useful.

As indicated the homogeneous theory is based primarily on a Koefod-Hansen (1957) extension of Taylor's (1921) pioneering work on diffusion by continuous movements. It considers only individual particle motion viewed from a Lagrangian reference frame in which the average fluid velocity is zero. No particle-particle or particle-wall interactions are dealt with but rather the particle-fluid interaction is assumed to dominate. Non-Stokesian behavior is taken into account through the application of the theory presented by Jones, et al. (1971) and Jones, Ostensen and Meek (1973).

The dynamical equation of motion describing particle behavior in a turbulent fluid flow was first derived by Tchen (1947). Modifications of Tchen's original equation to more correctly include pressure effects was made by Corrsin and Lumley (1956). Lumley (1957) showed that the resulting equation, when viewed in its most general sense, had incorporated within it on "essential non-linearity" due to the necessity of evaluating the fluid's velocity field at the particle's unknown position. As such, theoretical attempts at solving the equation have centered about particles constrained to remain throughout their history within a given region of strongly correlated fluid (i.e., an eddy). By such means the equation of motion reduces to one of time dependence only and the "essential non-linearity" is circumvented.

At first sight, solutions of such a simplified equation of motion appear to be of somewhat limited value. Many of the particles of practical interest may not remain within a given region of correlated fluid, but rather migrate, due to their free fall, from one region to another. However, in a statistical sense it is of little note whether the particle is constrained to remain within an eddy by arbitrarily setting its free-fall velocity to zero or whether it is allowed to move from one eddy to another. In the one case the particle experiences the distribution of turbulence states by remaining within an eddy which undergoes the distribution during its history; while in the other case the particle experiences the turbulence distribution by moving from one region of strongly correlated fluid to another. Assuming, in the latter case, that the particle's response time is small compared to its transit time, the average space scales of correlation are the same in both cases, being determined by the particle's inertial characteristics and the underlying fluid turbulence. The time scales of correlation are not the same in the two cases, however, due to differing convection velocities. Thus, solutions of the simplified equation of motion may, if properly interpreted, be used in the calculation of the sought-for particle velocity autocorrelation.

From the general theory of Wiener-Kinchine, it may be shown that the particle's velocity autocorrelation can be expressed in terms of a normalized particle energy spectrum, $F_{p,i}(\omega)$:

$$R_{p,i}(\tau) = \int_{-\infty}^{\infty} F_{p,i}(\omega) \cos(\omega\tau) d\omega \qquad (3.2\text{-}1)$$

where ω is the circular frequency. The early work of Soo (1956), Friedlander (1957) and Chao (1964) suggests that the particle's energy spectrum can be expressed as a function of the fluid's Lagrangian energy spectrum through a so-called particle response function. This response function is derived from the particle's simplified equation of motion [see Soo (1967) for a description of the derivation]

and is, therefore, strictly applicable to zero velocity free-fall particles constrained to move within a single correlated region of fluid. Thus, use of an energy spectrum determined with a response function derived for zero free-fall velocity particles requires some adjustment of Eq. (3.2-1) to account for non-zero free fall and the subsequent movement of the particle from one correlated region to another.

Motion of the particle will greatly affect its observed behavior in the time-frequency domain. To remove this dependence it is necessary to move into the wavenumber realm:

$$k \equiv \frac{\omega}{v_p'} \tag{3.2-2}$$

where k is the wavenumber, ω the corresponding frequency, and v_p' is the particle's convection velocity in the coordinate direction considered. Due to the equality of space scales in the two cases, normalization conditions on the particle energy spectra imply similarity of the spectra regardless of whether the particle is arbitrarily confined to a region of strongly correlated turbulence or whether it is allowed to roam about. Consequently, non-zero free-fall effects may be properly incorporated by transforming from a given state in the wavenumber domain, $F_{p,i}(k)$, into the frequency realm.

For the frame of reference considered in this work the instantaneous particle velocity in a given coordinate direction may be expressed as

$$v_{p,i}(t) = u_{p,i}(t) + f_i \tag{3.2-3}$$

where f_i is the i^{th} component of the particle's free-fall (or any deterministic) velocity. For a particle arbitrarily constrained to remain within a given eddy this free-fall velocity is set to zero. As a consequence such a particle has,

when viewed from a reference frame moving with the mean motion of the fluid, an observed frequency in the i^{th} coordinate direction of

$$\omega_o = k\, u'_{p,i} \tag{3.2-4}$$

where k is the space-related wavenumber. If the same particle is allowed to move about from eddy to eddy it has an observed frequency of

$$\omega = k\, v'_{p,i} \tag{3.2-5}$$

in the i^{th} coordinate direction.[1]

With this equivalence in mind Eqs. (3.2-4) and (3.2-5) may be combined, resulting in

$$\omega = \omega_o \left[1 + \left(\frac{f_i}{u'_{p,i}} \right)^2 \right]^{1/2} \tag{3.2-6}$$

which can be seen to reduce to ω_o as $f_i \to 0$ and to $\omega_\infty = k f_i$ for $f_i \gg u'_{p,i}$. Normalization conditions on the particle's energy spectrum require that the nonzero free-fall velocity spectrum be related to that of the zero free-fall velocity spectrum by

$$F_{p,i}(\omega) = \frac{F_{p,i}(\omega_o)}{\left[1 + \left(f_i / u'_{p,i} \right)^2 \right]^{1/2}} \tag{3.2-7}$$

Identifying

$$\ell_i = \left[1 + \left(f_i / u'_{p,i} \right)^2 \right]^{1/2} \tag{3.2-8}$$

---

[1] In this development it is to be understood that ω is specific to a selected coordinate direction (i = 1, 2, or 3).

the expression for the particle's velocity autocorrelation becomes:

$$R_{p,i}(\tau) = \int_{-\infty}^{\infty} F_{p,i}(\omega_o) \cos(\beta_i \omega_o \tau)\, d\omega_o \qquad (3.2\text{-}9)$$

Determination of this autocorrelation thus reduces to a determination of a proper zero free-fall energy spectrum which is determined in part from the particle's equation of motion. Extensive consideration of this function has been made by Jones et al (1971, 1972) and by Meek (1972) and will not be repeated here.

Subsequent analysis using a derived expression for $F_{p,i}(\omega_o)$ shows that particle motion in an homogeneous turbulence can be characterized by three parameters, two involving inertial effects due to particle size and density and the other parameter reflecting free fall effects. Of the two inertial parameters one, designated β, involves the ratio of a fluid sphere to that of the same size solid sphere. The other parameter, designated ξ, is a ratio of the response time of the particle (as determined by its inertial characteristics) to the fluid's characteristic time of correlation in the Lagrangian frame. The third parameter, designated T_i, describes the loss of correlation a particle experiences as it moves from one region of strongly correlated fluid to another.

3.3 Inhomogeneous Flow

As noted earlier effective incorporation of inhomogeneous flow features into the general framework of the homogeneous theory requires a rather detailed specification of the flow system and its inhomogenities. Consequently the present work will concentrate on pipe flow in which the fluid turbulence is stationary and homogeneous in the longitudinal or flow direction. Despite these somewhat arbitrary constraints it is felt that the method presented can be extended to other, equally arbitrary systems.

Consider the pipe flow system in question divided into N equally spaced imaginary annular elements. If N is large, it may be argued with some validity that the turbulence contained within each individual element is approximately homogeneous. As such the theory developed in the previous section may be applied in a piece-wise manner to each element so that an axial autocorrelation may be written for each.

$$R_{p,z}(\tau, j) = \int_{-\infty}^{\infty} Q_z(\omega_o)\, F_{f,z}(\omega_o, j) \cos\left(\zeta_j\, \omega_o \tau\right) d\omega_o \qquad (3.3\text{-}1)$$

Here $Q_z(\omega_o)$ is the particle's response function derived from the particle equation of motion (see Jones et al 1971 and 1972). Notice that insofar as the particle is concerned the inhomogenity of the underlying fluid flow is felt primarily through the fluid energy spectrum characteristic of each element, $F_{f,z}(\omega_o, j)$. Some slight influence is also felt through ζ_j. The average correlation experienced by the particle will thus be a function of the amount of time spent in each annular element

$$\langle R_{p,z}(\tau) \rangle = \sum_{j=1}^{N} \frac{t_j}{T^*} R_{p,z}(\tau, j) \qquad (3.3\text{-}2)$$

where $\frac{t_j}{T^*}$ represents the fraction of the total time, T^*, the particle spends in the j^{th} element. Normalization constraints require:

$$\sum_{j=1}^{N} \frac{t_j}{T^*} = 1 \qquad (3.3\text{-}3)$$

In a pipe where radial symmetry is applicable we allow the summation in Eq. (3.3-2) to go to an integral over the radial coordinate as the number of

intervals goes to infinity. The amount of time the particle spends in each region is replaced by the dimensionless radial position probability density function.

$$\text{prob}(r, r+dr) = P(\eta)\, d\eta \tag{3.3-3}$$

where

$$\eta = r/R \tag{3.3-4}$$

and R is the inside radius of the pipe.

Using the above definitions Eq. (3,2-1) can be written as

$$\langle R_{p,z}(\tau) \rangle = \int_0^1 R_{p,z}(\tau, \eta)\, P(\eta)\, d\eta \tag{3.3-5}$$

Here $R_{p,z}(\tau,\eta)$ is the homogeneous axial particle autocorrelation function determined for a given value of η. The earlier theory for particles in the range $0.1 \leq \beta \leq 3.0$ predicts that for homogeneous turbulence

$$R_{p,z}(\tau, \eta) = \exp\left(-\tau/T_{p,z}\right) \tag{3.3-6}$$

where $T_{p,z}$ is the particle time constant given by

$$T_{p,z} = J_{f,z}/\zeta \tag{3.3-7}$$

and $\mathcal{J}_{f,z}$ is the axial fluid convected time scale and ζ is the free fall parameter defined earlier.

For the nonhomogeneous case consideration must be made of the radial variation of $\mathcal{J}_{f,z}$ and ζ. Inherent in the parameter ζ is the particle axial rms velocity $u'_{p,z}$. Little is known about the radial variation of $u'_{p,z}$ in a pipe. From earlier (WRC-58) data $u'_{p,z}$ and thus ζ are constant to a first order approximation. As such no η dependence of ζ will be assumed. Effects of $u'_{p,z}$ variation can be investigated later if found to be of importance. Furthermore, $\mathcal{J}_{f,z}$ is expected to be a function of the radial coordinate, η, thus giving the relation for a nonhomogeneous flow

$$T_{p,z}(\eta) \cong \mathcal{J}_{f,z}(\eta)/\zeta \tag{3.3-8}$$

Estimates of $\mathcal{J}_{f,z}$ from the trend of data for the Eulerian time macroscale suggest (see Fig. 3.3-1) that the radial variation of the Lagrangian time macroscale may be adequately represented by a linear fit of the form

$$\mathcal{J}_{f,z}(\eta) = \mathcal{J}_{f,z}(0)/(a_0 + a_1\eta) \tag{3.3-9}$$

or a second order fit of the form

$$\mathcal{J}_{f,z}(\eta) = \mathcal{J}_{f,z}(0)/(a_0 + a_1\eta + a_2\eta^2) \tag{3.3-10}$$

where a_0, a_1, and a_2 are fit constants to be determined experimentally and $\mathcal{J}_{f,z}(0)$ is the value of the convected time scale at $\eta = 0$ (the pipe centerline). Using Eq. (3.3-10), Eq. (3.3-8) may be written as:

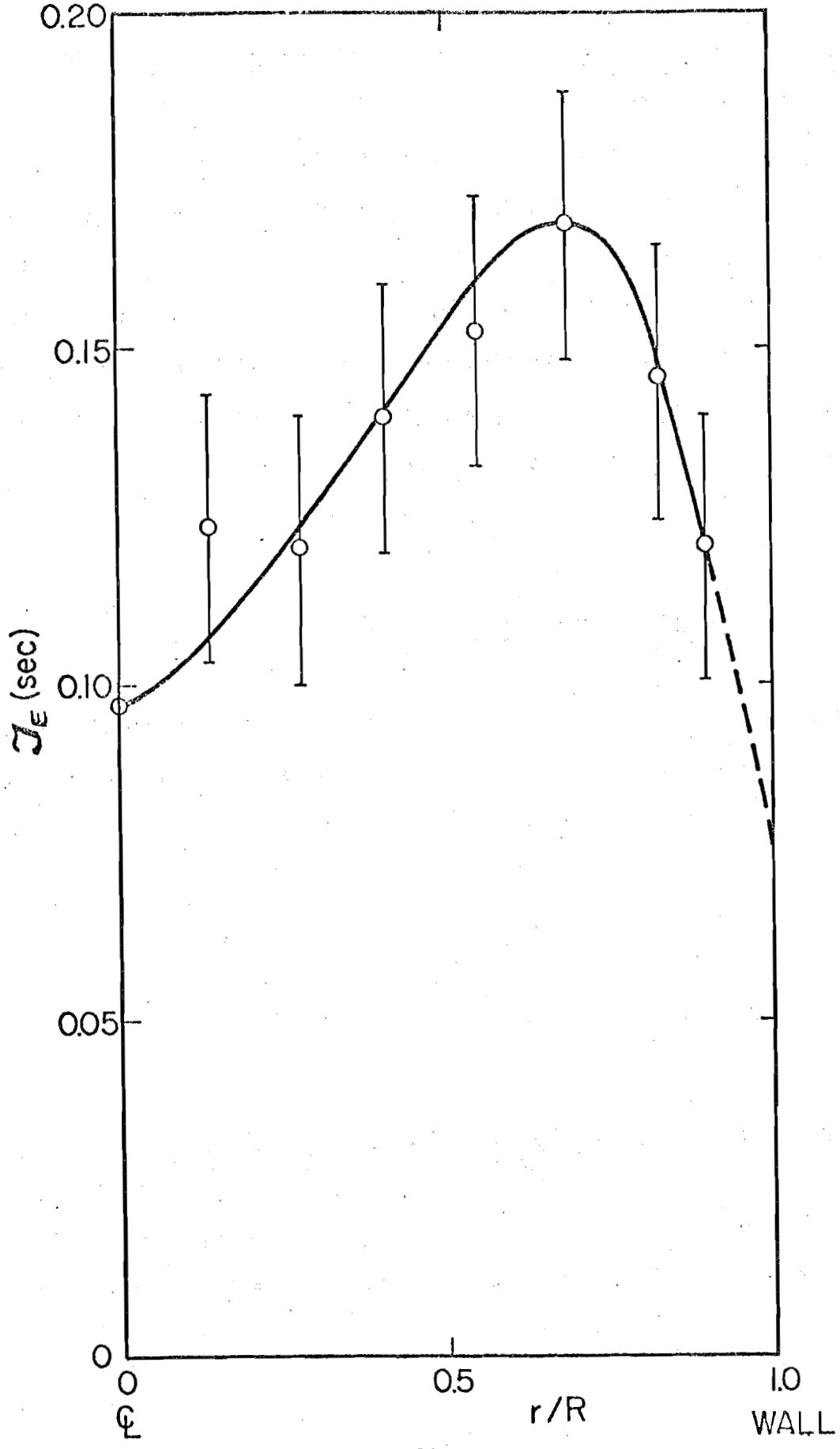

Fig. 3.3-1 Radial Variation of $\mathcal{I}_E$ in a pipe at Re = 50,000.

$$T_{p,z}(\eta) = \mathcal{J}_{f,z}(0) \Big/ \rho(a_0 + a_1\eta + a_2\eta^2) \tag{3.3-11}$$

where Eq. (3.3-6) becomes

$$R_{p,z}(\tau,\eta) = \exp\left[-\tau\rho(a_0+a_1\eta+a_2\eta^2)\Big/\mathcal{J}_{f,z}(0)\right] \tag{3.3-12}$$

and Eq. (3.3-5) can thus be rewritten as

$$\langle R_{p,z}(\tau)\rangle = \int_0^1 P(\eta)\exp\left[-\tau\rho(a_0+a_1\eta+a_2\eta^2)\Big/\mathcal{J}_{f,z}(0)\right]d\eta \tag{3.3-13}$$

It remains now to discern an appropriate form for $P(\eta)$. The data from experiments are insufficient to describe a precise form for $P(\eta)$. Here an approximate form will be utilized for $P(\eta)$.

A determination of the probability distribution for particle radial position can be made by appealing to the physical phenomenon under investigation. Kada and Hanratty (1960) noted a uniform distribution of solid particles in their experiments. Indeed, fully suspended dilute two phase flows are quite often homogeneously distributed. Assuming a uniform distribution of particles per unit cross sectional area of the pipe, the probability of finding a particle in a radial increment $d\eta$ about η is proportional to the annular area at η as seen in Fig. 3.3-2.

Thus the normalized form for the uniform distribution probability function, $P_u(\eta)$, is

$$P_u(\eta)\,d\eta = 2\eta\,d\eta \tag{3.3-14}$$

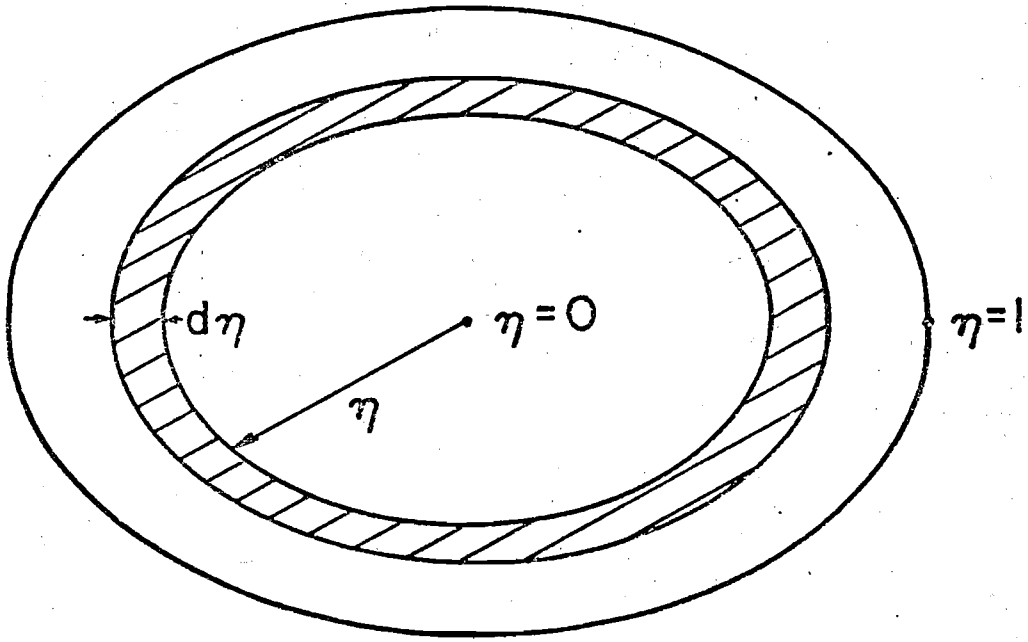

Fig. 3.3-2 Incremental Annular Area for the Modified Uniform Theory.

To accurately predict the actual experimental results from the present system account must be taken of the experimental rejection of particle runs in which the particle trajectory swerves out of the calibrated "core" region of the pipe. Runs with a mean radius near η_{max}, the radial limit of the calibrated core region, have a large probability of being instantaneously outside η_{max} and thus being rejected during analysis. The largest of the mean radii, $\overline{\eta_r}$, appearing in the experimental data are somewhat less than the maximum allowed radius, η_{max}. If for each run a Gaussian distribution of instantaneous radial positions about the mean $\overline{\eta_r}$ is assumed, then the maximum mean radius seen in a histogram plot will be about $\eta_{max} - \sigma_r$, where σ_r^2 is the variance of the η values about $\overline{\eta_r}$. That is, about 33 percent of the runs with $\overline{\eta_r} = \eta_{max} - \sigma_r$ will be rejected as being beyond the "core" boundary as shown in Fig. 3.3-3.

As the mean radial position $\overline{\eta_r}$ moves closer to η_{max}, the particle run has an increasing probability of rejection. The probability of rejection is two times the area of the Gaussian defined by $(\overline{\eta_r}, \sigma_r)$, that is outside η_{max}. This is pictured in Fig. 3.3-4.

Thus,

$P_A(\eta)$ = probability of acceptable run = (1 - prob. of rej.)

= 1 - 2(area of Gaussian outside η_{max})

$$= 1 - 2\left[\frac{1}{\sigma_r\sqrt{2\pi}}\int_{\eta_{max}}^{\infty} \exp\left[(\eta - \overline{\eta_r})^2/2\sigma_r^2\right] d\eta\right] \qquad (3.3\text{-}15)$$

or we can let $\overline{\eta_r}$ be redefined as η.

$$P_A(\eta) = \operatorname{erf}\left(\frac{\eta_{max} - \eta}{\sigma_r\sqrt{2}}\right) \qquad (3.3\text{-}16)$$

$P_A(\eta)$ is shown in Fig. 3.3-5.

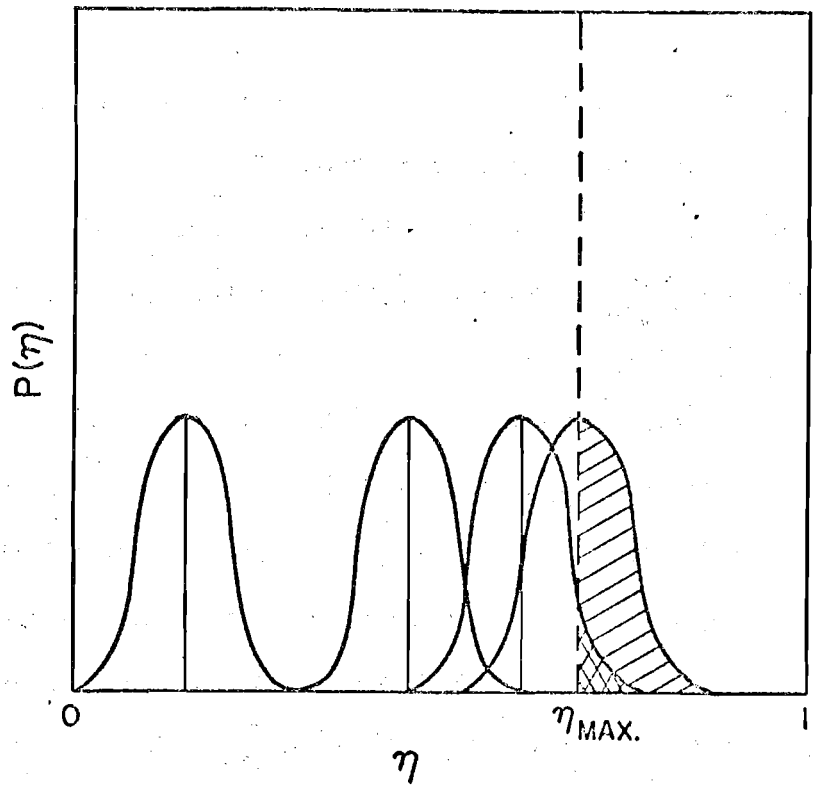

Fig. 3.3-3 Probability of Rejection for Runs With Various Mean Radii.

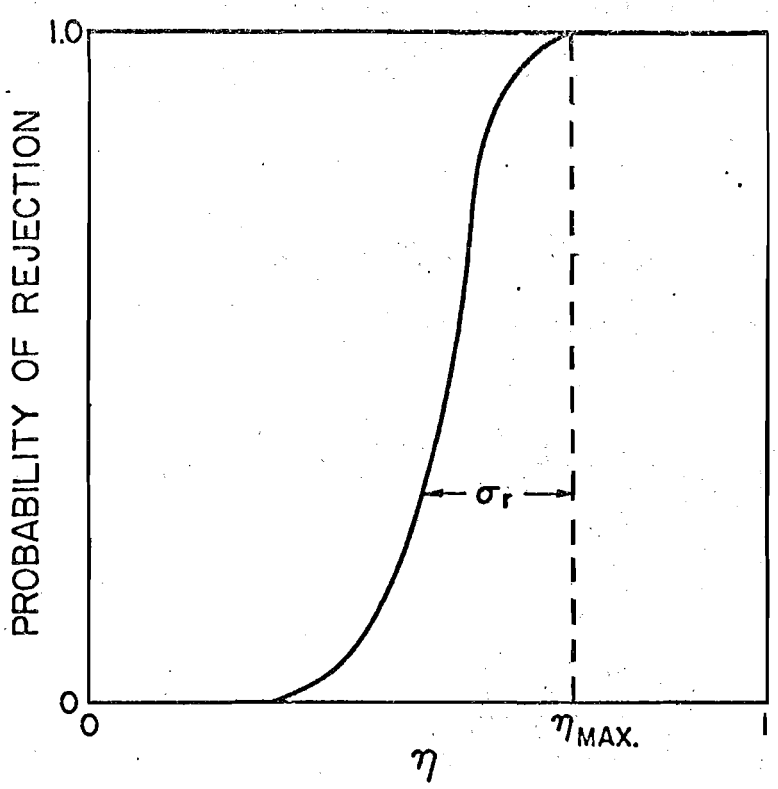

Fig. 3.3-4 Probability of a Particle Run Being Rejected.

Thus the modified probability density for a uniform distribution of particles with rejection criterion, $P_m(\eta)$, is

$$P_m(\eta) = P_u(\eta) \cdot P_A(\eta) \tag{3.3-17}$$

$$P_m(\eta) = A_m \eta \, erf\left(\frac{\eta_{max} - \eta}{\sigma_r \sqrt{2}}\right) \tag{3.3-18}$$

The normalization condition must again hold

$$\int_0^{\eta_{max}} P_m(\eta) d\eta = 1 \tag{3.3-19}$$

Thus

$$A_m = \left\{ erf\left(\frac{\eta_{max}}{\sigma_r\sqrt{2}}\right)\left(\frac{\eta_{max}^2}{2} + \frac{\sigma_r^2}{2}\right) + \right.$$
$$+ \exp\left(\frac{-\eta_{max}^2}{\sigma_r^2 2}\right)\left(\frac{\eta_{max}\sigma_r\sqrt{2}}{\sqrt{\pi}} - \frac{\eta_{max}\sigma_r}{\sqrt{2\pi}}\right) - \tag{3.3-20}$$
$$\left. - \frac{\eta_{max}\sigma_r\sqrt{2}}{\sqrt{\pi}} \right\}^{-1}$$

$P_m(\eta)$ is shown in Fig. 3.3-6 for some representative values of η_{max} and σ_r.

By utilizing Eqs. (3.3-18) and (3.3-9) in Eq. (3.3-5):

$$\left\langle R_{p,z}(\tau) \right\rangle = A_m \exp\left(\frac{-\tau \beta a_o}{J_{f,z}(0)}\right) \times$$
$$\times \int_0^{\eta_{max}} \eta \, erf\left(\frac{\eta_{max} - \eta}{\sigma_r\sqrt{2}}\right) \exp\left(\frac{\tau \beta a_1 \eta}{J_{f,z}(0)}\right) d\eta \tag{3.3-21}$$

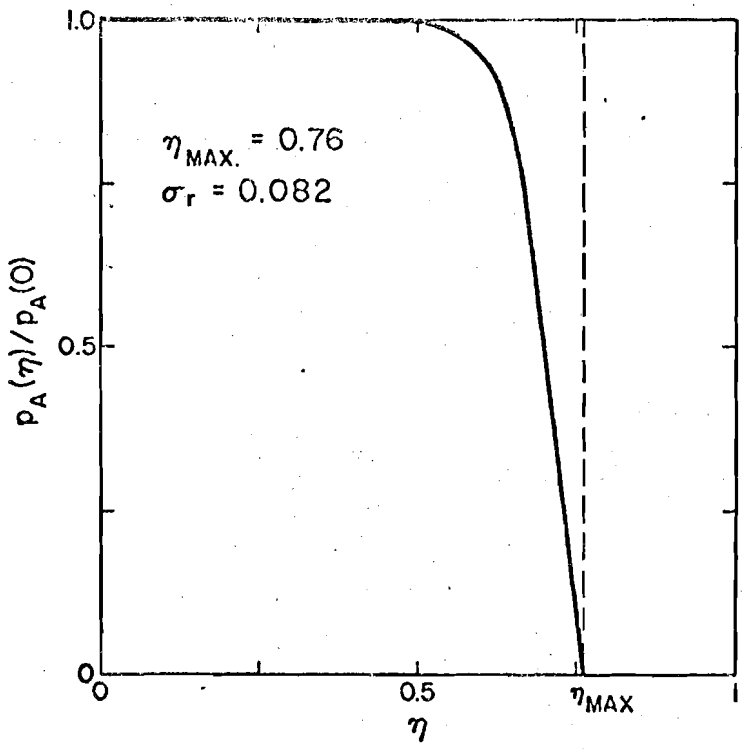

Fig. 3.3-5 Probability of an Acceptable Particle Run.

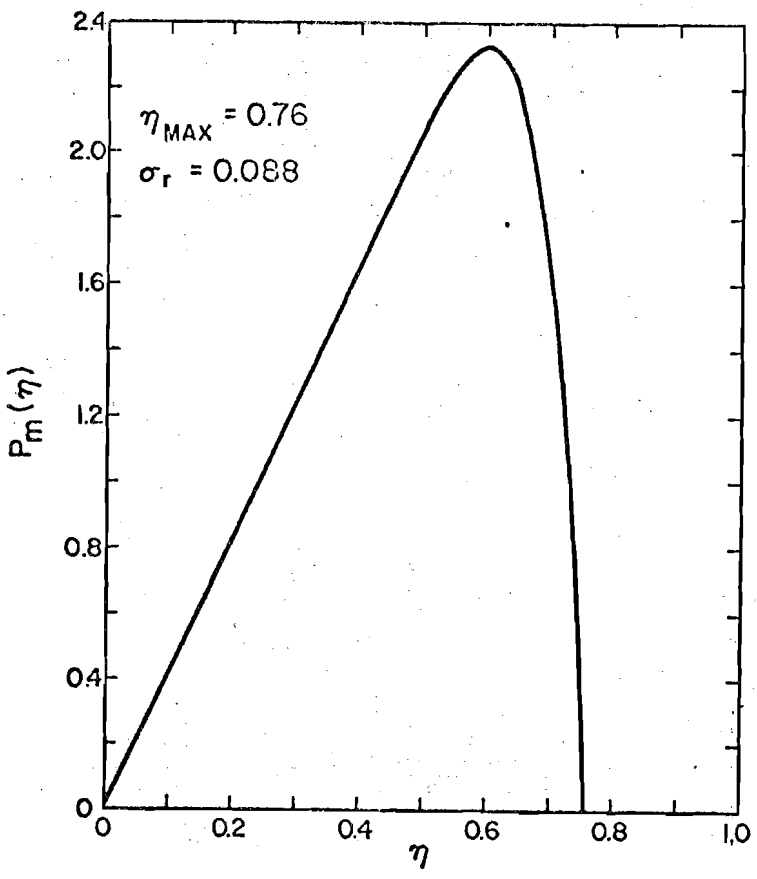

Fig. 3.3-6 Modified Uniform Distribution for Individual Run Mean Radii.

By evaluating the integral in Eq. (3.3-21) it is found after some calculation

$$\langle R_{p,z}(\tau)\rangle = C \cdot h(a', \sigma_r, \eta_{max}) \tag{3.3-22}$$

where

$$h(a', \sigma_r, \eta_{max}) = \left\{ \frac{\sigma_r\sqrt{2}}{a'^2} \exp\left(\frac{a'\eta_{max}}{\sigma_r\sqrt{2}}\right) erf\left(\frac{\eta_{max}}{\sigma_r\sqrt{2}}\right) + \right.$$

$$+ \exp\left(\frac{a'^2}{4}\right)\left[\frac{\sigma_r\sqrt{2}}{2} - \frac{\sigma_r\sqrt{2}}{a'^2} - \frac{\eta_{max}}{a'}\right]\left[erf\left(\frac{\eta_{max}}{\sigma_r\sqrt{2}} - \frac{a'}{2}\right) - erf\left(\frac{-a'}{2}\right)\right] + \tag{3.3-23}$$

$$\left. + \frac{\sigma_r\sqrt{2}}{a'\sqrt{\pi}}\left[1 - \exp\left(\frac{a'^2}{4}\right)\exp -\left(\frac{\eta_{max}}{\sigma_r\sqrt{2}} - \frac{a'}{2}\right)^2\right]\right\}$$

and

$$C = A_m\sqrt{2}\sigma_r \exp\left(\frac{-\tau a_0 b}{J_{f,z}(0)}\right)\exp(a'\eta_{max}) \tag{3.3-24}$$

and

$$a' = \frac{-\tau a_1 b\sqrt{2}\sigma_r}{J_{f,z}(0)} \tag{3.3-25}$$

The above equations are valid only for $\tau \neq 0$ or $a' \neq 0$. The integral in Eq. (3.3-21) must be evaluated in a different manner for the case $\tau = 0$. For $\tau = 0$ in Eq. (3.3-21):

$$\langle R_{p,z}(0)\rangle = A_m \int_0^{\eta_{max}} \eta\, erf\left(\frac{\eta_{max} - \eta}{\sigma_r\sqrt{2}}\right) d\eta \tag{3.3-26}$$

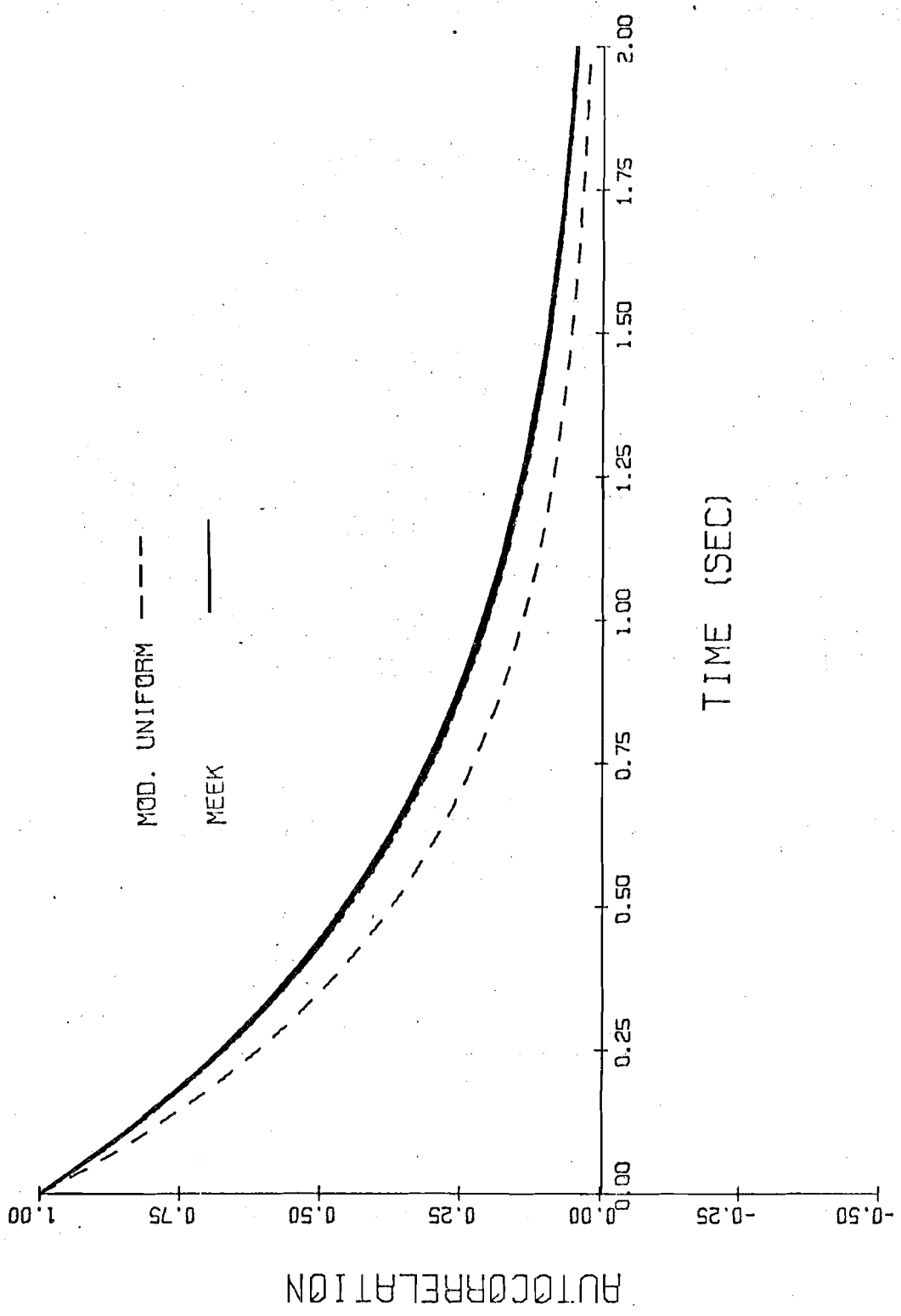

Fig. 3.3-7 Theoretical Predictions for the Axial Particle Autocorrelation.

But this integral is simply A_m^{-1} as defined by Eqs. (3.3-19) and (3.3-20). Thus, $\langle R_{p,z}(0) \rangle = 1$ as it should be for an autocorrelation.

A comparison between theoretical predictions for the axial particle autocorrelation function, $R_{p,z}(\tau)$, is shown in Fig. 3.3-7. The curves shown are based on calculations from Eq. (3.3-6) for the homogeneous theory, and Eq. (3.3-22) for the modified uniform theory. Typically observed experimental values were used for the input parameters $J_{f,z}(0)$, $\zeta, \sigma, \bar{\eta}, \sigma_r$ and η_{max}. The modified uniform theory predicts a smaller time macroscale than the homogeneous theory. This is an important result especially for particles with low free fall velocity and will be discussed further.

3.4 Anisotropic Flow

In the case of anisotropic flow systems prediction of particle behavior is complicated by the rather specific relationship of the anisotropy to the flow system involved. An approximate engineering model will therefore be proposed to incorporate anisotropic effects. Emphasis will be placed on formalism rather than application to a specific case.

From the general theory of linear regression it is known that determination of correlation between two quantities allows a statistical inference of one from a knowledge of the other. In the present context this involves Lagrangian particle motion:

$$u_{p,i} = \frac{\langle u_{p,i} \mid u_{p,j} \rangle}{\langle u_{p,j}^2 \rangle} u_{p,j} \qquad (3.4\text{-}1)$$

This expression must be regarded as purely a statistical one and cannot be expected to provide information beyond that implicit in linear regression. If velocities are normalized to their RMS values Eq. (3.4-1) becomes:

$$u'_{p,i} = R_{ij}\, u'_{p,j} \qquad (3.4\text{-}2)$$

where the prime denotes normalization and Rij is the zero lag time velocity correlation matrix. From the form of Eq. (3.4-2) it is evident that the velocity correlation matrix serves (in a formal sense) to provide a linear transformation from one set of velocity components, referred to a given set of basis vectors, into another set of components referred to the same basis. Indeed the transformation involved is an orthogonal one preserving the length of the original vector. Using standard techniques of matrix mechanics it is possible to perform a principal axis transformation to diagonalize the velocity correlation matrix. Re-normalization of the resultant matrix produces a matrix which is formally similar to that for isotropic flow.

To furnish an engineering approximation to incorporate anisotropy it is suggested that the various components of particle correlation derived previously for isotropic flow be substituted into this matrix and an inversion of the above process be applied. Such a step implicitly assumes the identity of the principal axis matrix to be that of isotropic flow. It further requires the transformation matrix used in the inversion process to be a constant as a function of lag time. Both of these assumptions in all likelihood are approximate and certainly cannot be rigorously justified. However, used as rough predictive devices they should prove useful. A further approximation that should also be of use is that of inferring the transformation matrix from knowledge of the more readily obtainable fluid velocity correlation matrix. Although not as accurate such a procedure should provide an acceptable measure

of the actual transformation matrix.

An unavoidable shortcoming of this approach, related directly to its empiricism, is the inability of such a model to include effects due to particle size. Once the transformation matrix is known the isotropic matrix can easily be inverted to allow prediction of the anisotropic situation. However, since this transformation is dependent solely upon the structure of the anisotropic flow no further effects due to particle size beyond those included in the isotropic expressions can be incorporated. Recent experimental evidence presented in Chapter Two suggests size to be a definite factor at least insofar as lateral velocity correlation is concerned. The inability of the present approach to include such behavior must be regarded as an indicator of its limitations.

4. MODEL VERIFICATION AND APPLICATIONS

4.1 Prediction of Particle Free Fall and Inertial Effects

In examining the nature of the combined influence of free fall velocity and inertial effects, we have developed a model which incorporates these through the parameters T_{pi}, β and ξ introduced in Section 3.2. The FFP series provides experimental information against which the model is compared. In addition, other experimental data in the open literature enables a wider range of parameterization verification of the model.

For the case in which a uniform axial drift velocity, f; an isotropic, homogeneous fluid turbulence fluid field, u_{fi}; a particle response function, $Q(\omega_o)$; and a range on the particle density parameter of $0.1 \leq \beta \leq 3.0$, the theory developed by Meek (1972) and presented in Section 3.2 is valid. Equation (3.2-9) can then be approximated directly as

$$R_{p,i}(\tau) \cong \exp\left(-\tau/T_{p,i}\right) \tag{4.1-1}$$

where

$$T_{p,i} = \mathcal{J}_{f,i} / \zeta_i \tag{4.1-2}$$

and ζ_i is given by Eq. (3.2-8). For the full range of the density parameter ($0.0 \leq \beta \leq 3.0$) the simplified result of Eq. (4.1-1) does not hold for $\beta < 0.1$ and the more detailed results of Meek (1972) should be consulted.

By following Taylor (1921) the dispersion for the various i-directions can be obtained using $R_{pi}(\tau)$ in the expression

$$\overline{X_{p,i}^2(t)} = 2\,\overline{u_{p,i}^2} \int_0^t \int_0^T R_{p,i}(\tau)\, d\tau\, dT \tag{4.1-3}$$

Substituting $R_{pi}(\tau)$ from Eq. (4.1-1) gives the axial particle dispersion as

$$\overline{X_{p,z}^2(t)} = 2\,\overline{u_{p,z}^2}\; T_{p,z}\left[t - T_{p,z}\left(1 - \exp\left(-t/T_{p,z}\right)\right)\right] \tag{4.1-4}$$

Assuming the turbulence to be isotropic the corresponding lateral dispersion is given by

$$\overline{X^2_{p,r}(t)} = \overline{X^2_{p,\theta}(t)} = \overline{u^2_{p,z}}\ T_{p,z}\left[t - T_{p,z}\left(1 - \exp\left(-t/T_{p,z}\right)\right)\right] \tag{4.1-5}$$

where

$$R_{p,r}(\tau) = R_{p,\theta}(\tau) = \left(1 - \frac{\tau}{2T_{p,z}}\right)\exp\left(-t/T_{p,z}\right) \tag{4.1-6}$$

Meek and Jones (1973) have presented the parallel development for small, heavy particles where $\beta \to 0$ but f_i is finite. The corresponding correlation and dispersion relations in the axial and lateral directions are:

$$R_{p,z}(\tau) = \frac{1}{1-\xi}\left[\exp\left(-\tau/T_{p,z}\right) - \xi\exp\left(-\tau/(\xi T_{p,z})\right)\right] \tag{4.1-7}$$

$$R_{p,r}(\tau) = R_{p,\theta}(\tau) = \frac{1}{1-\xi}\left[\left(1 - \tau/(2T_{p,z})\right)\exp\left(-\tau/T_{p,z}\right) - \xi\left(1 - \tau/(2T_{p,z}\xi)\right)\exp\left(-\tau/(\xi T_{p,z})\right)\right] \tag{4.1-8}$$

$$\overline{X^2_{p,z}(t)} = \frac{2\overline{u^2_{p,z}}}{1-\xi}\left\{\left[tT_{p,z} - T^2_{p,z}\left(1 - \exp\left(-t/T_{p,z}\right)\right)\right] - \xi^2\left[tT_{p,z} - \xi T^2_{p,z}\left(1 - \exp\left(-t/T_{p,z}\right)\right)\right]\right\} \tag{4.1-9}$$

and

$$\overline{X^2_{p,r}(t)} = \overline{X^2_{p,\theta}(t)} = \frac{\overline{u^2_{p,z}}\ tT_{p,z}}{1-\xi}\left\{\left[1 - \exp\left(-t/T_{p,z}\right)\right] - \xi^2\left[1 - \exp\left(-t/(\xi T_{p,z})\right)\right]\right\} \tag{4.1-10}$$

where

$$\overline{u^2_{p,z}}\ /\ \overline{u^2_{f,z}} = 1/(1+\xi) \tag{4.1-11}$$

A direct comparison of these predictions with lateral correlation and dispersion measurements presented by Snyder and Lumley (1971) shows good agreement. Figure 4.1-1 shows the lateral correlations for sets of their experimental data in comparison to predictions by Eq. (4.1-8). Although perfect agreement is lacking the trends and functional behavior of the predictions are correct. The corresponding dispersions predicted by Eq. (4.1-10) for two of their sets of data are compared in Fig. 4.1-2 and excellent agreement is observed. Thus, employing such a predictive scheme with reasonable estimates of the fluid turbulence structure ($\overline{u_{f,z}^2}$ and $\mathcal{J}_{f,z}$) and of the particle characteristics (α, β, f_z) should provide acceptable dispersion predictions for many practical applications. Since isotropic turbulence has been assumed, the lateral Lagrangian integral time scale for the fluid turbulence structure, $\mathcal{J}_{f,r}$, is half the corresponding axial value, $\mathcal{J}_{f,z}$.

To demonstrate the effects of crossing trajectories brought in by finite free fall velocities, examinations of the ratio of particle-to-fluid integral time scales employed is useful. Defining the integral time scale for the particle as

$$T_{p,i} = \int_0^\infty R_{p,i}(\tau)\, d\tau \tag{4.1-12}$$

the ratio of scales for the axial direction is given by

$$T_{p,z} / \mathcal{J}_{f,z} = (1+\xi) \Big/ \left(1 + f_z^2 / \overline{u_{p,z}^2}\right)^{1/2} \tag{4.1-13}$$

This relation shows that as f_z increases the particle integral time scale rapidly decreases. The inertial effects, through ξ, tend to increase $T_{p,z}$ and even dominate the relation when $f_z^2 < \overline{u_{p,z}^2}$. Figure 4.1-3 shows the predicted ratios for the three cases of Snyder and Lumley considered earlier and demonstrates the need to consider the inertial effects in these low β cases.

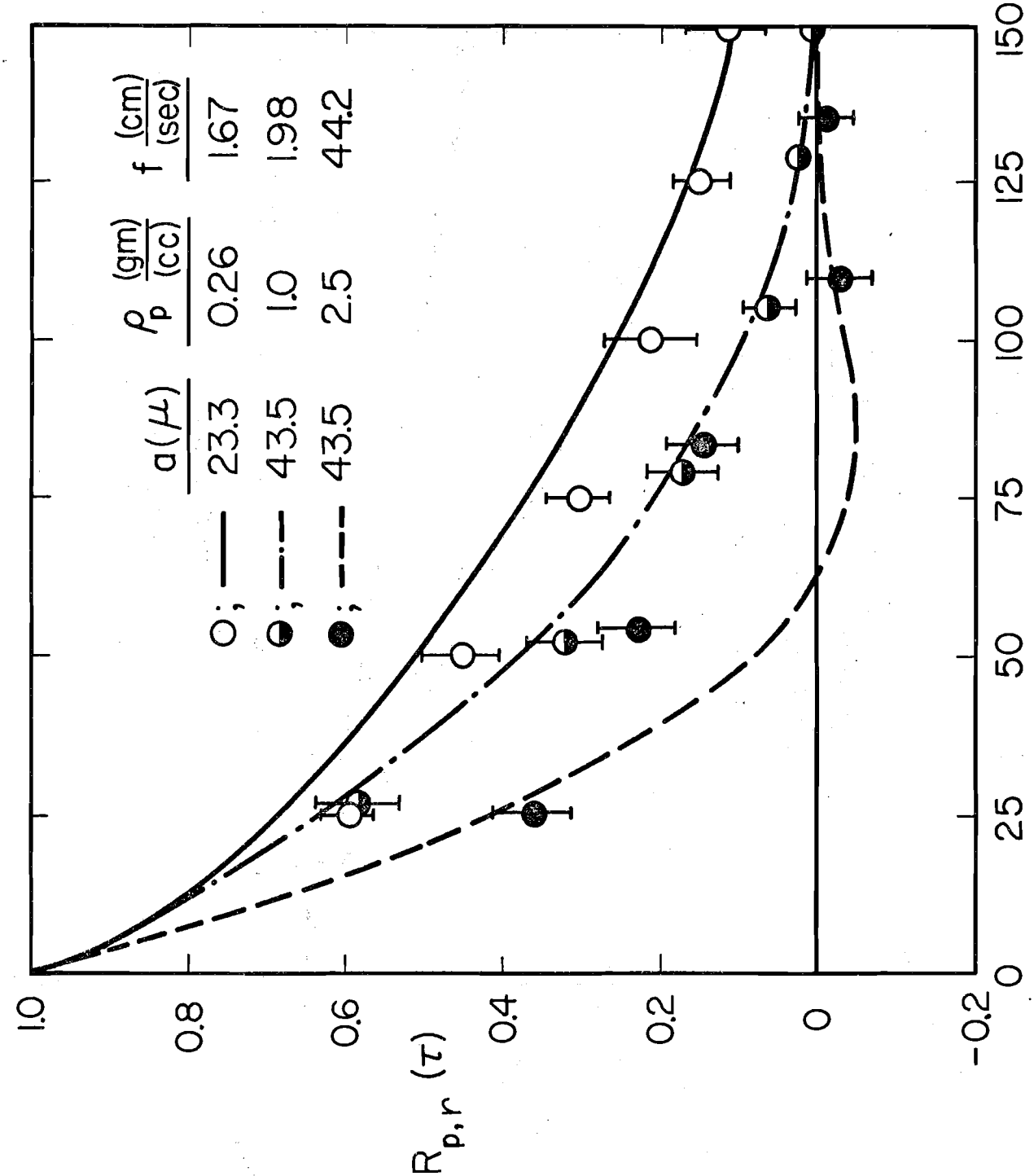

Fig. 4.1-1 Comparison of Analytical Predictions of Lateral Correlation Coefficients with Measurements of Snyder and Lumley (1971).

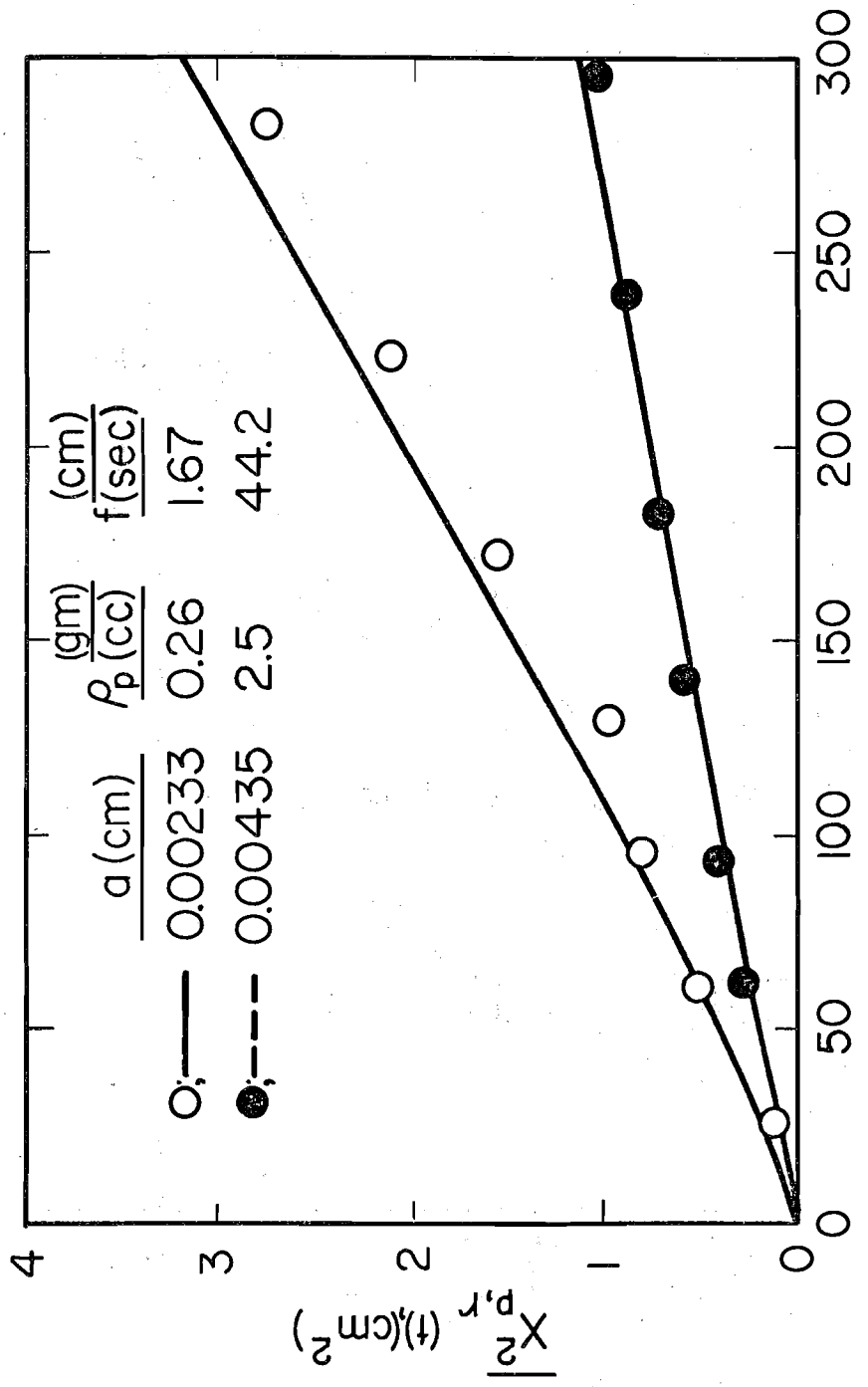

Fig. 4.1-2 Comparison of Analytical Predictions of Lateral Dispersion with Measurements of Snyder and Lumley (1971).

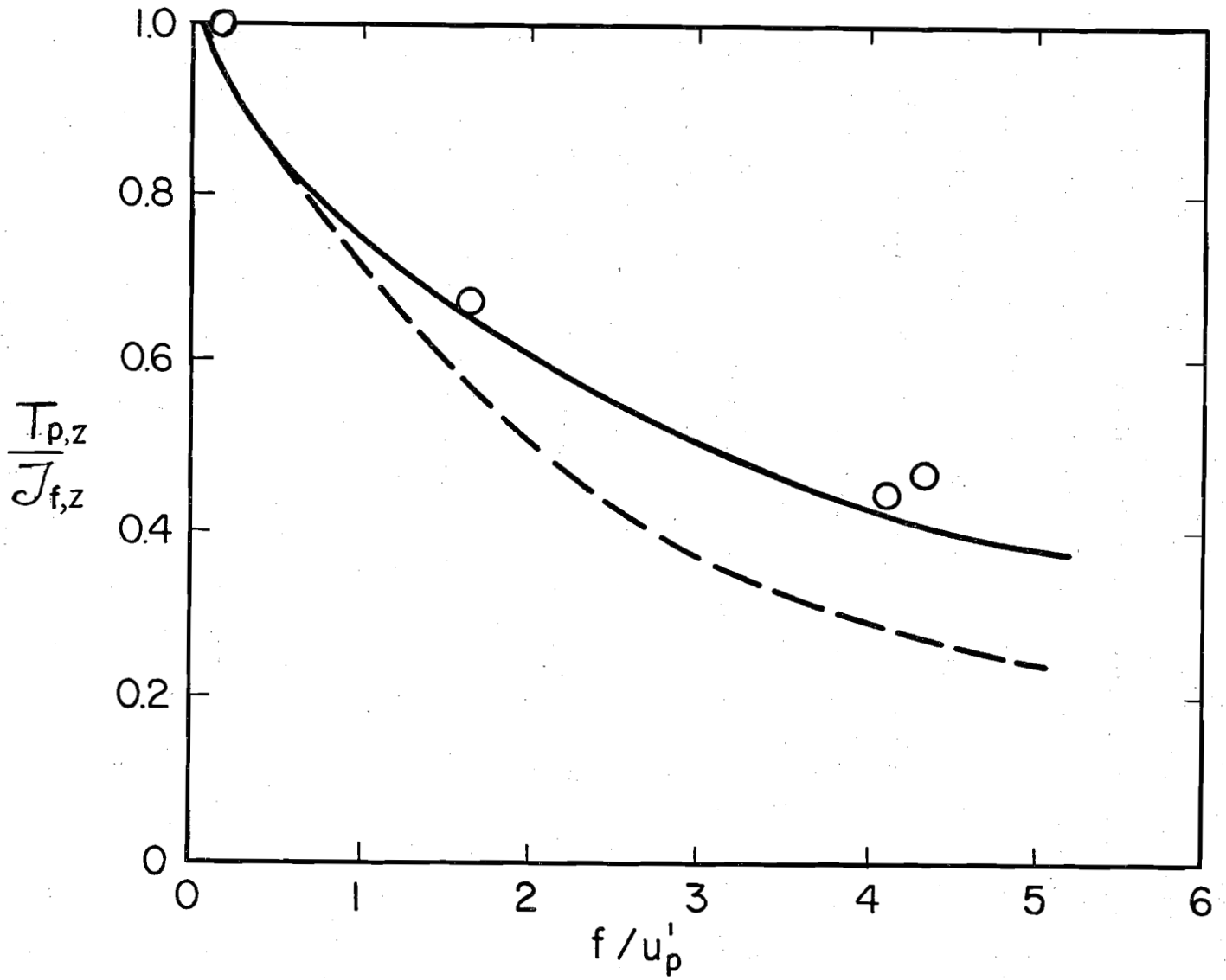

Fig. 4.1-3 Comparison of Analytical Predictions of Integral Time Scales with Measurements of Snyder and Lumley (1971): Solid Line, with Inertial Effects; Dashed Line, Neglecting Inertial Effects.

For the range of β near unity, where the free fall parameterization can readily be varied with particles of a few millimeters diameter, both the FFP and SP series data can be used to check the proposed models for particle correlation, dispersion and integral time scale. The data obtained by Howard (1974) is presented in Appendix B in which the FFP and SP series $R_{pi}(\tau)$ for axial, radial and azimuthal direction are compared for each series. The corresponding computer presentation of other statistical quantities is also included.

To illustrate the agreement of Meek's theory with experimental results the axial particle autocorrelation is compared with data for FFP1 including a comparison with an additional evaluation with the radial distribution of particles included (Modified Uniform theory) which has been discussed in Chapter 3. (See Fig. 4.1-4). Due to the relatively large size of the particle to the lateral turbulence scale the use of isotropy in the theoretical prediction of the lateral particle correlations is in significant disagreement with observations. Figure 4.1-5 compares predicted and observed axial dispersion for FFP1 and shows excellent agreement. This was generally found to hold for axial dispersion for positive free fall particles but not for large negative free fall cases. The specific reason for this lack of agreement is not resolved.

Results with $\beta \simeq 0.75$ and $\beta \simeq 1.1$ and with 3 mm and 5 mm diameter particles have been attempted in this apparatus, but difficulties with either very rapid transit times or very long transit times for the two β-values, respectively, have prevented procurement of reliable data with adequate resolution. Some preliminary data for a 5 mm particle with β=0.73 are included with the F F P series data in Appendix B. But inadequate resolution prevents establishment of specific trends from being affirmed for the extension of the β parameter.

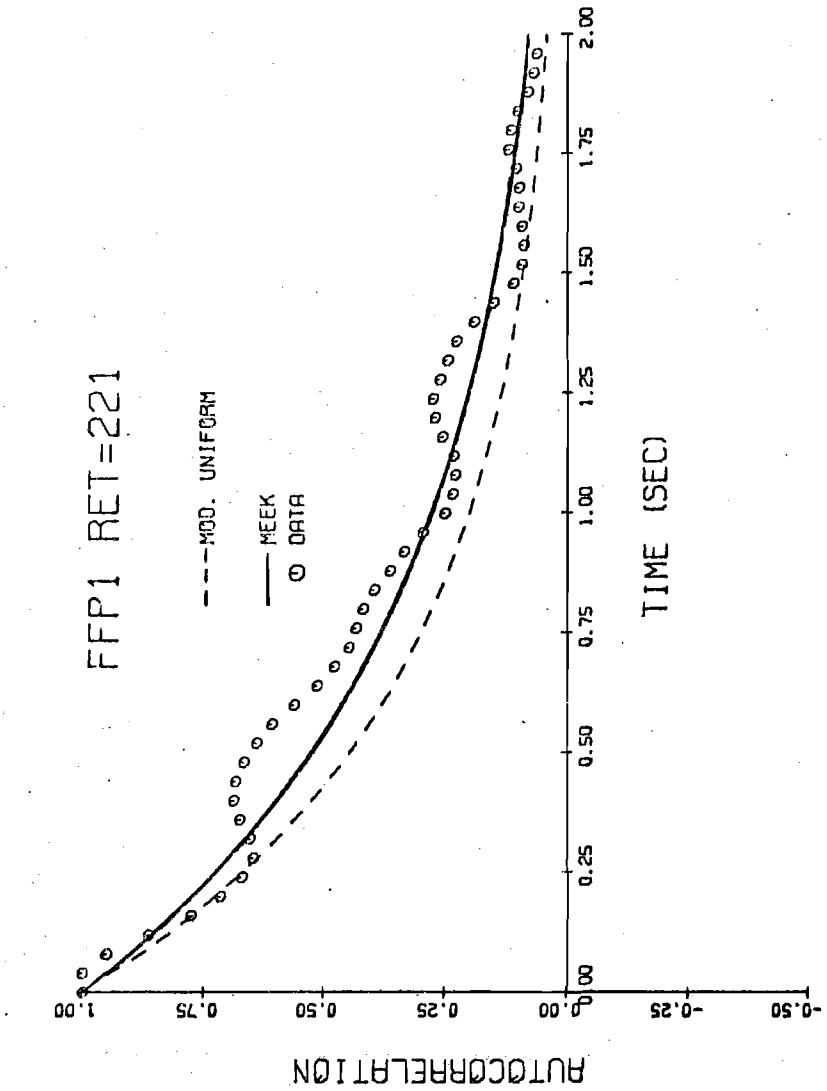

Fig. 4.1-4 Comparison of Analytical Predictions of Axial Autocorrelation with Measurements by Howard (1974) for FFP1 Particle.

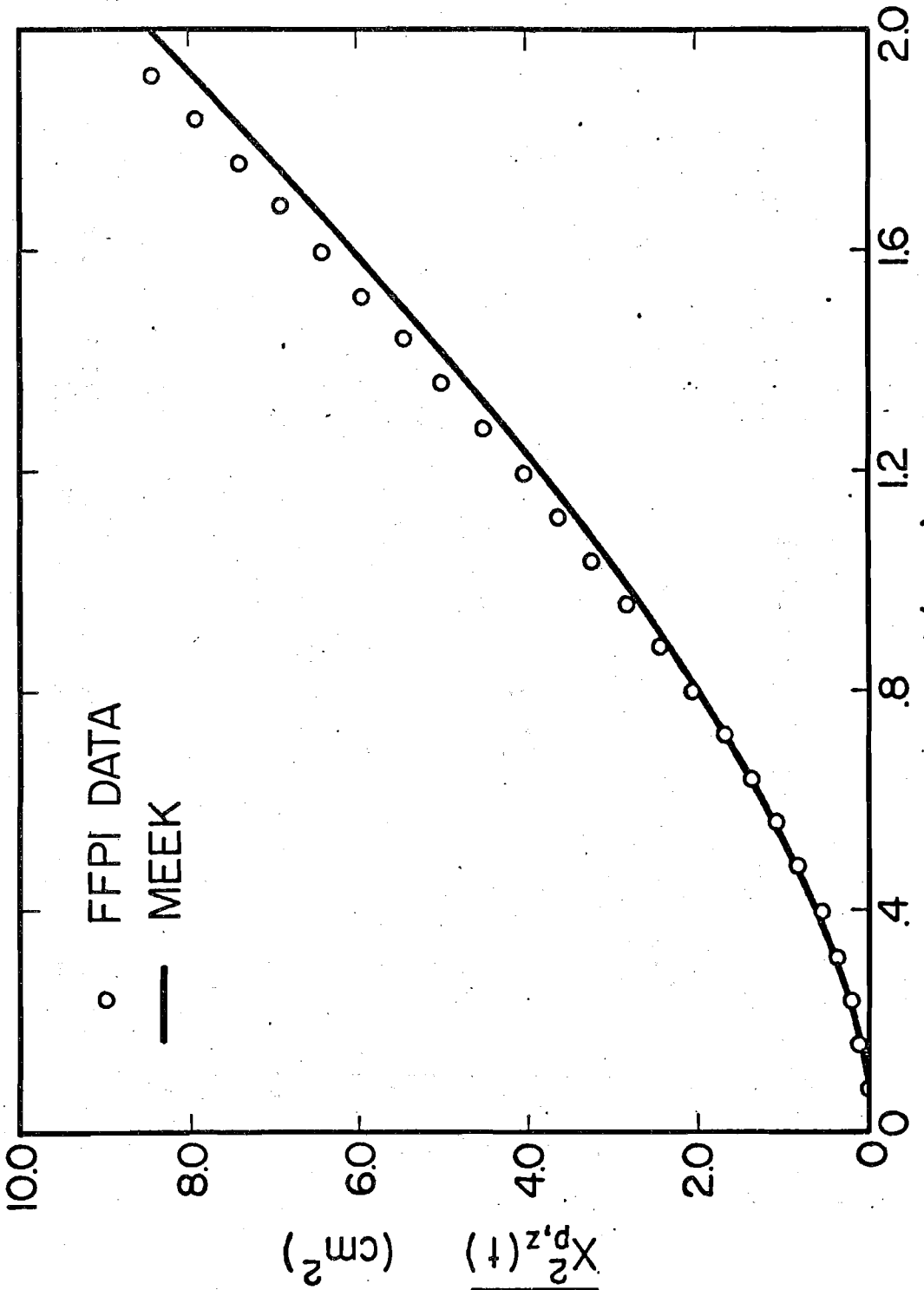

Fig. 4.1-5 Comparison of Experimental Axial Dispersion With Predictions from Meek's Theory

4.2 Prediction of Particle Size Effects

The theory developed in Chapter 3 basically deals with the prediction of particle motion in the axial direction. We have seen in Chapter 2 that turbulence is a three dimensional phenomena with three dimensional structure. For the lateral directions it was more difficult experimentally to fulfill the theoretical requirement that the particle must be small compared with the micro-scale of the turbulence than was the case for the axial direction. If the particle size does not fulfill this requirement, what method can be used to help predict particle motion? It is believed that as the particle size becomes smaller and smaller, its response becomes more like a fluid particle. For the axial direction and for particles of finite size but smaller than the turbulent micro-scale, the size variation of particle motion enters in the parameter α. For the case of particles somewhat larger than the fluid spatial microscale (as occurred for lateral directions where scales are smaller) we make recourse to experiments to yield empirical data.

Data from the SP-Experiments are plotted in Fig. 4.2-1. Table 4.2-1 provides background time scales. We can see that our expectations are verified. As the particle size becomes smaller ($\alpha \mathcal{J}_{f,z}$ gets larger) the particle time scale ratio $\mathcal{T}_{p,z}/\mathcal{T}_{p,r}$ tends toward the limit expected for fluid particles. The data of Sabot, Renault & Compte-Bellot (1973) suggests for turbulence in a pipe with pipe Reynolds number of 1.35×10^5 that the fluid time scale ratio is

$$\mathcal{J}_{f,z}/\mathcal{J}_{f,r} = 4.8$$

as shown in Fig. 4.2-1. An empiricle fit to these data yields

$$\mathcal{T}_{p,z}/\mathcal{T}_{p,r} = 4.8 - 3.1 \exp(-.26 \alpha \mathcal{J}_{f,z})$$

Thus for a given size, α, and fluid macroscale, $\mathcal{J}_{f,z}$, we may calculate the ratio $\mathcal{T}_{p,z}/\mathcal{T}_{p,r}$. If we estimate $\mathcal{T}_{p,z}$ from the theory as developed in Chapter 3,

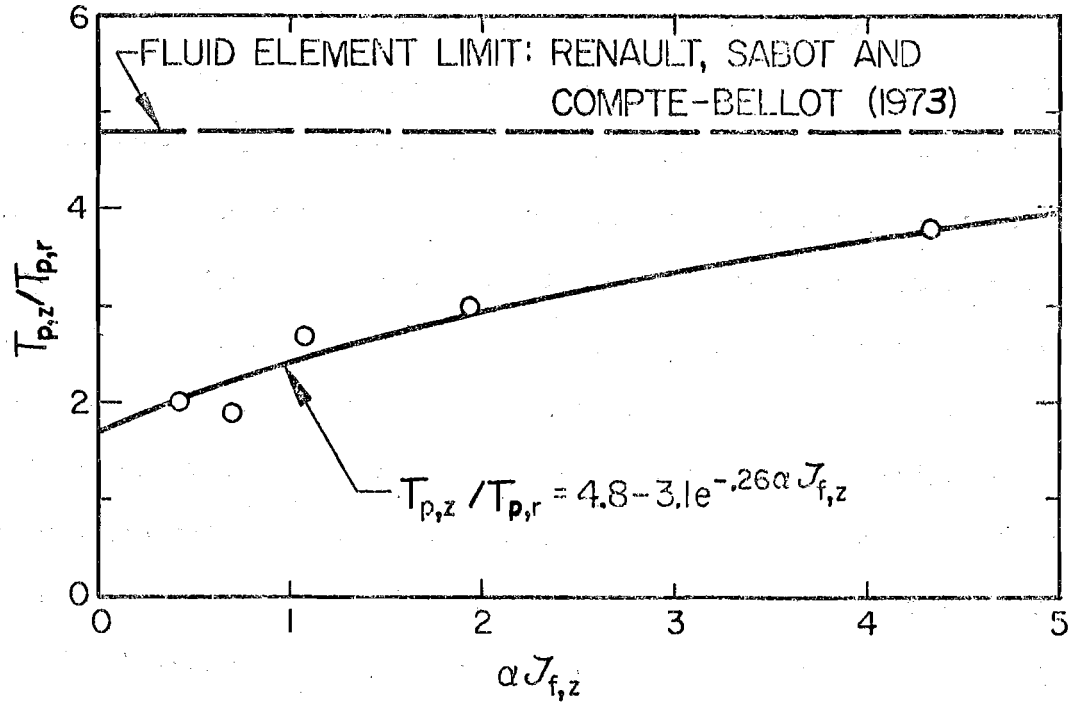

Figure 4.2-1 Ratio of Axial-to-Lateral Integral Time Scales for Fluid and for Particles.

Table 4.2-1 Axial-to-Lateral Particle Integral Time Scales

Particle	α	$\alpha \mathcal{J}_{fz}^{*}$	T_{pz}/T_{pr}
SP2A,C,D (6.5mm)	.25	.42	2.0
SP3 (4mm)	.65	1.08	2.7
SP4 (3mm)	1.16	1.93	3.0
SP5 (2mm)	2.61	4.33	3.8
FFP (5mm)	.42	.70	1.9

*$\mathcal{J}_{fz}$ = 1.66 seconds for Re_{pipe} = 50,000

we may also estimate $T_{p,r}$, a parameter important in predicting the lateral dispersion of the particle. Thus, we are able to empirically predict the effect of particle size on lateral particle dispersion. This is significant in engineering applications particularly to environmental problems in which the spread of plumes in the atmosphere and in lakes and rivers is a primary concern in meeting dissipation and dilution standards.

4.3 Applications to Related Problems

In the controlled experiments detailed observations of fluid and particle turbulence were obtained. This will be the exception in engineering applications where much of the existing fluid turbulence field is not measured. However, in the development of the model, only a few key parameters of the turbulent field are required. In general, good estimates can readily be made in boundary layer flows, in open channel flows and in plumes for turbulence intensity and integral scales. The types of particles with their size distribution are also usually known. These are the only ingredients which are needed to predict dispersions when the form of the particle autocorrelation functional is taken to be a single parameter exponential. The size and shape parameterizations presented above give good indication of the range of particle sizes for which the model can be applied with accuracy.

4.4 Procedure For Predicting Dispersion

From the definition of dispersion given by Taylor (1921) and its modification by Kampé de Fériet (1939) we observe that particle dispersion is directly related to its autocorrelation function

$$\overline{X_{p,i}^2(t)} = 2\overline{u_{p,i}^2}\int_0^t (t-\tau)\, R_{p,i}(\tau)\, d\tau \qquad (4.4\text{-}1)$$

For very short times compared to the particle time macroscale, $t \ll T_{p,i}$ we note that $R_p(\tau) \tilde{=} 1$ and thus,

$$\overline{X^2_{p,i}(t)} \cong \overline{u^2_{p,i}}\, t^2 \quad , \quad t \ll T_{p,i} \tag{4.4-2}$$

For times very long compared with the particle time macroscale we have $t \gg T_{p,i}$ thus

$$\overline{X^2_{p,i}(t)} \cong 2\overline{u^2_{p,i}}\, t \int_0^t R_{p,i}(\tau)\, d\tau \tag{4.4-2}$$

or

$$\overline{X^2_{p,i}(t)} \cong 2\overline{u^2_{p,i}}\, t\, T_{p,i} \quad , \quad t \gg T_{p,i} \tag{4.4-3}$$

For <u>axial dispersion</u> (in the flow direction) the theory of Meek (1972) enables $T_{p,i}$ to be estimated from

$$T_{p,z} = \mathcal{J}_{f,z} / \zeta \tag{4.4-4}$$

where

$$\zeta = \left[1 + \left(f_z / \sqrt{\overline{u^2_{p,z}}}\right)^2\right]^{1/2} \tag{4.4-5}$$

This enables us to calculate $\overline{X^2_{pz}(t)}$ for both long and short times compared to the particle macroscale. For intermediate times we use Meek's relation

$$R_{p,z}(\tau) = \exp\left(-\tau / T_{p,z}\right) \tag{4.4-6}$$

to calculate $\overline{X^2_{pz}(t)}$. An example of such dispersion is shown in Fig. 4.1-5.

For dispersion in the <u>lateral direction</u>, the theory of Meek does not apply directly. However, we can estimate the value of the radial time macroscale, T_{pr}, from measurements of the spatial structure of our turbulent flow field. We note that

$$T_{p,r} \cong T_{p,z}\left(\Lambda_{rr}/\Lambda_{zz}\right)\left(\overline{u_{f,r}^2}/\overline{u_{f,z}^2}\right) \tag{4.4-7}$$

where spatial integral scale ratio, $\Lambda_{rr}/\Lambda_{zz}$, is determined by analogy with measurements in a turbulent flow similar to the flow being considered. The ratio $\overline{u_{f,r}^2}/\overline{u_{f,z}^2}$ is likewise estimated or measured, and $T_{p,z}$ is estimated by Meek's theory from the Lagrangian fluid time macroscale.

Thus, lateral dispersion is given by

$$\overline{X_{p,r}^2(t)} = \overline{u_{p,r}^2}\, t^2 \quad , \quad t \ll T_{p,r} \tag{4.4-8}$$

$$\overline{X_{p,r}^2(t)} = 2\,\overline{u_{p,r}^2}\, t\, T_{p,r} \quad , \quad t \gg T_{p,r} \tag{4.4-9}$$

and

$$\overline{X_{p,r}^2(t)} = 2\,\overline{u_{p,r}^2} \int_0^t (t-\tau)\, R_{p,r}(\tau)\, d\tau \tag{4.4-10}$$

for the intermediate times. The functional form for $R_{p,r}(\tau)$ is not known at this time. However, one possible estimate would be

$$R_{p,r}(\tau) = \exp\left(-\tau/T_{p,r}\right) \tag{4.4-11}$$

The drawback to this estimate is that it has no negative correlation loop commonly observed in lateral correlations. Thus, dispersion should be overpredicted by this assumed form for $R_{p,r}(\tau)$.

It must be noted that in all cases it is assumed that the size of the particle is at least several times smaller than the microscale of the turbulence. If this condition of smallness is not met, then the lateral dispersion would increase because $T_{p,r}$ would increase. Howard (1974) has verified this behavior by experimental evaluation of dispersion for various size particles.

For negatively buoyant particles, where Meek's theory seems to fail, available experimental results indicate that dispersion is approximately equal in both the lateral and axial directions. The time scale for negatively buoyant particles is found to be less than that of positive free fall particles of the same free fall Reynolds number by a factor of 0.6. Further research into the behavior of the negatively buoyant particles is necessary to uncover the basis for their unique behavior and to determine appropriate procedures for estimating their dispersion.

5. SUMMARY AND CONCLUSIONS

The three phases of this research study have primarily emphasized the behavior of single particles suspended in a turbulent fluid. This work relates directly to dilute suspensions of small particles where particle-particle interaction is negligible and where particle loadings have negligible influence on the fluid turbulence structure. The results of the study, therefore, form a base to which cases with finite particle loadings can be compared. The establishment of such a base study has been accomplished with this study.

Influence of particle free fall velocity, inertia, size and shape have been studied. Except for particle shape, analytical models have been developed in which the physical characteristics of the particle and the structural characteristics of the fluid turbulence field are incorporated. These models have been tested with experimental data obtained in studies here in water and with experimental results reported in the literature for other fluids. Comparisons have been presented in Chapter 4 which showed general confirmation of the model.

In the experimental study the effect of particle shape for fixed volumetric displacement, using spheres as the base, showed no discernable variation between spheres, cubes and tetrahedrons. For most small particles it is concluded that basing their physical parameters on the displaced volume and density of an equivalent sphere is a good approximation.

Studies on the effects of particle size showed that, for reasonable agreement between model prediction and observed behavior, the particle diameter must be several times smaller than the integral length scale of the turbulence field. However, in cases where the axial and lateral scales of turbulence differ substantially, the predictions of particle behavior in the direction which satisfies the size - scale criterion are found to be in good agreement with observations where as in the direction which violates this criterion substantial disagreement (under prediction) occurs.

Parametric variation of free fall (heavier than fluid) particles the analytical model was capable of accommodating these crossing trajectory effects. However, currently available experimental results for negative free fall (lighter than fluid) particles reveal significant discrepancy between observed and predicted behavior. No rational explanation has been developed to explain this observation.

Particles with substantially different inertial levels than the equivalent fluid particle have been studied. Only experimental cases in which the particle density exceeded the fluid density have been studied. In these cases good agreement was found between model predictions and experimental observations.

For cases in which the particle drag coefficient substantially differs from the Stokes' (viscous dominated) case, a means of accounting for the deviation between them has been developed by Jones, Ostensen and Meek (1973).

The research has also provided a unique set of experimental data of specified accuracy with well controlled and documented parameterization of particle parameters and fluid field structure. Because of the detailed statistical structure included in the data, their further use in model development and testing is anticipated. Preliminary use has been made in extending the analysis to account for non-homogeneous fluid turbulence field structure. It is also anticipated in future work on non-dilute suspensions that the observation of deviations of particle statistical behavior from the single particle case will be important in model development for two-phase flow cases.

To meet the practical objective of these studies, an engineering model has been developed and tested which predicts the behavior of particles in dilute suspension in fluid turbulence. Only the prime features of the fluid turbulence (intensity, $\sqrt{\overline{u_{fi}^2}}$, and convective integral time scale, T_{fi}), the particle physical parameters (diameter, d_p, and relative density, ρ_p/ρ_f) and particle free fall velocity

(f_i) are necessary inputs to the model. It has been shown that for most practical applications these quantities can be readily estimated or measured. Thus, dispersion of particles emitted from stacks into the atmospheric boundary layer, of sand or other suspended particulate in streams and of water droplets from spray nozzles or from cooling towers can be predicted from this model. Such predictions are of prime importance in the areas of water pollution via sedimentation, particle transport and oxygenation as well as in atmospheric dispersion. The latter relates directly to methods prescribed by the Environmental Protection Agency for evaluating the behavior of atmospheric emissions.

APPENDIX A: EXPERIMENTAL FLUID DATA

Understanding underlying turbulent flow field in which the particles move is of major importance in predicting particle motion. For this reason we include some important measurements made in the turbulent pipe flow at a Reynolds number of about 50,000 which was used during all particle experiments.

The mean axial fluid velocity profile is shown in Fig. A-1 compared with the results of Laufer (1954). Figure A-2 shows the axial fluid turbulent intensity profile in the pipe as well as radial and azimuthal intensity obtained by Burchill (1970) in fully developed pipe flow at Re = 50,000. The core flow used for particle measurements is the region from the pipe centerline to a radius of 7 cm or r/R = 0.76. The fluid convected frame time macroscale, $\mathcal{J}_{f_z}$ is shown in Fig. A-3. Radial variation of the axial fluid space macroscale Λ_{zz}, is shown in Fig. A-4. These measurements were made with two hot film anemometers separated axially in the pipe flow as described by Howard (1974). Corresponding measurements for radial separation of the two probes gave Λ_{zr} for probe separations about r/R=0 and r/R=0.276 of 0.476 inches and 0.61 inches, respectively. The Eulerian time macroscale and microscale are presented in Fig. A-5 as taken by Meek (1972).

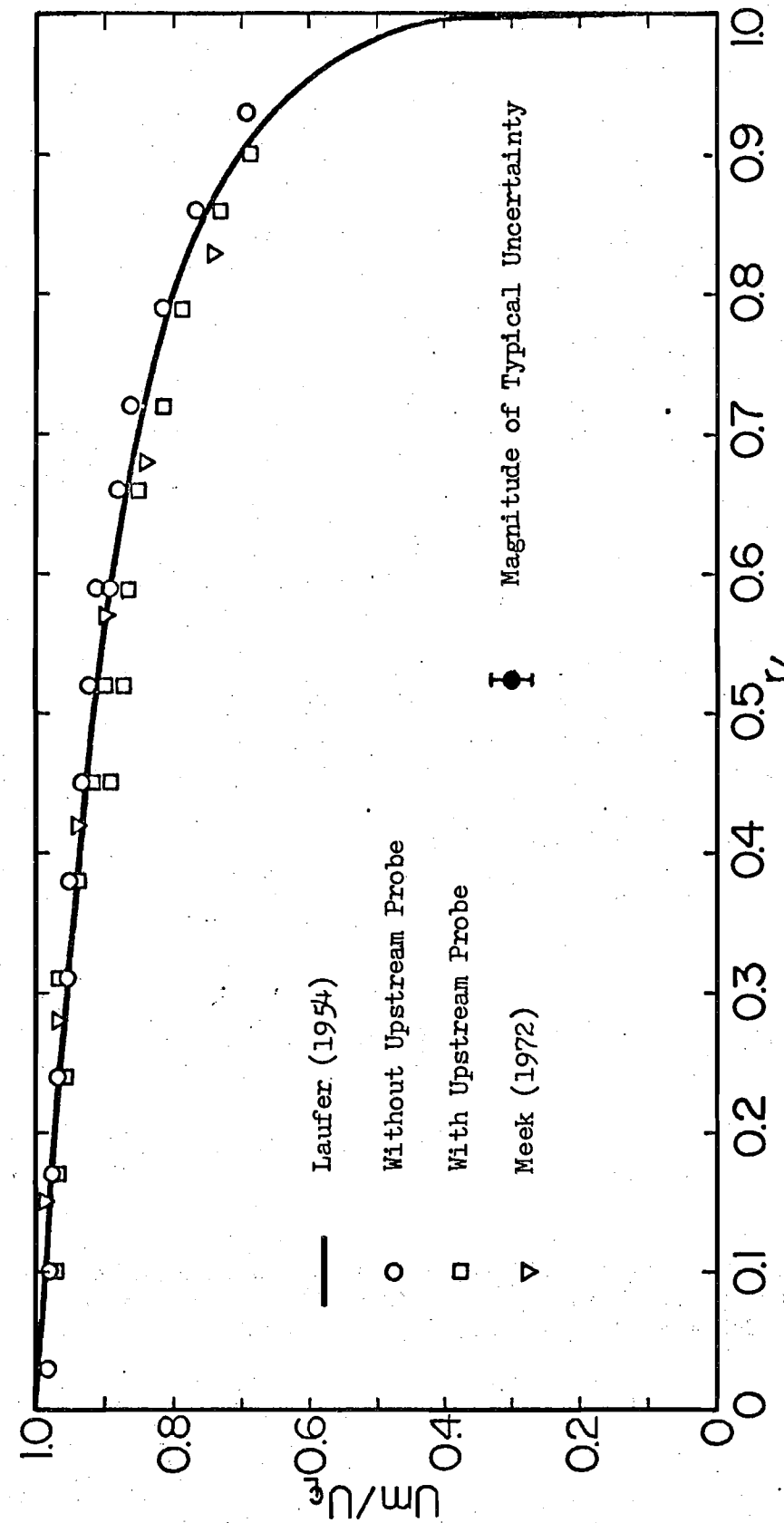

Fig. A-1. Mean Velocity Profile in a Pipe at Re = 50,000.

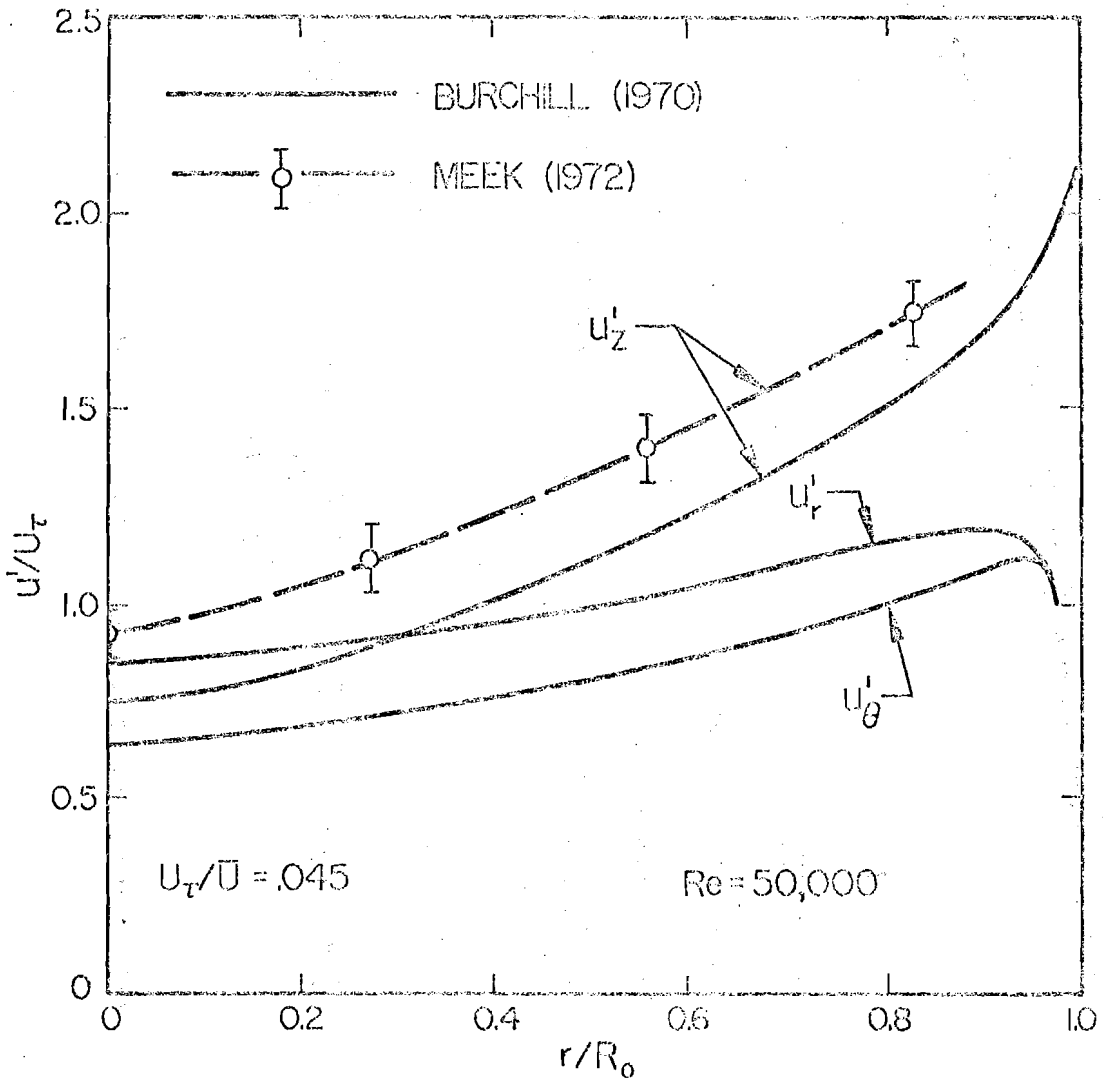

Fig. A-2. Radial Variation of Eulerian Fluid Turbulence Intensities in Fully Developed Pipe Flow (Burchill, 1970) and in the Test Section (Meek, 1972).

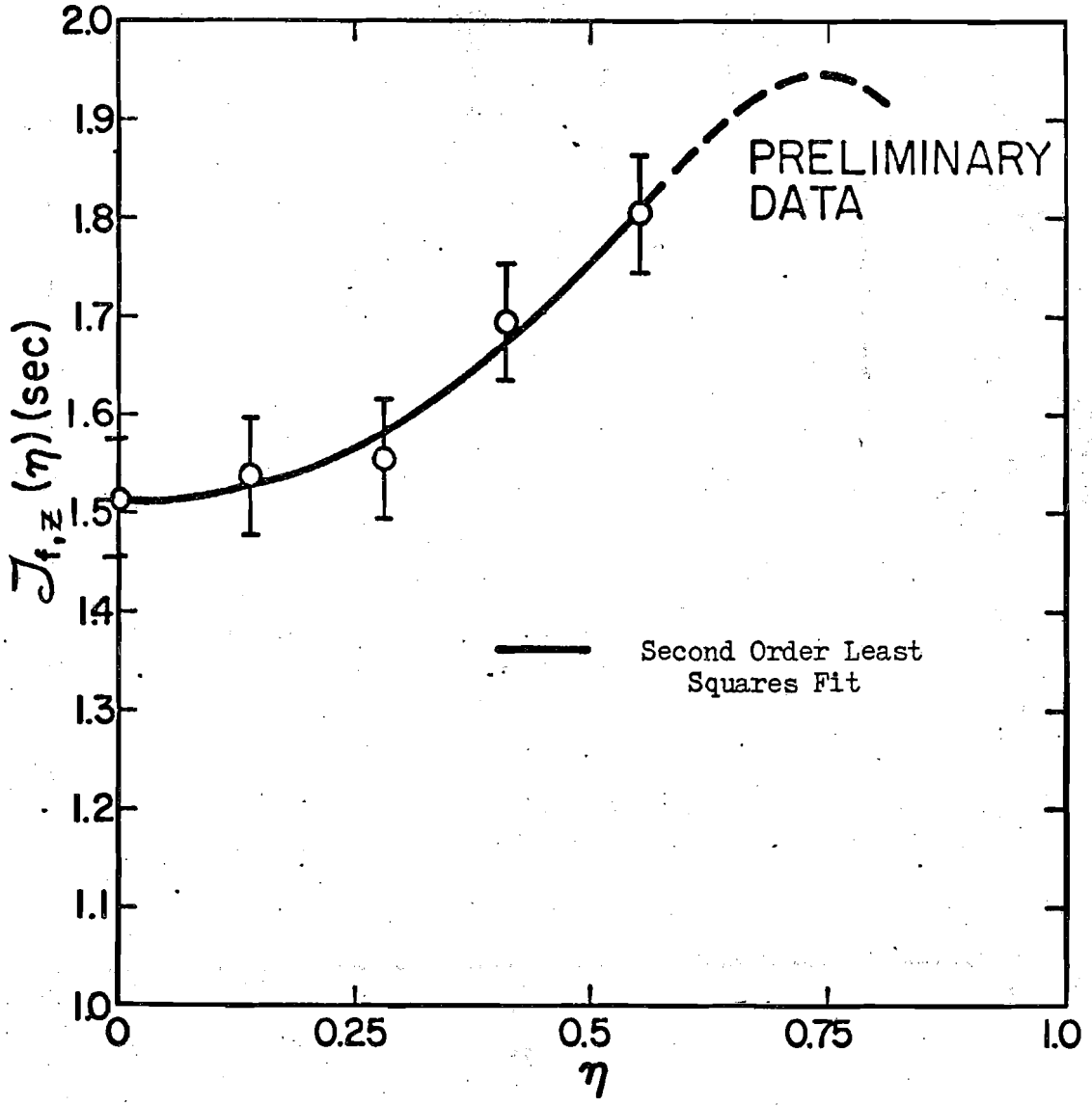

Fig. A-3. Radial Variation of the Fluid Convected Frame Time Macroscale, $\mathcal{J}_{f,z}$.

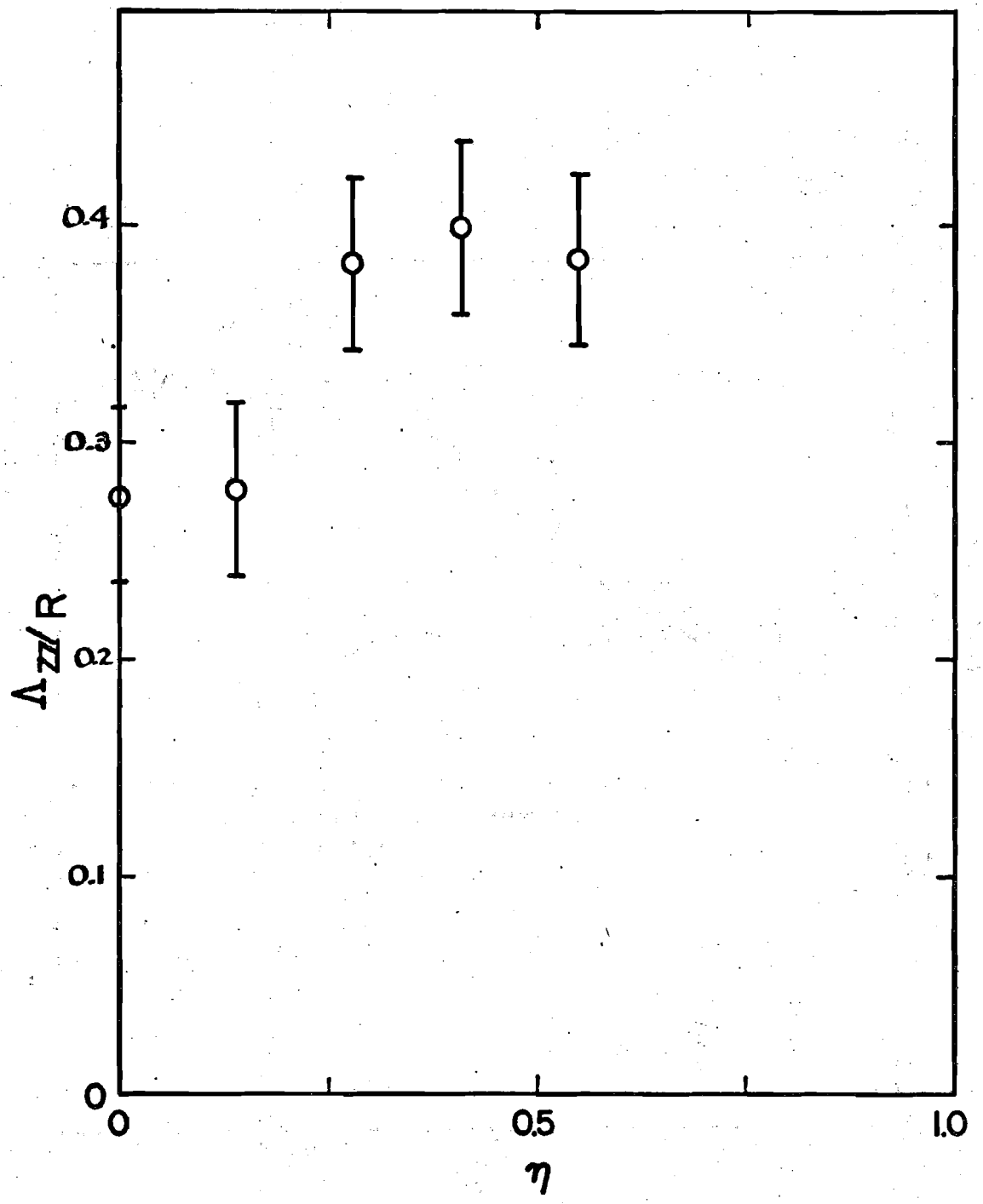

Fig. A-4. Radial Variation of the Fluid Axial Space Macroscale, Λ_{zz}.

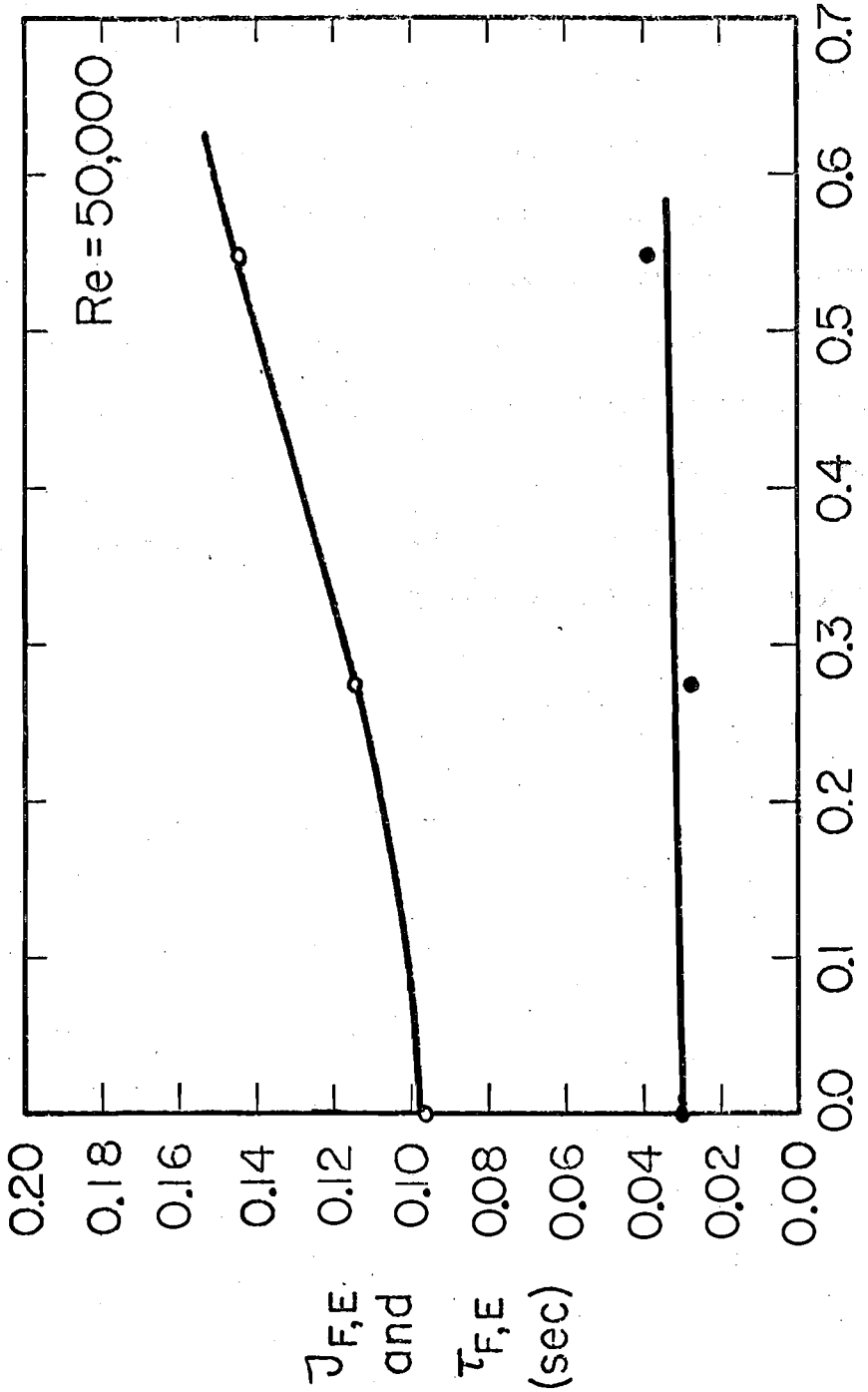

Fig. A-5. Radial Variation of the Fluid's Time Macroscale and Microscale.

- o Macroscale
- • Microscale

APPENDIX B: EXPERIMENTAL PARTICLE DATA

This Appendix presents particle data obtained by Howard (1974). The earlier data of Meek (1972) as well as the data for the shape studies have been presented earlier by Jones et al. (1972) and are not repeated here. Tables B-1, B-2, B-3 and B-4 present the physical properties, quiescent behavior, statistical behavior (including mean, variance, macroscale, microscale and model structure) of the particles in the FFP and SP series experiments. Figures B-1 through B-11 include the ensembled autocorrelations and spectra for each of the series of particle experiments. A comparison of the R_{pz}, R_{pr} and $R_{p\theta}$ for each series is included in Figs. B-12 through B-17. For further details the reader is referred to the theses of Meek (1972) and Howard (1974).

Table B-1: Physical Properties and Quiescent Dynamic Behavior for the FFP and SP Series

Series	Diameter d(mm.)	Density ρ_p(g/cc)	Reynolds Number Re_Q	Quiescent Free Fall Vel. f_Q(cm/sec)	Quiescent Drag Coeff. $C_{D,Q}$	Approx. Weight (mg)	Size Parameter α (sec^{-1})	Density Parameter β
FFP1	5	1.0077	135	2.35	0.91	65.5	0.42	0.9949
FFP2A	5	0.9962	-85	-1.48	1.12	65.5	0.42	1.0025
FFP2B	5	0.9951	-101	-1.76	1.03	65.5	0.42	1.0033
FFP3	5	0.9997	-13	-0.23	3.57	65.5	0.42	1.0002
FFP4	5	1.0005	21	0.37	2.56	65.5	0.42	0.9996
FFP5	5	1.0038	86	1.50	1.11	65.5	0.42	0.9975
FFPS	5	1.55	1498	26.1	0.54	101.5	0.42	0.7317
SP2A,C,D	6.5	1.0065	198	2.65	0.79	144.0	0.25	0.9957
SP3	4	1.0142	130	2.83	0.93	33.6	0.65	0.9906
SP4	3	1.0256	110	3.17	1.00	14.1	1.16	0.9832
SP5	2	1.0544	81	3.52	1.15	4.2	2.61	0.9650

Table B-2: Statistical Quantities for Particles in the FFP and SP Experiments

Series	Number of Runs	Mean Position		rms Position		Mean Velocity			rms Velocity		
		r	θ	r'	θ'	$\overline{v_r}$	$\overline{v_\theta}$	$\overline{v_z}$	v_r'	v_θ'	v_z'
FFP1	39	3.66	3.16	0.79	0.72	-.02	.00	3.84	.83	.91	2.06
FFP2A	37	3.92	2.96	0.89	0.80	-.03	-.05	-2.99	.70	.82	1.95
FFP2B	19	3.66	2.67	0.76	0.87	.02	.04	-1.51	.64	.80	1.98
FFP3	9	3.91	3.49	1.06	0.96	-.05	.11	1.69	.78	.95	2.03
FFP4	24	4.35	2.84	0.90	0.46	.01	-.04	0.45	.73	.94	2.48
FFP5	26	3.56	3.00	0.81	0.48	.01	-.03	2.60	.69	.81	1.92
FFPS	25	3.62	3.50	0.97	0.82	.11	-.09	23.2	2.50	2.28	5.19
SP2A,C,D	50	3.57	2.99	0.80	0.89	.01	.11	2.91	.78	.97	1.95
SP3	20	3.21	3.88	0.66	0.71	-.02	-.09	3.73	.75	.85	1.56
SP4	31	3.37	3.52	0.73	0.44	-.02	.03	3.91	.78	.81	1.58
SP5	72	3.38	2.98	0.64	0.58	.03	.01	3.48	.76	.84	1.60

Table B-3: Scales of the Particle Motion for FFP and SP Series

Series	No. of Runs	Macroscales			Microscales		
		$\mathcal{J}_{p,r}$	$\mathcal{J}_{p,\theta}$	$\mathcal{J}_{p,z}$	$\tau_{p,r}$	$\tau_{p,\theta}$	$\tau_{p,z}$
FFP1	39	.30	.38	.76	.46	.49	.40
FFP2A	37	.43	.54	.70	.44	.46	.50
FFP2B	19	.49	.40	.60	.42	.49	.44
FFP3	9	.60	.92	1.34	.43	.60	.48
FFP4	24	.42	.43	1.00	.43	.33	.57
FFP5	26	.46	.53	1.04	.55	.50	.51
FFPS	25	.13	.18	0.68	.12	.12	.58
SP2A,C,D	50	.28	.40	.79	.30	.16	.13
SP3	20	.20	.32	.88	.41	.48	.30
SP4	31	.26	.22	.83	.30	.23	.33
SP5	72	.19	.21	.86	.31	.31	.38

Table B-4: Turbulent Dynamic Behavior for the FFP and SP Series

Series	f_T(cm/sec)	Re_T	$C_{D,T}$	ζ	ξ	T_p^*(sec)
FFP1	3.84	221	0.34	2.12	1.45	0.78
FFP2A	-2.99	-172	0.28	1.83	1.44	0.91
FFP2B	-1.51	- 87	1.40	1.26	1.44	1.32
FFP3	1.69	97	0.07	1.30	1.44	1.28
FFP4	0.45	26	1.61	1.02	1.44	1.63
FFP5	2.60	149	0.37	1.68	1.45	0.99
FFPS	23.20	1336	0.47	5.12	4.79	0/32
SP2A,C,D	2.91	217	0.65	1.80	2.45	0.92
SP3	3.73	171	0.53	2.59	0.93	0.64
SP4	3.91	135	0.66	2.67	0.53	0.62
SP5	3.48	80	1.17	2.39	0.24	0.69

* $\overline{\mathcal{T}_{f,z}}$ = 1.66 seconds = $\mathcal{T}_{f,z}(\bar{\eta})$

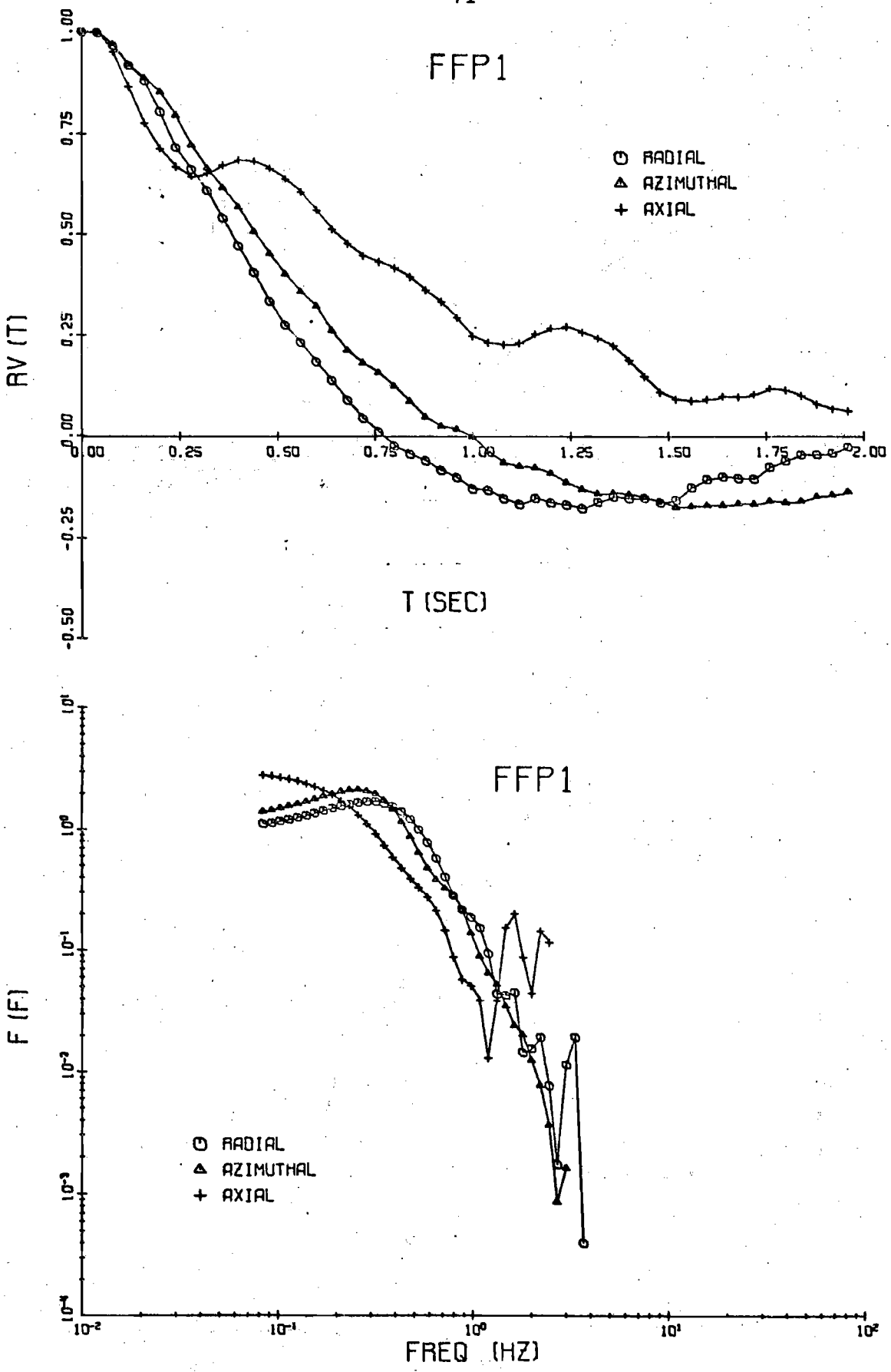

Fig. B-1. Particle Autocorrelations and Spectra for FFP1 Particle.

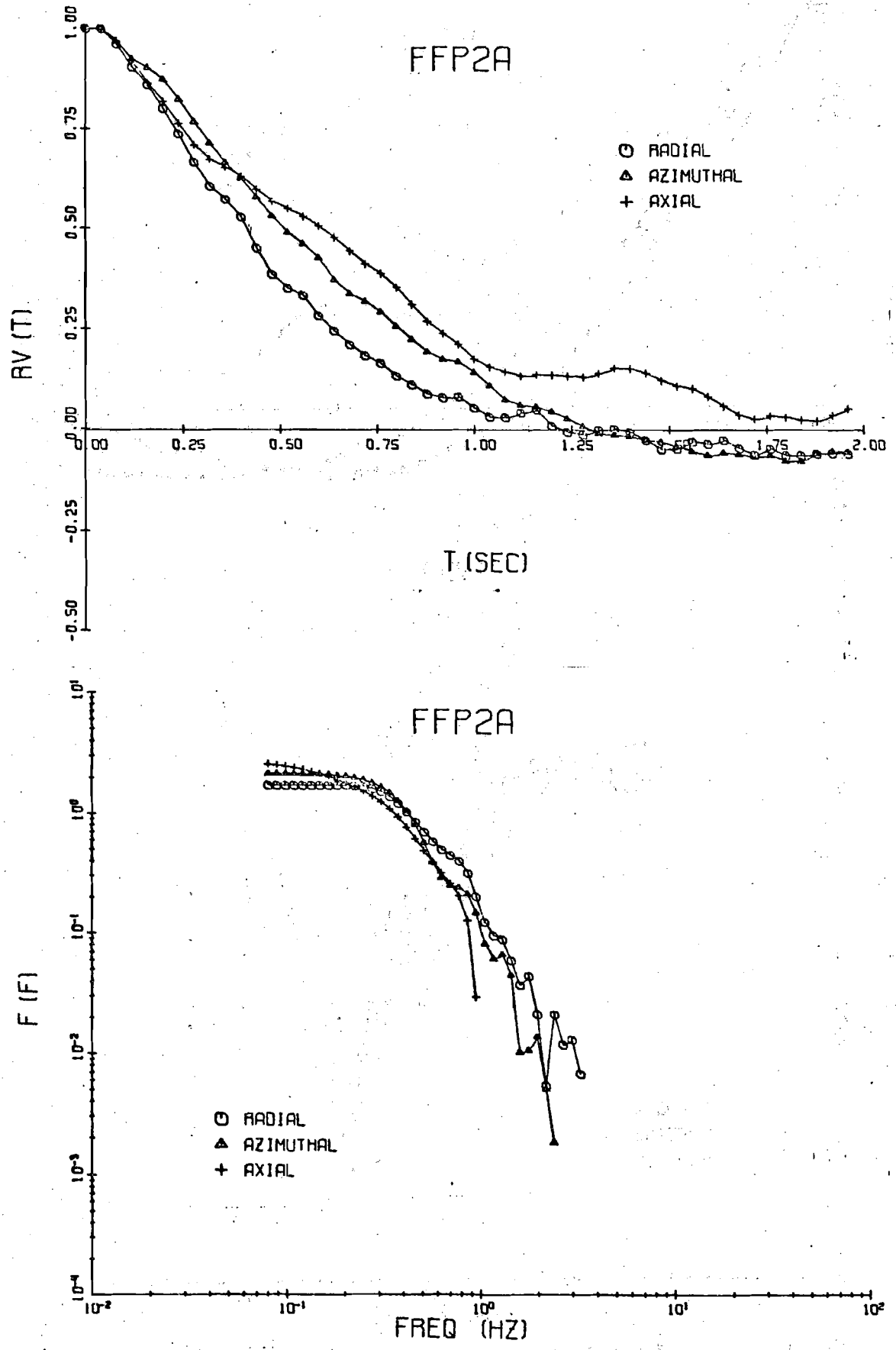

Fig. B-2. Particle Autocorrelations and Spectra for FFP2A Particle.

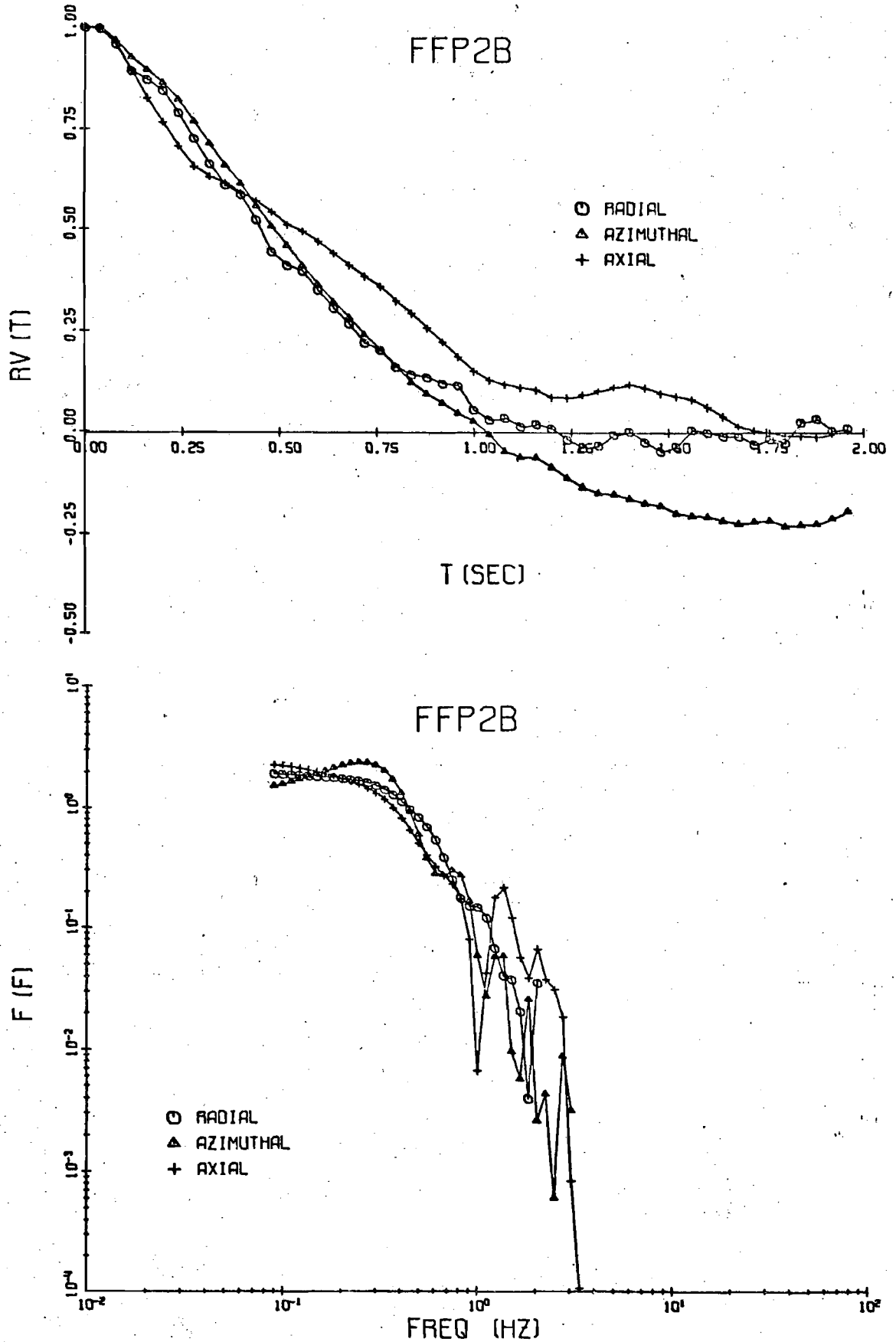

Fig. B-3. Particle Autocorrelations and Spectra for FFP2B Particle.

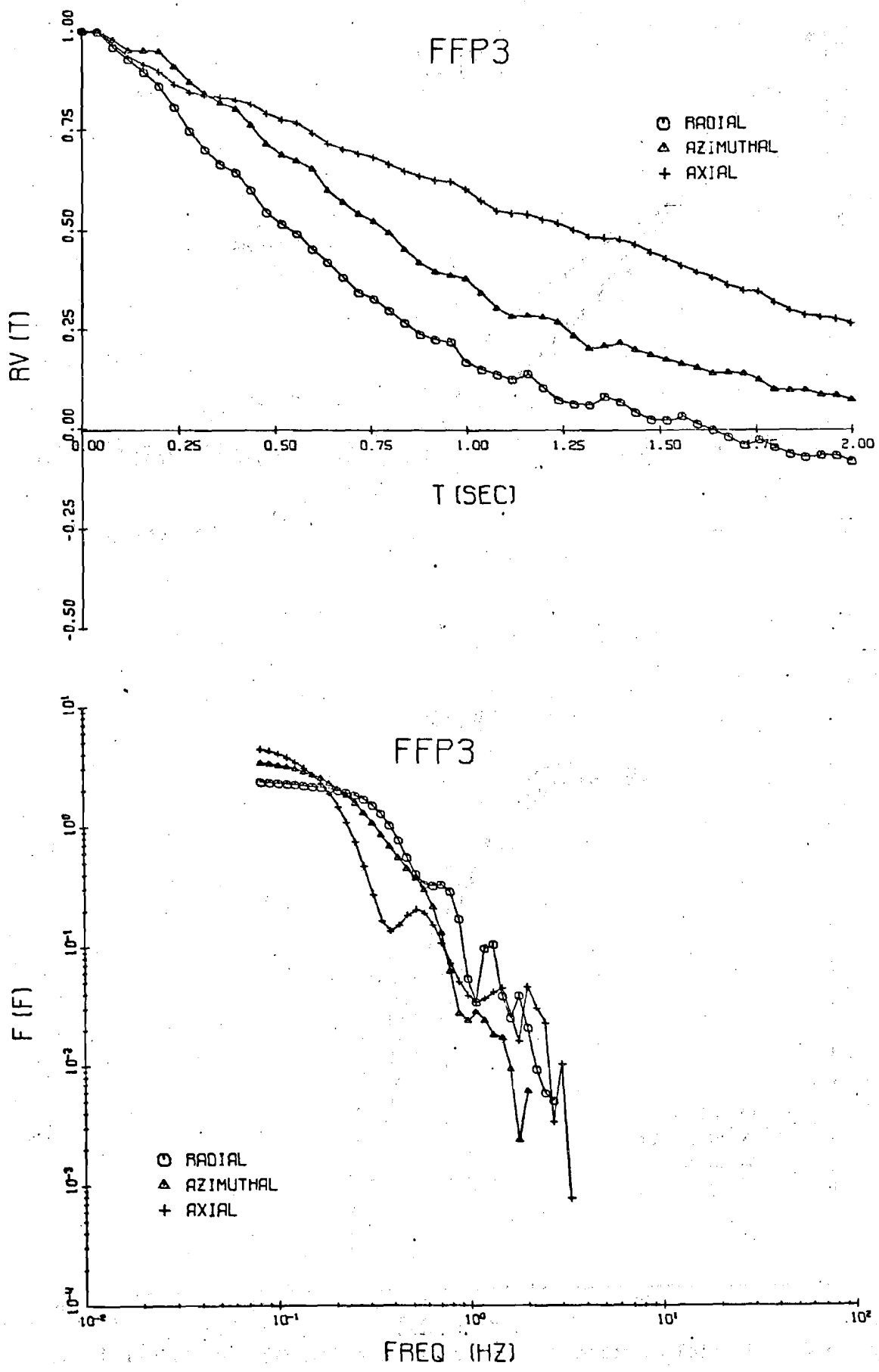

Fig. B-4. Particle Autocorrelations and Spectra for FFP3 Particle.

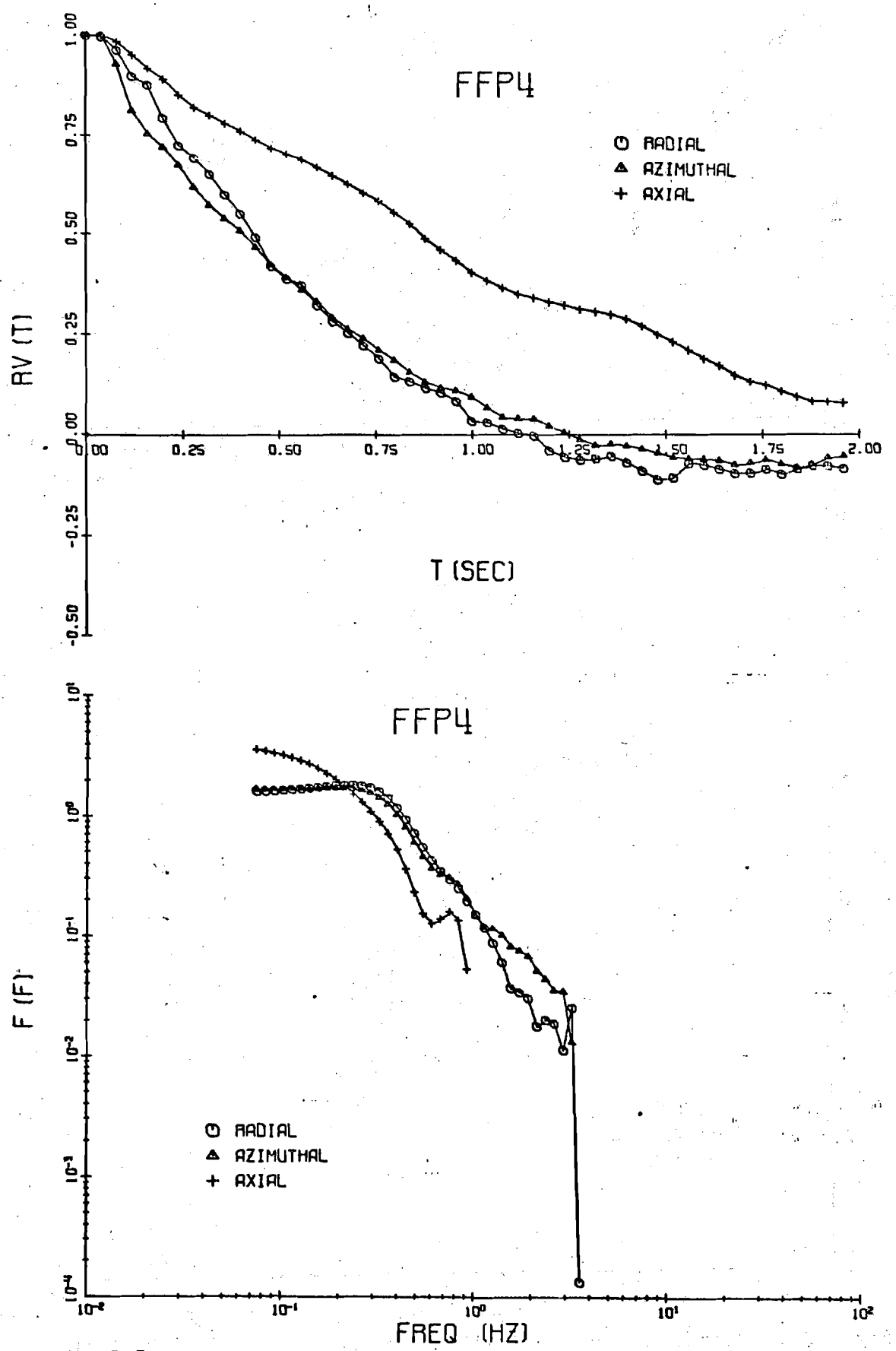

Fig. B-5. Particle Autocorrelations and Spectra for FFP4 Particle.

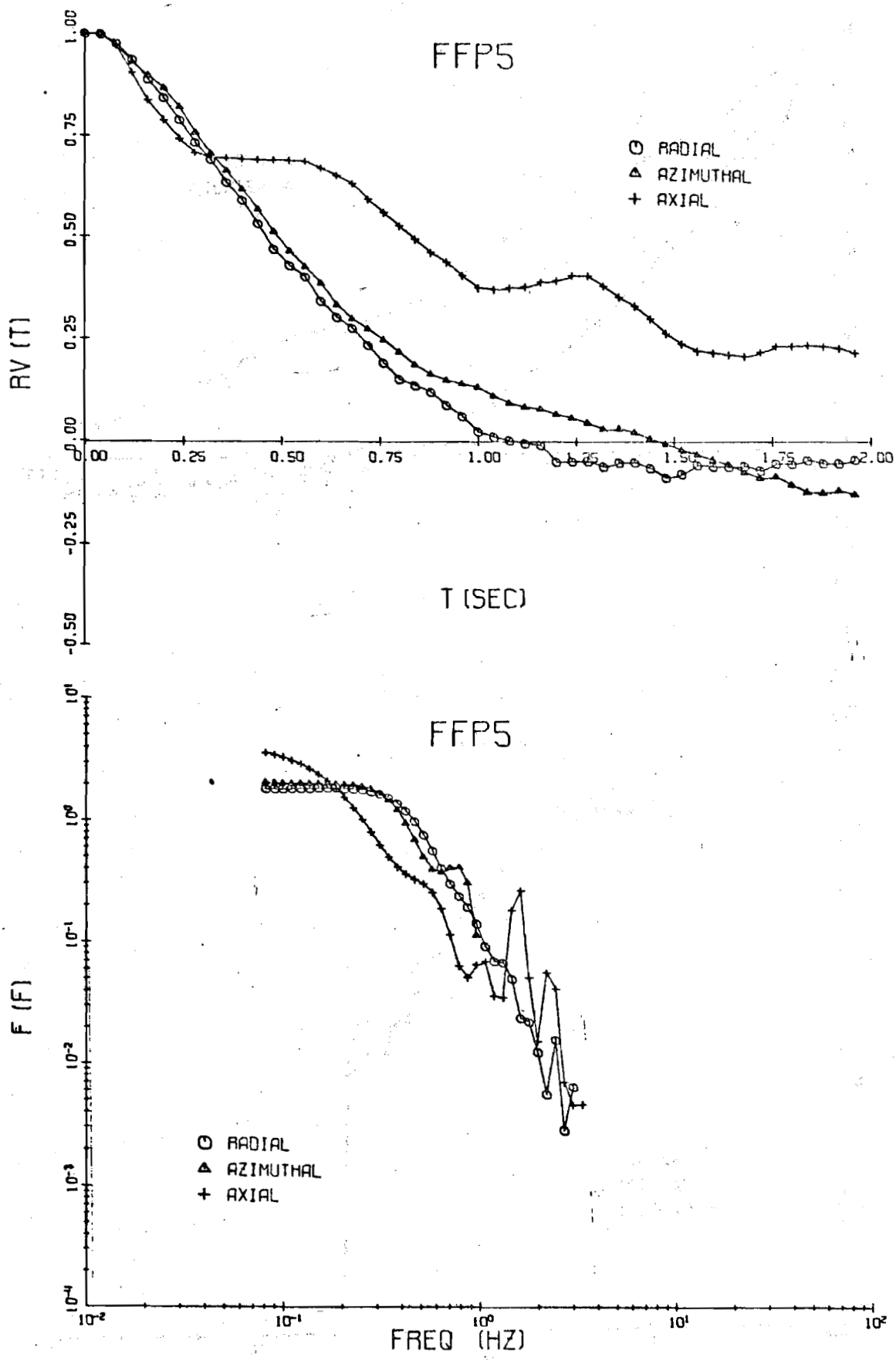

Fig. B-6. Particle Autocorrelations and Spectra for FFP5 Particle.

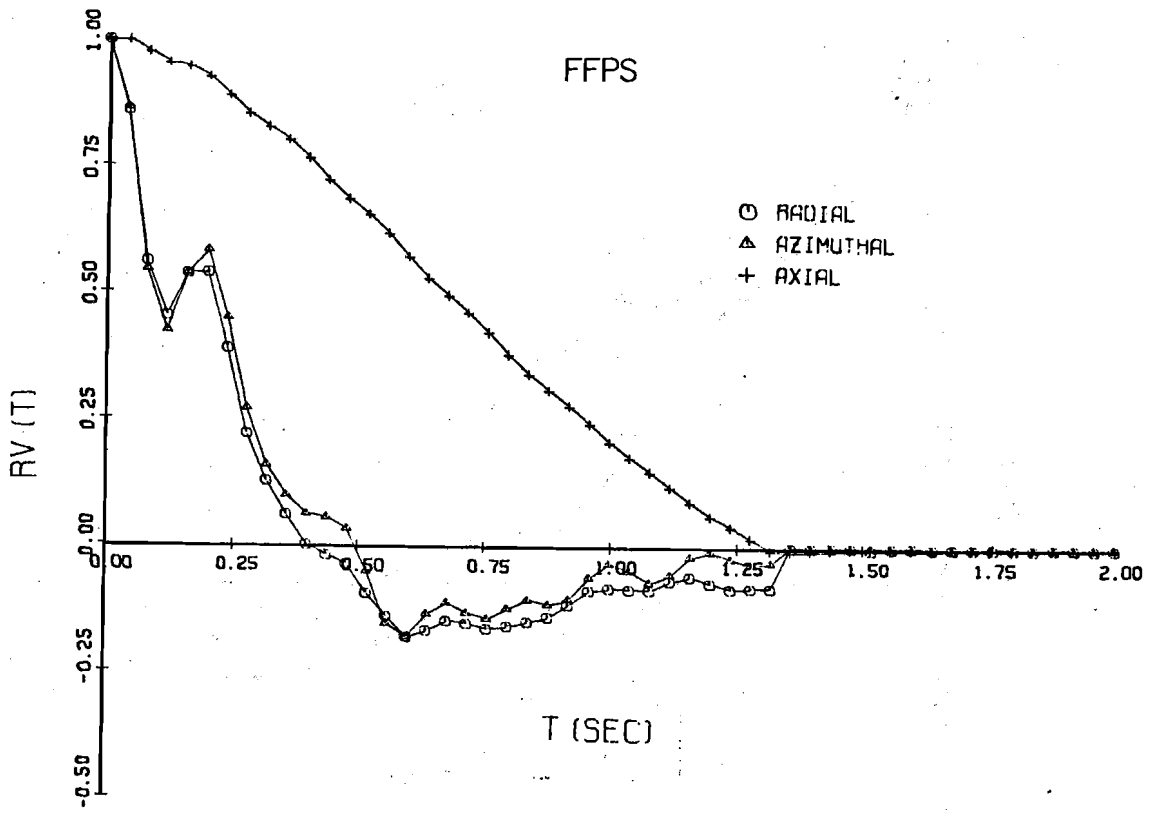

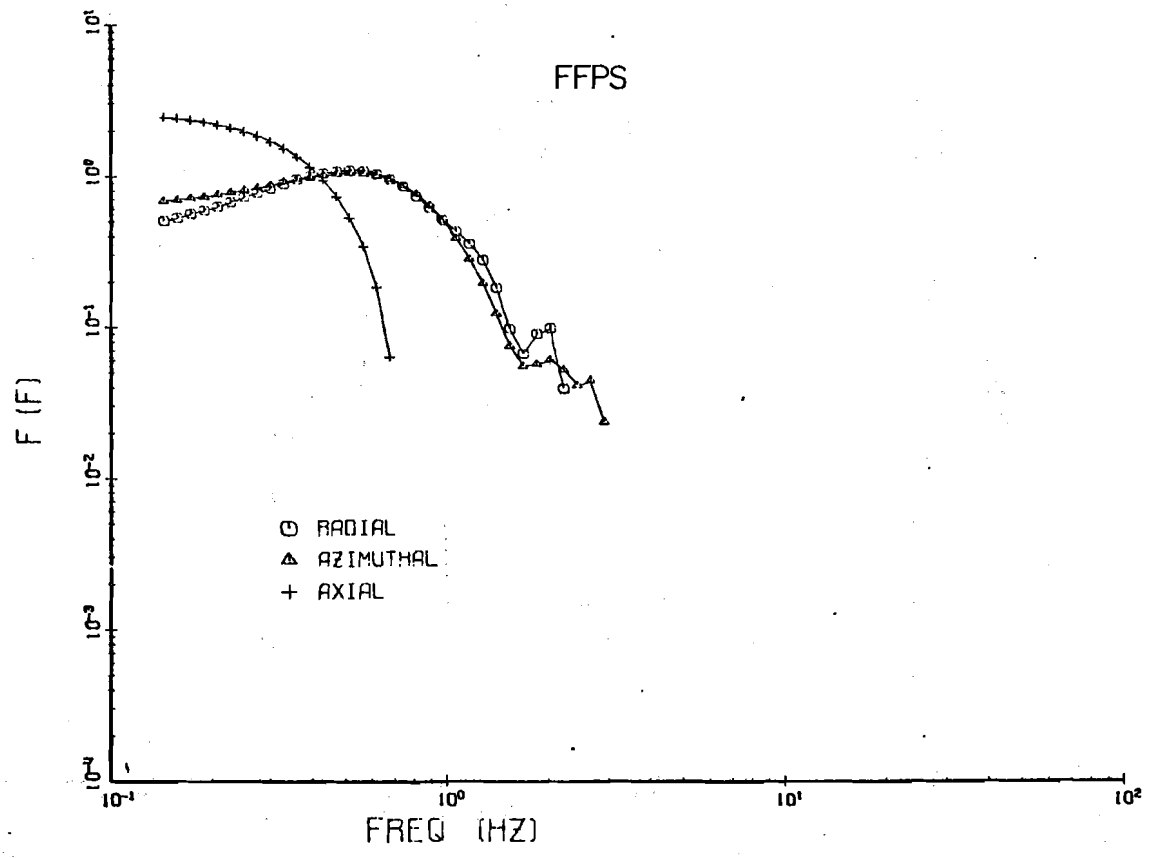

Fig. B-7. Particle Autocorrelations and Spectra for FFPS Particle.

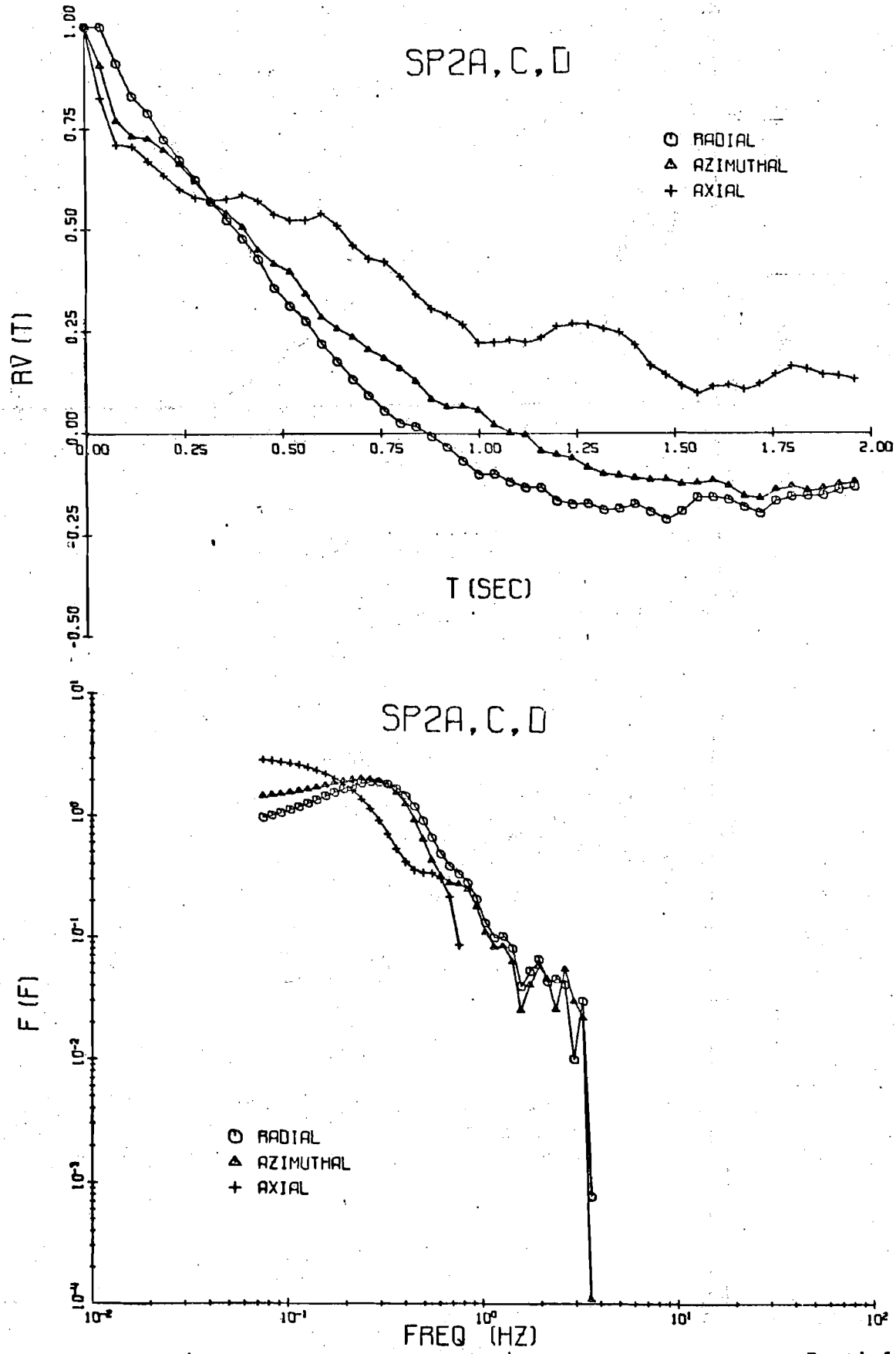

Fig. B-8. Particle Autocorrelations and Spectra for SP2A,C,D Particle.

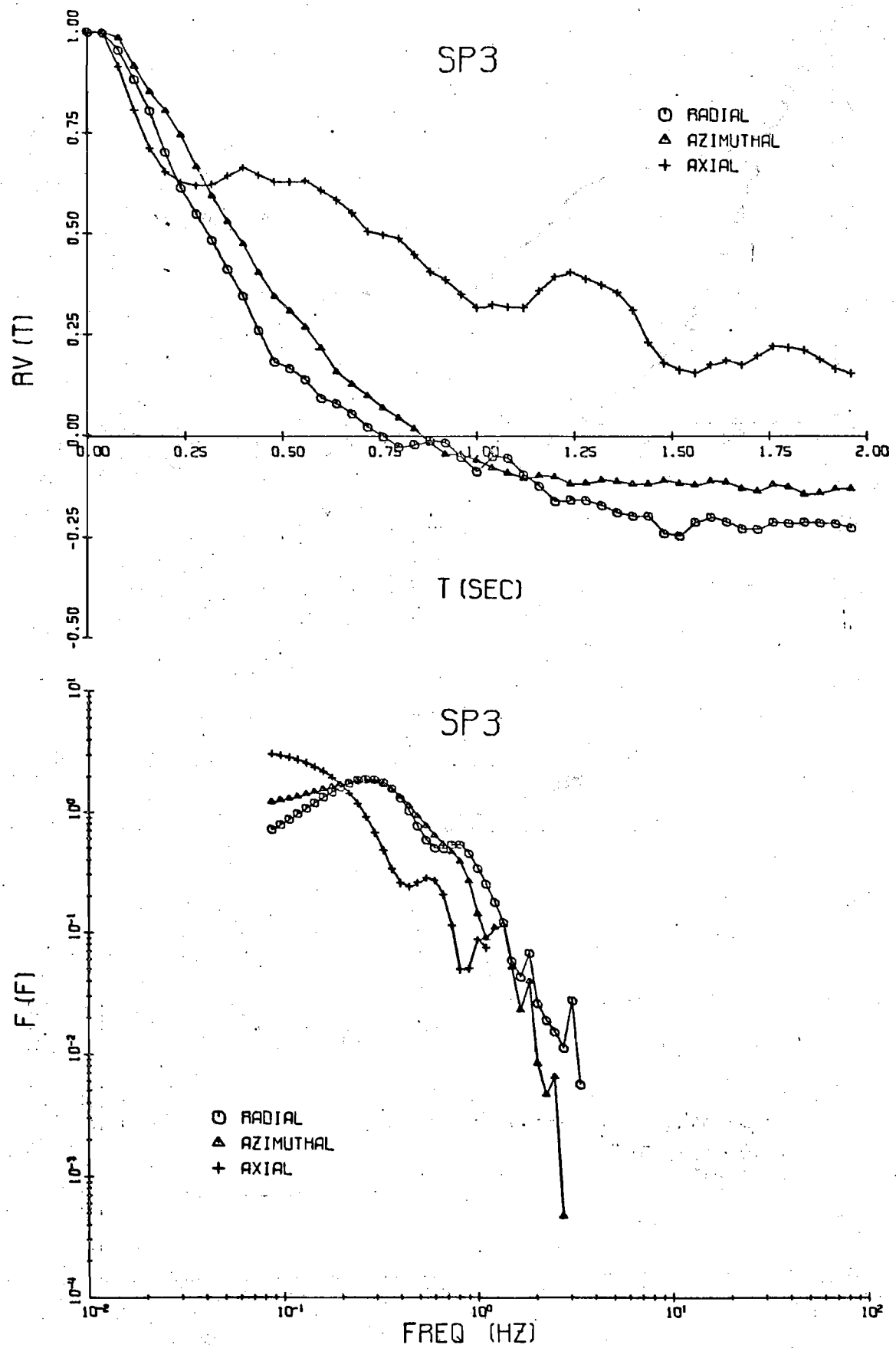

Fig. B-9 Particle Autocorrelations and Spectra for SP3 Particle.

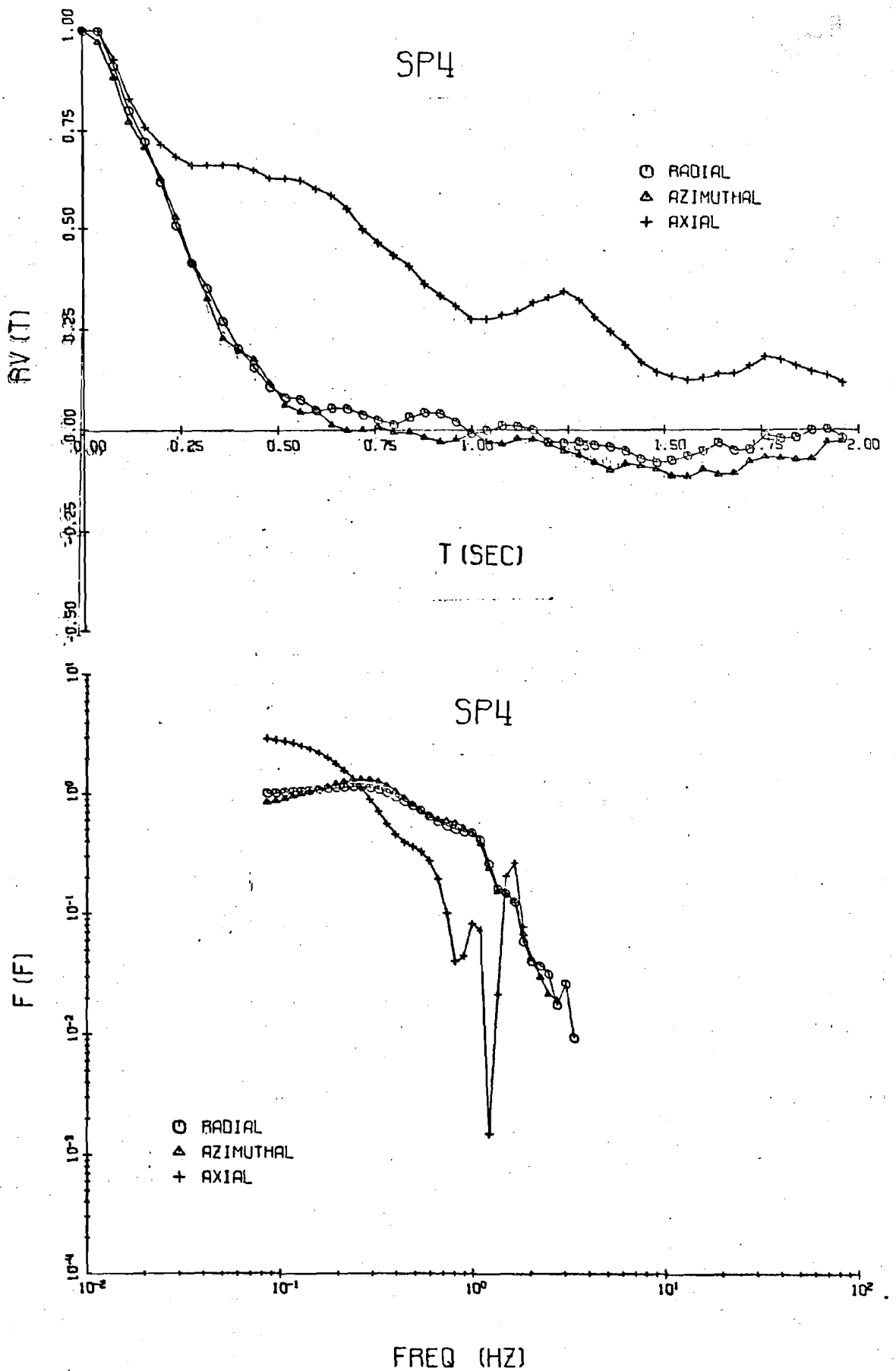

Fig. B-10 Particle Autocorrelations and Spectra for SP4 Particle.

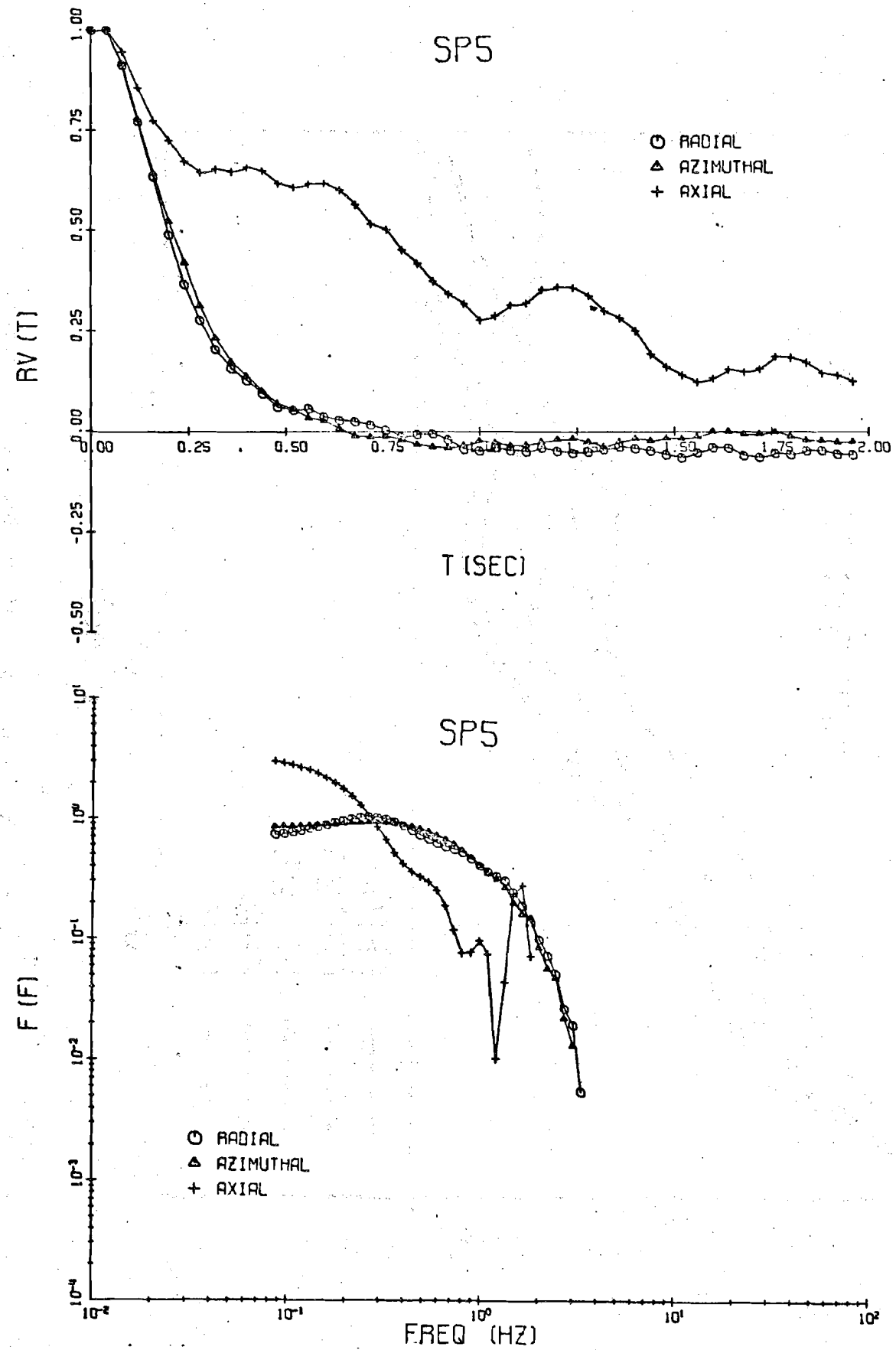

Fig. B-11 Particle Autocorrelations and Spectra for SP5 Particle.

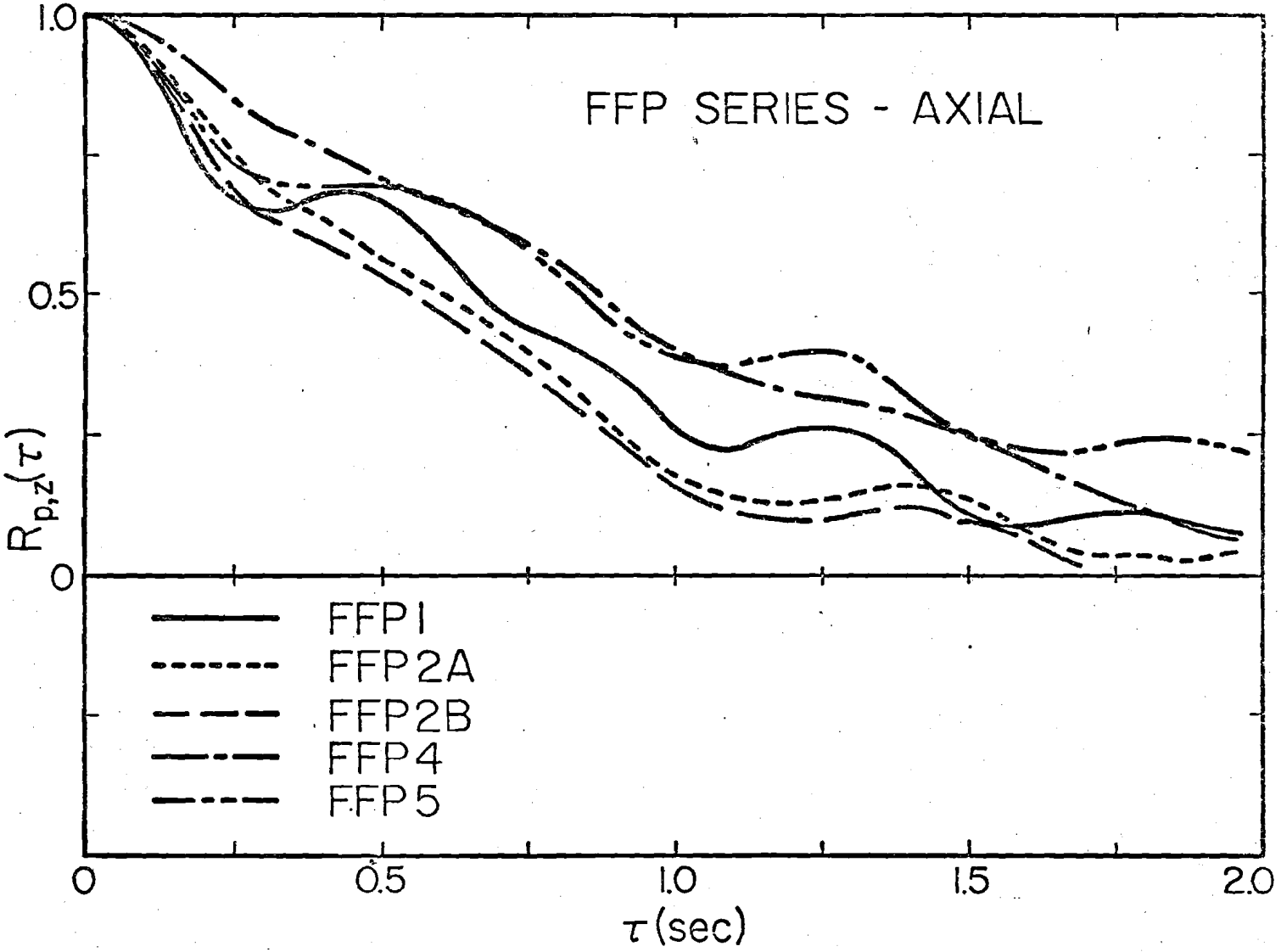

Fig. B-12 Axial Particle Autocorrelations for the FFP Series.

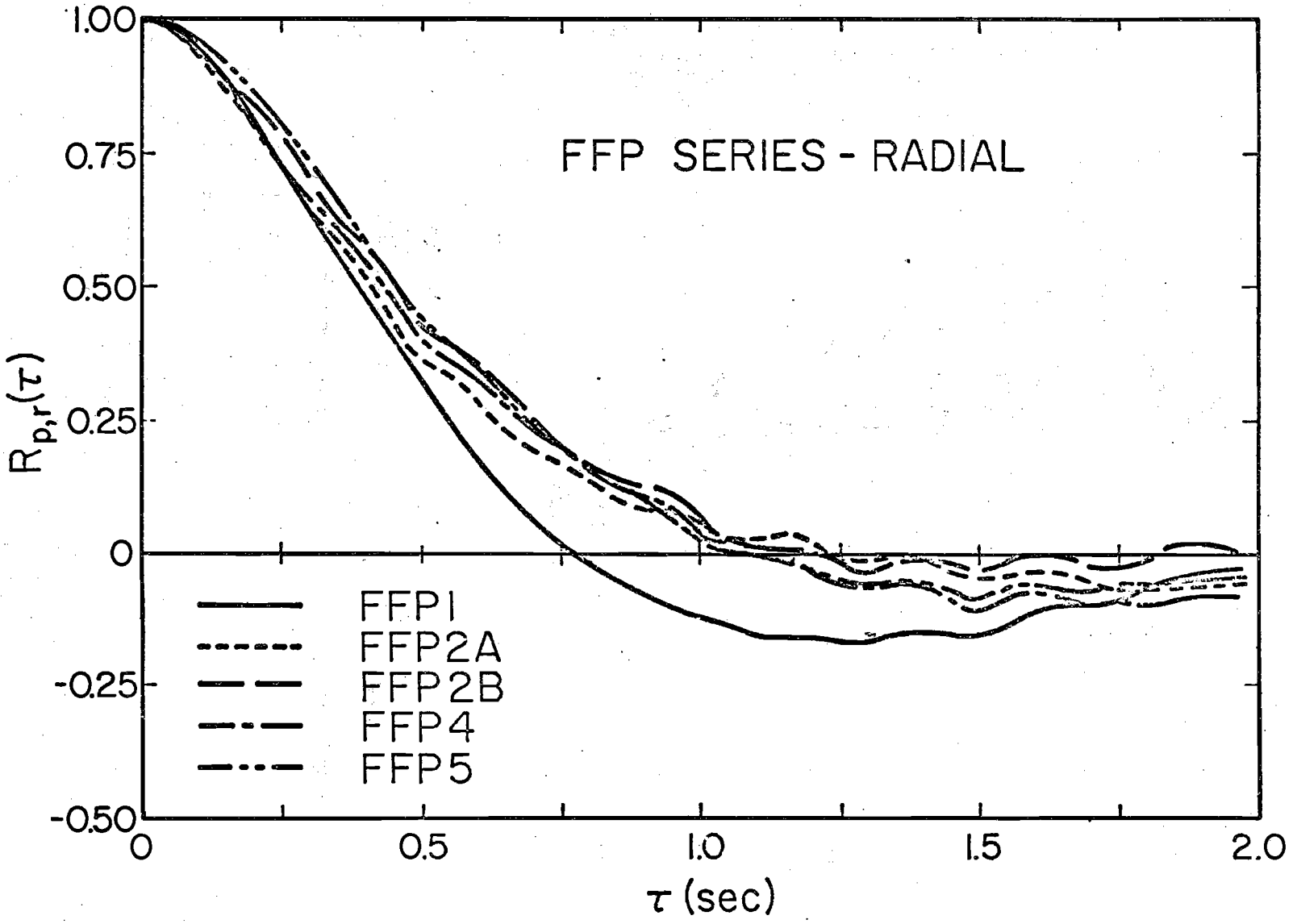

Fig. B-13 Radial Particle Autocorrelations for the FFP Series.

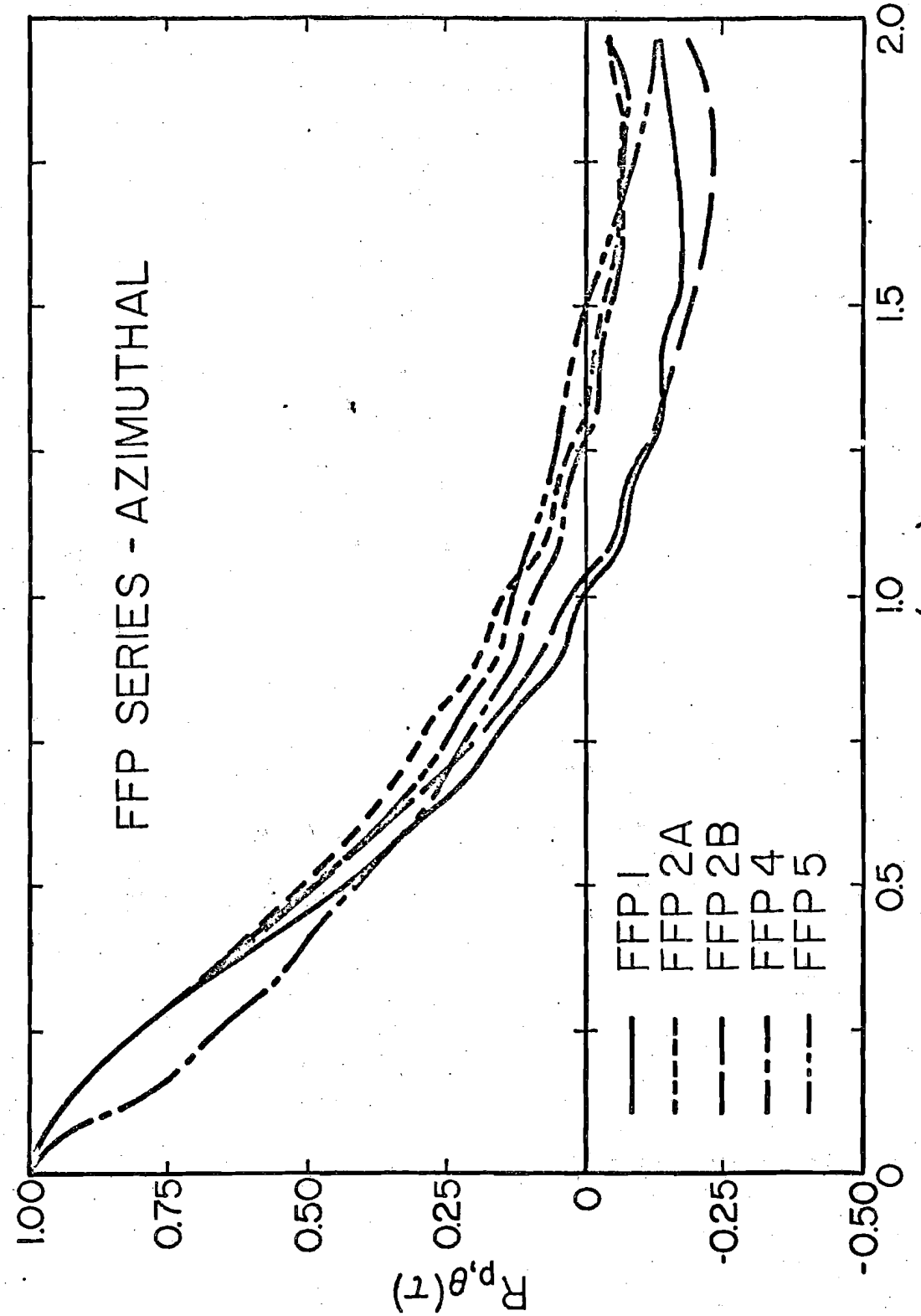

Fig. B-14 Azimuthal Particle Autocorrelations for the FFP Series.

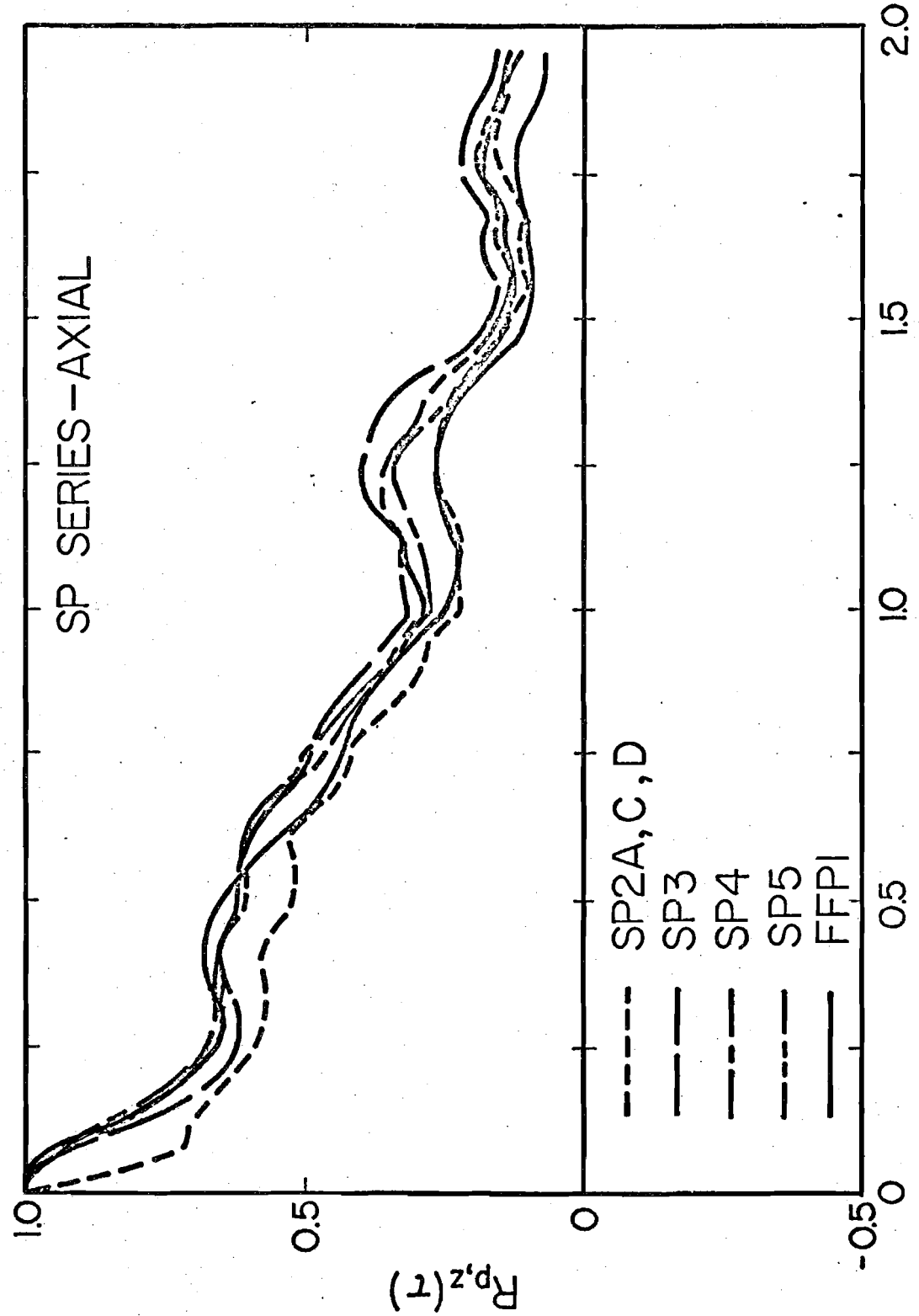

Fig. B-15 Axial Particle Autocorrelations for the SP Series.

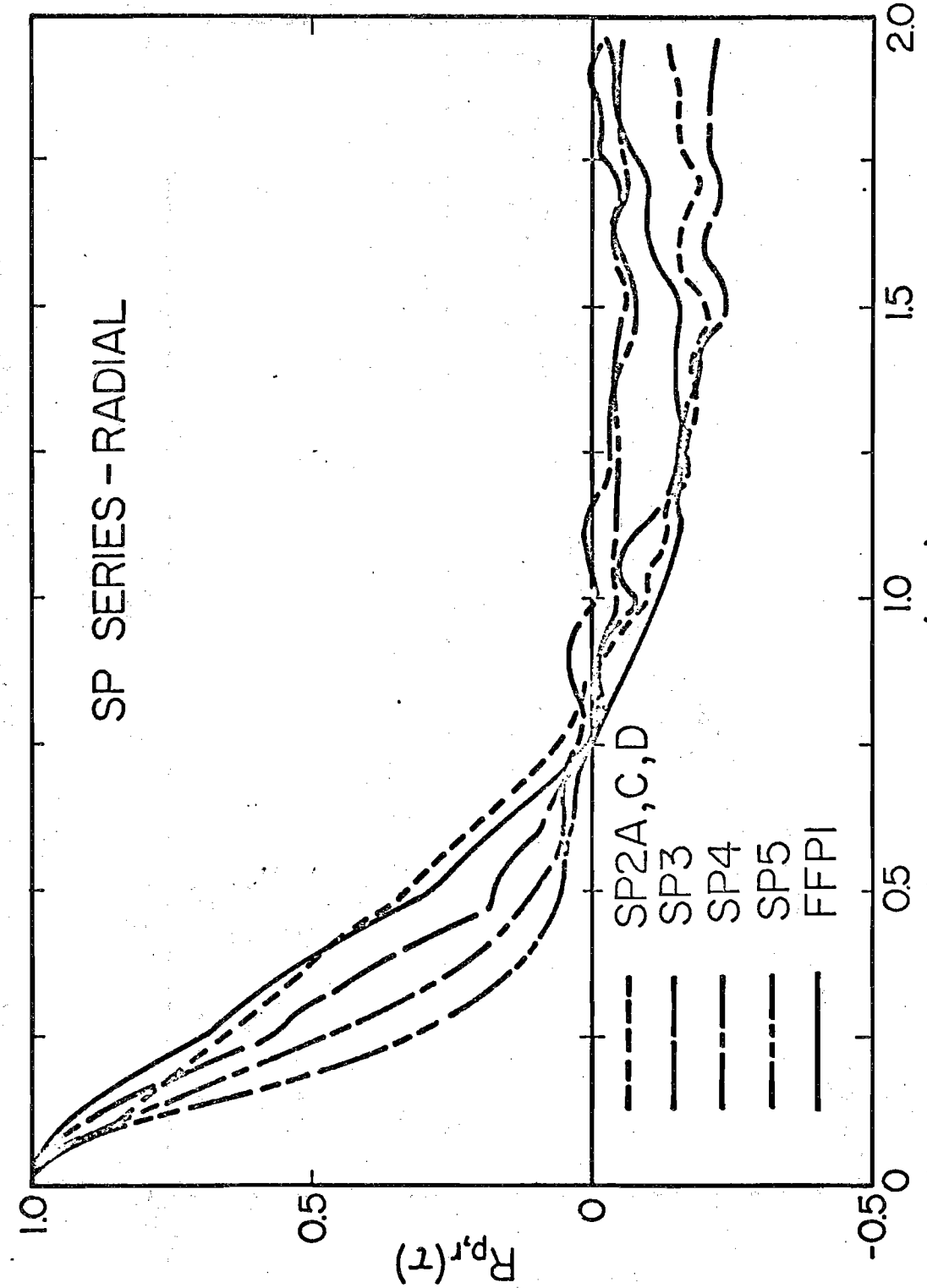

Fig. B-16 Radial Particle Autocorrelations for the SP Series.

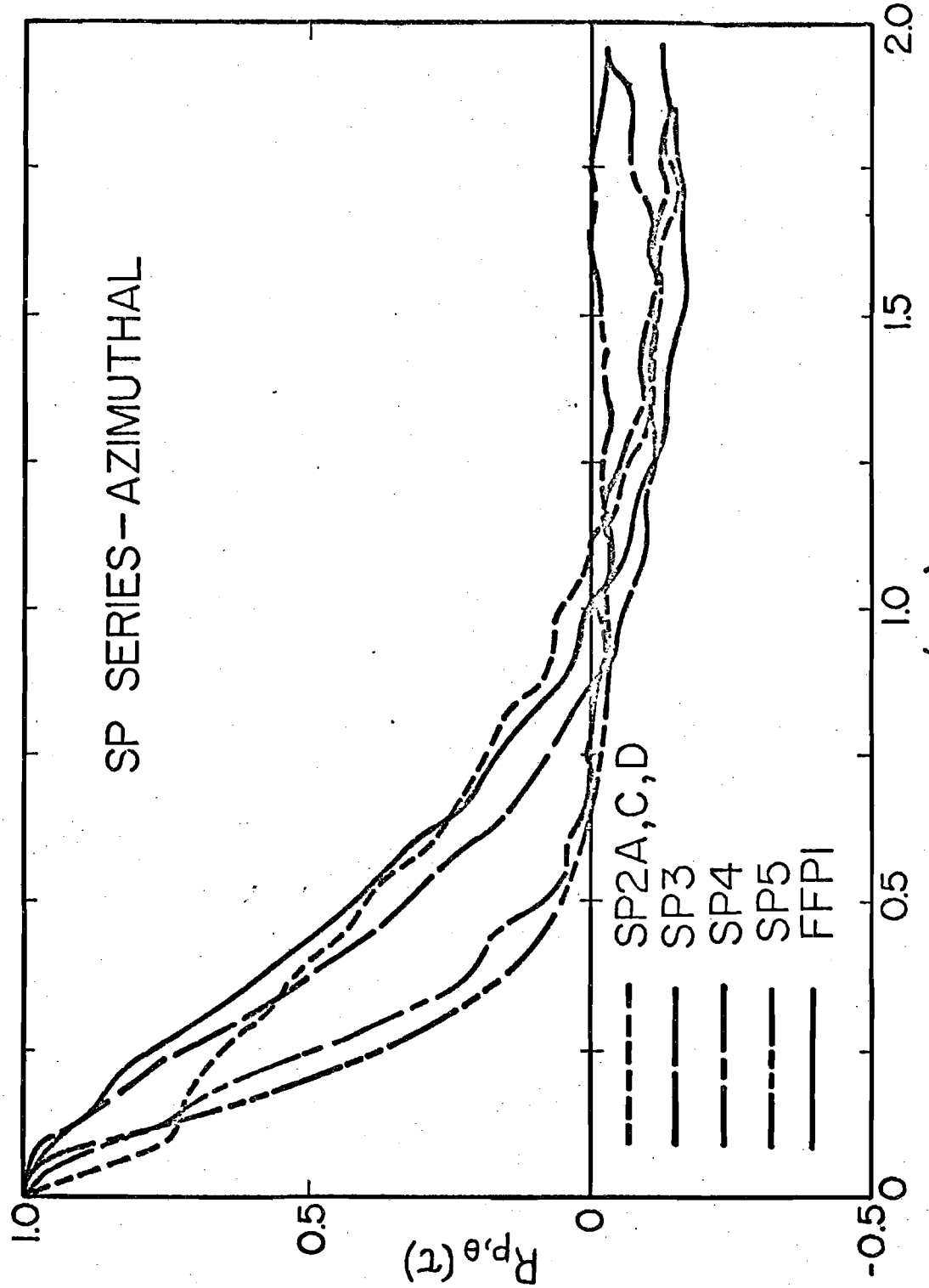

Fig. B-17 Azimuthal Particle Autocorrelations for the SP Series.

APPENDIX C: DATA PROCESSING PROCEDURES AND TECHNIQUES

C.1 Fluid Measurement System and Data Processing

Fluid turbulence measurements were obtained in a closed loop system shown schematically in Fig. C.1-1. Water is pumped from the storage tank to the header tank which provides pump isolation from the test section flow. A Borda mouth entrance with vanes, screens and a rake provides the necessary inlet conditioning for nearly fully developed and stationary turbulence throughout the 17 feet long test section. The exit elbow is treated with a honeycomb resistance to prevent flow asymmetry at the test section outlet. Steady flow and temperature control were provided to insure retention of calibration of the sensing anemometry and constant fluid properties.

The test section used for fluid measurements is an aluminum tube of 7.25 inches inside diameter with several access ports along its length. The dual ports shown as A, B, C, D and E in Fig. C.1-2 are spaced on 3 feet center-to-centers with ports A2, A3, B2, B3, C2, and C3 spaced on one side only to provide 1 foot center-to-center axial positioning.

Anemometer sensors were located in traversing mechanisms to provide radial separation (Meek, 1972) or axial separation (Howard, 1974). For radial separation ports 1, E, D, C, B, A and 0 can be employed with 1, A and 0 providing traverses across two orthogonal diameters to check for assymmetry. The ports on one foot axial separations provided adequate positioning flexibility to examine the convected field structure of the turbulence. Several probe support extensions shown in Fig. C.1-3 provided variation in axial separation for these measurements. Figure C.1-4 schematically shows the orientation of the probes in use with radial offset to eliminate upstream probe wake effects.

The probe supports held standard quartz coated, six-mil diameter, hot-film anemometer sensors. Two parallel data channels were used to sense the axial

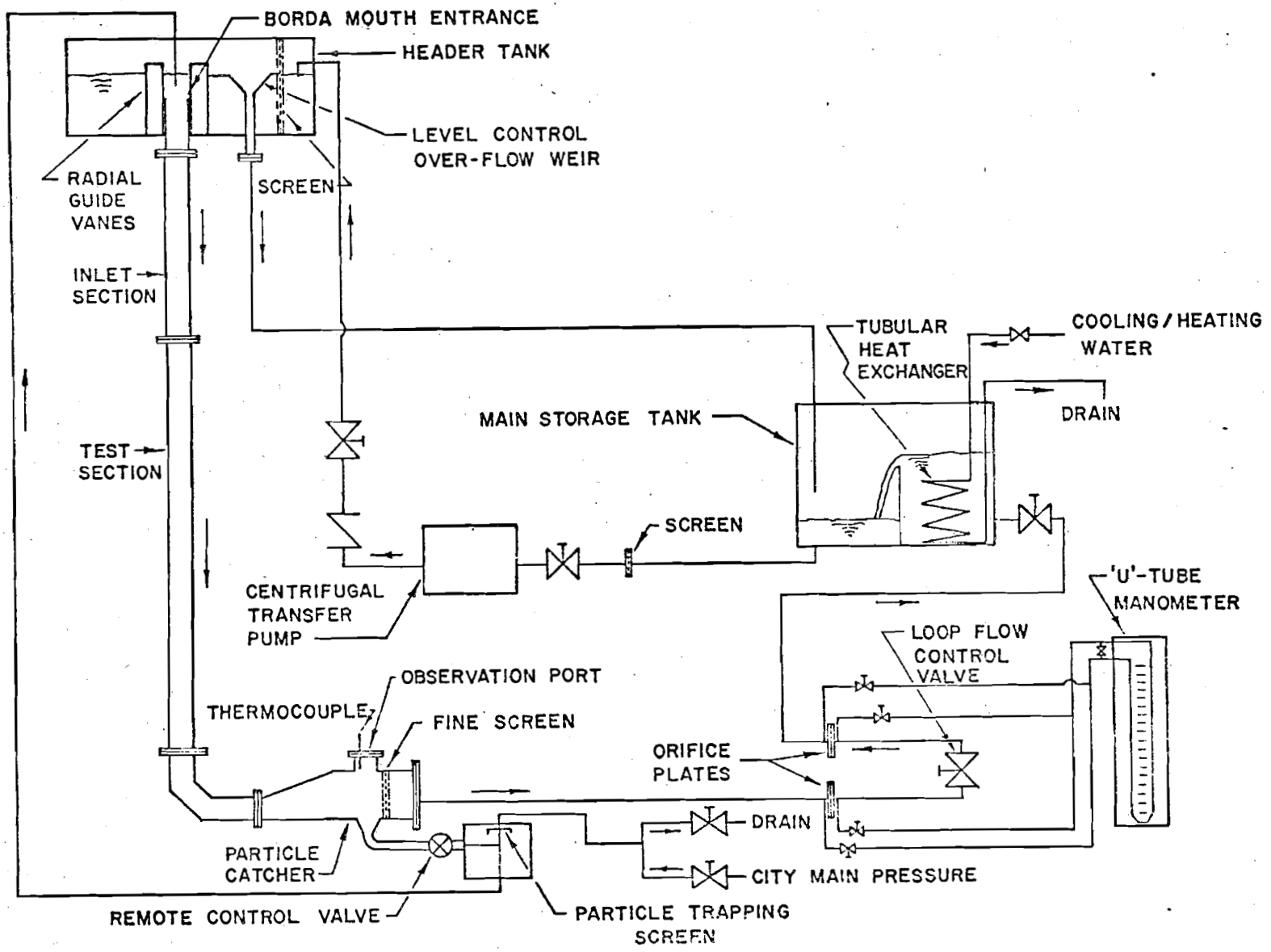

Fig. C.1-1 Fluid Flow Loop Used for Fluid and Particle Measurements.

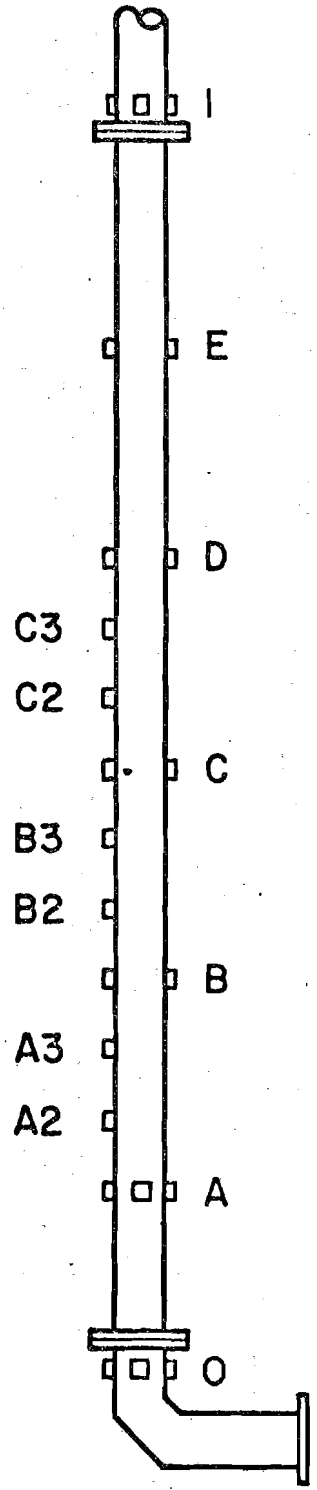

Fig. C.1-2 Test Section and Access Ports Used for Fluid Measurements.

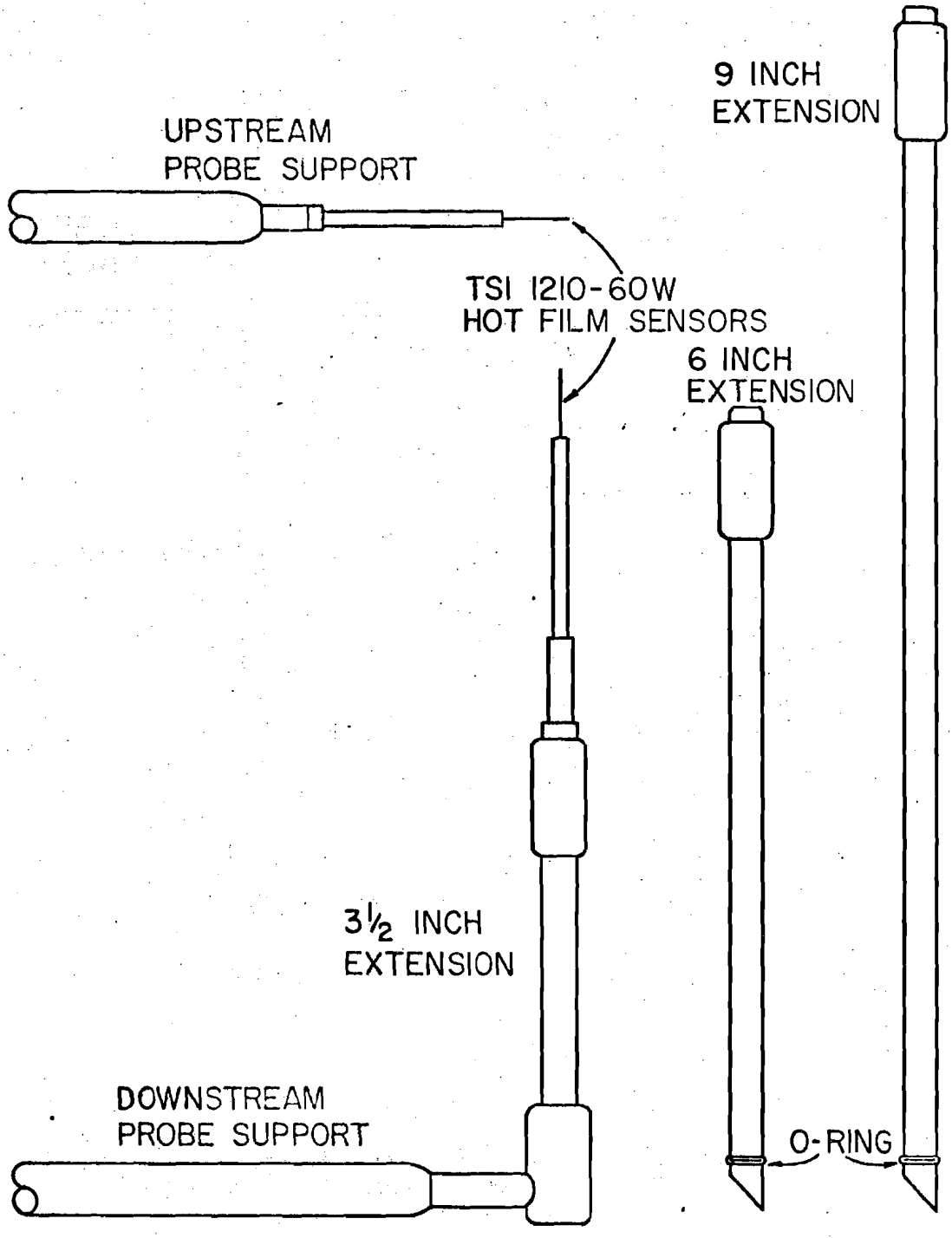

Fig. C.1-3 Anemometer Probe Supports

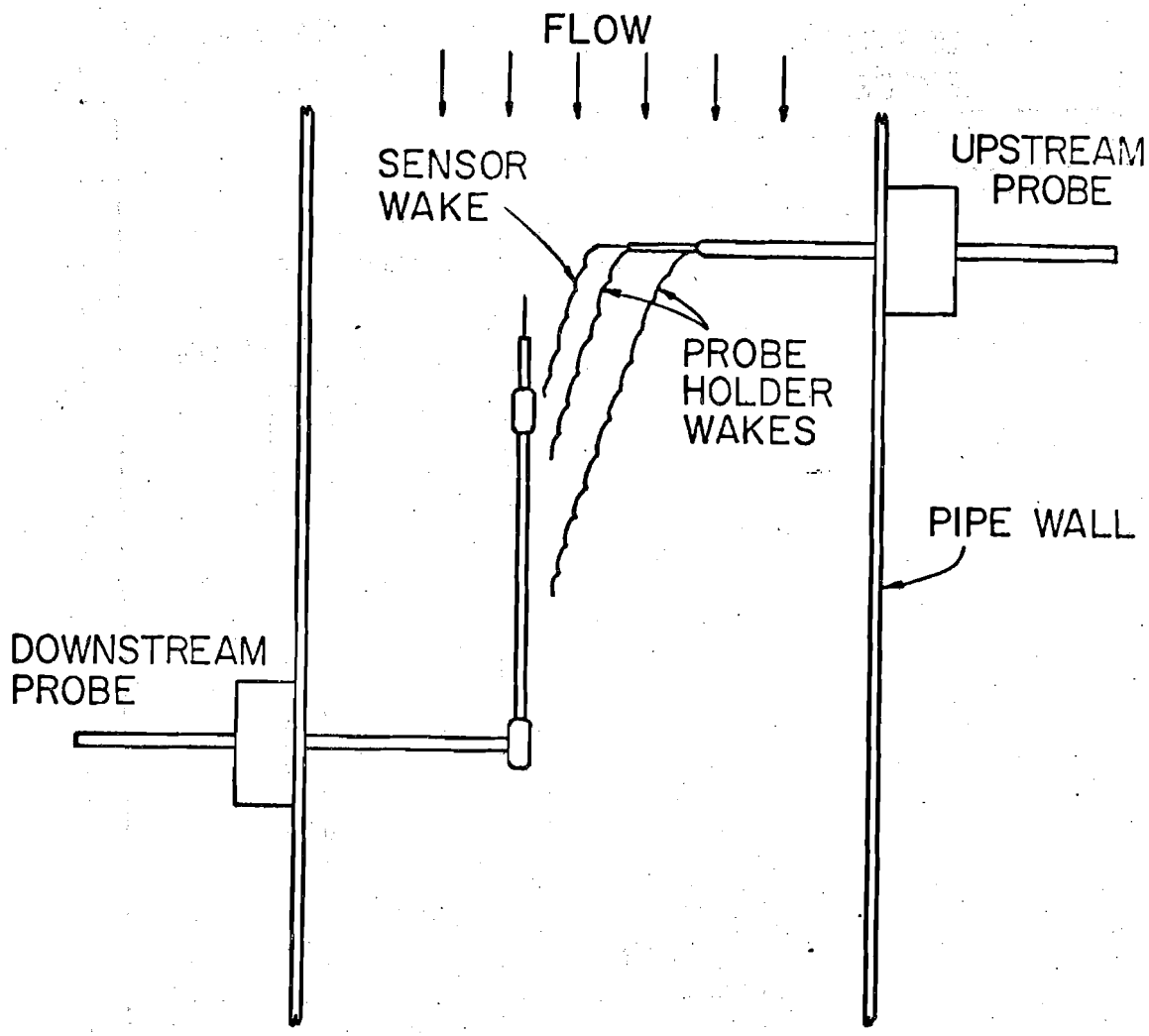

Fig. C.1-4 Probe Arrangement for Axial Separation with Radial Offset to Eliminate Upstream Probe Wave Effects.

velocity at each of the two locations. Fig. C.1-5 shows the electronic data procurement system employed to record the data. The recorded data was off-line processed through appropriate filters, correlation analyzer, rms voltmeter and digital voltmeter shown in Fig. C.1-6. Separate and/or superimposed plots of autocorrelation and cross correlation data were obtained directly from the correlation analyzer. Values of selected individual correlation points were determined via a digital voltmeter.

Howard (1974) has explicitly presented procedures for obtaining and processing the two-point, space-time correlations in this system including examination and correction of upstream probe wake effects and interpretation of the space-time correlation data. The procedures are in common use in two-point space-time data processing and are not repeated here. Results from the fluid turbulence measurements are presented in Appendix A.

C.2 Particle Measurement System and Data Processing

The experimental facility used was the same as that used in fluid measurements (Fig. C.1-1) with the replacement of the 17 feet long aluminum test section with smooth transparent lucite section of identical dimensions. Details of the system for inserting and retrieving the radioactively labelled test particle have been given previously by Jones (1966), Meek (1972), Howard (1974) and Jones, et al. (1971, 1972). Descriptions of the position monitoring system and the particle manufacture have also been given in these reports. Only a brief presentation of the data procurement system will be included so that the discussion of processing will be more complete.

A series of eight photomultiplier tubes with NaI crystals are placed on a carriage which traverses the length of the test section at the mean speed of the tagged particle as it passes downward through the test section. The geometric

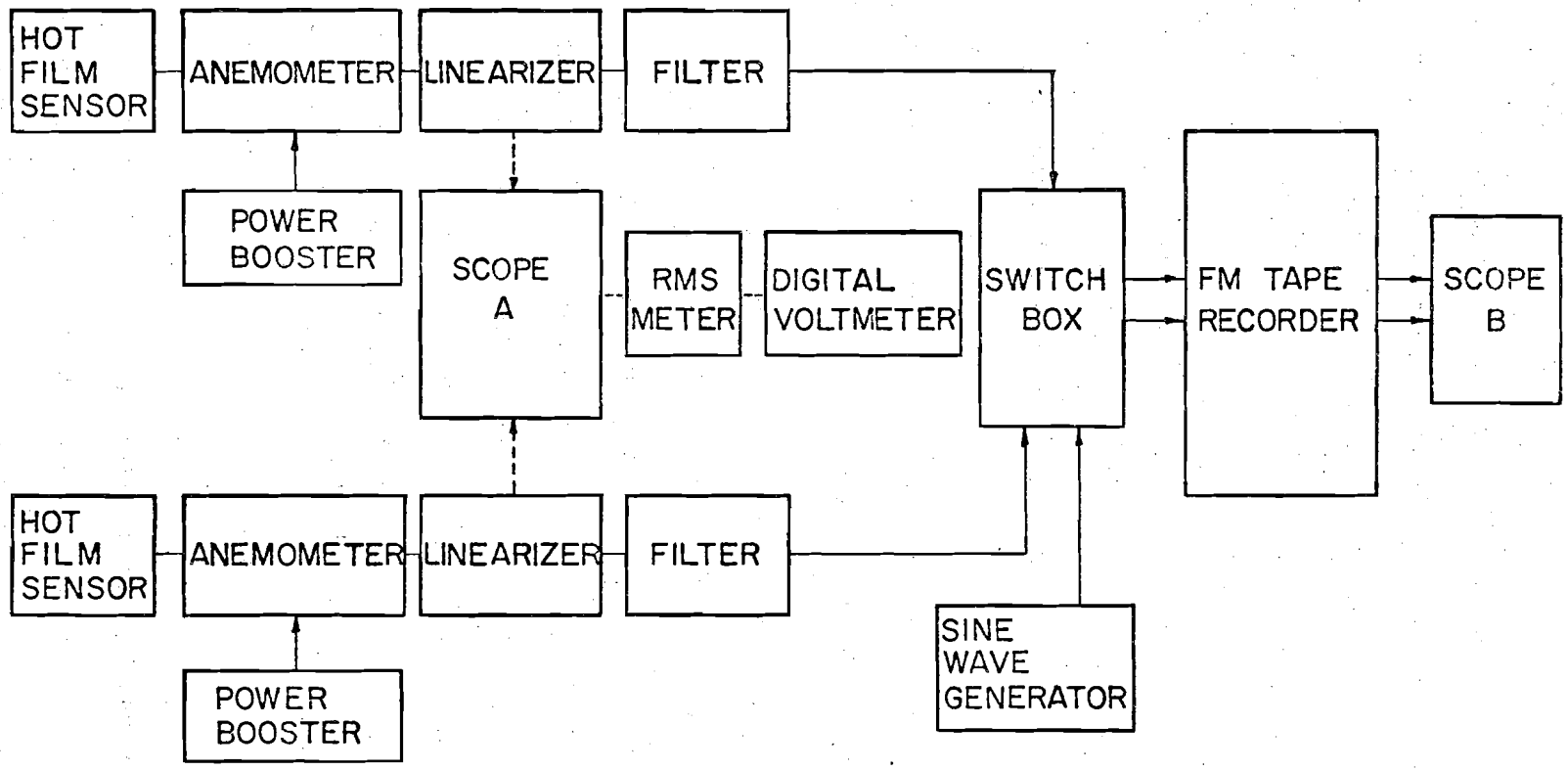

Fig. C.1-5 Fluid Turbulence Data Procurement System.

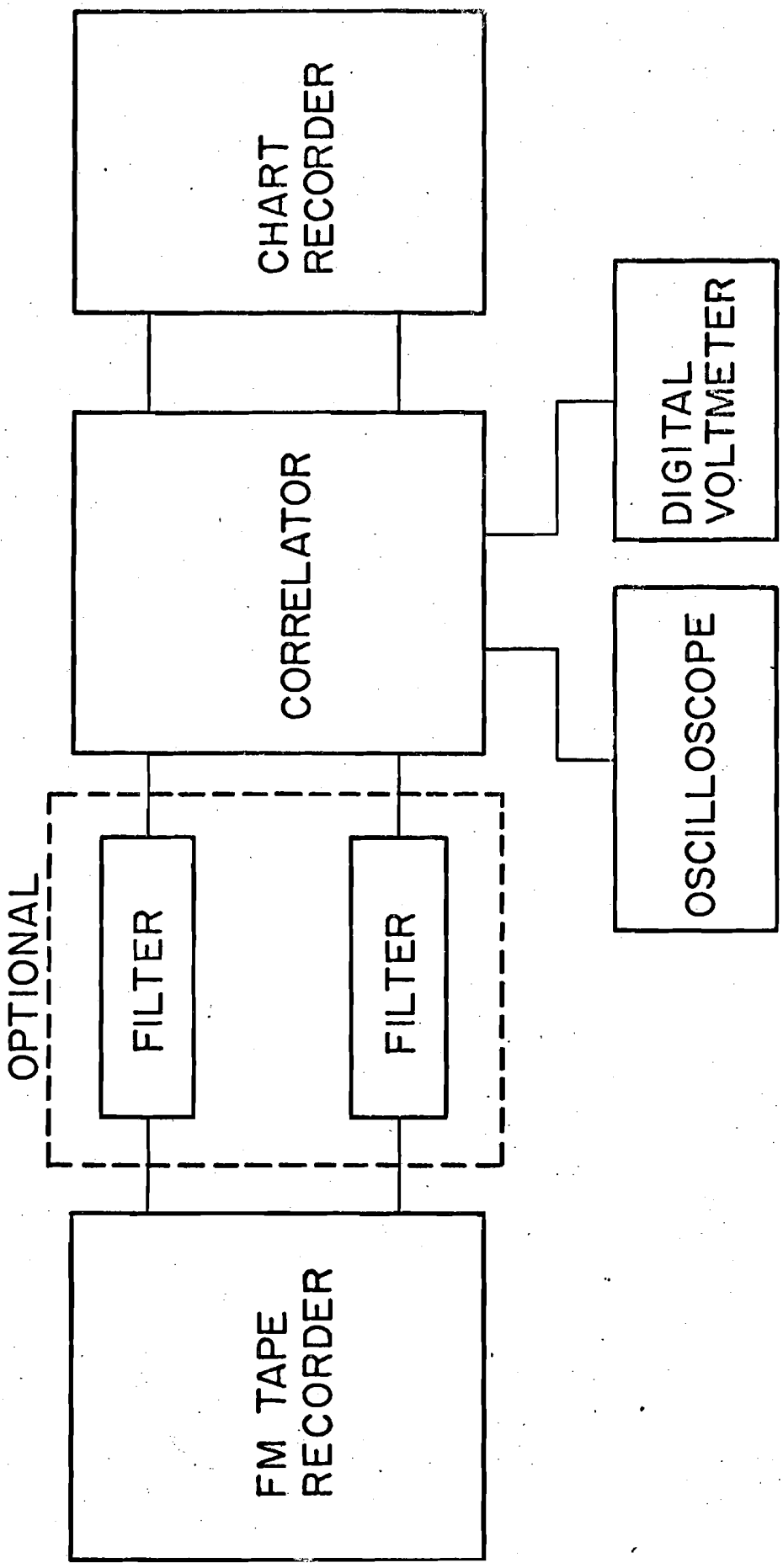

Fig. C.1-6 Fluid Turbulence Data Processing System.

location of these sensors provides outputs from pairs of tubes related to the lateral (X and Y) and to the axial (Z) location of the particle with respect to a calibrated region of the carriage. The carriage axial location is also monitored, thus providing a continuous set of signals of particle location in the test section. These signals are filtered, differenced and recorded for a series of runs with the same particle. Analyses are performed on each run and the resultant statistical structure values are ensembled to provide an improved statistical estimate of the particular particle behavior. Figure C.2-1 shows a schematic of this data processing.

The actual particle position in the imaginary calibrated right circular cylindrical region within the test section (radius 6 cm and height 10 cm) is determined from the three differenced signals (T,U,V) through third order polynomial relations for each cartesian direction as

$$X_i = a_{i1} + a_{i2}T + a_{i3}T^2 + a_{i4}T^3 + a_{i5}U + a_{i6}TU +$$
$$+ a_{i7}T^2U + a_{i8}U^2 + a_{i9}TU^2 + a_{i10}U^3 + a_{i11}V + a_{i12}TV +$$
$$+ a_{i13}T^2V + a_{i14}UV + a_{i15}TUV + a_{i16}U^2V + a_{i17}V^2 +$$
$$+ a_{i18}TV^2 + a_{i19}UV^2 + a_{i20}V^3 \qquad \text{(C.2-1)}$$

where
$$T = X1 - X2 \qquad \text{(C.2-2)}$$
$$U = Y1 - Y2 \qquad \text{(C.2-3)}$$
$$V = ZEH + ZWH - ZEL - ZWL \qquad \text{(C.2-4)}$$

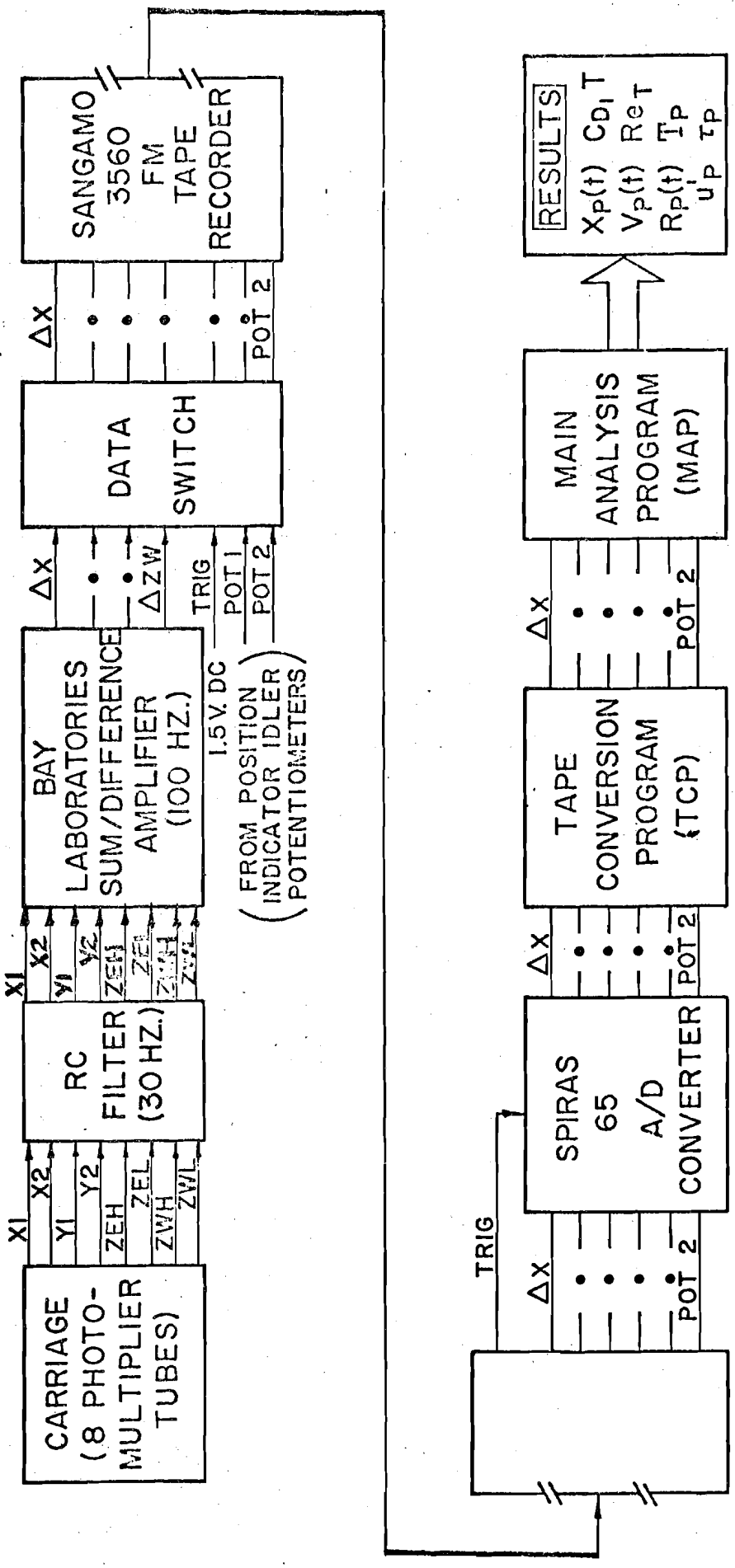

Fig. C.2-1 Schematic of Particle Data Acquisition and Analysis System.

and a_{ij} (i = 1, 3 and j = 1, 20) are coefficients determined from least squares fitting calibration data. These calibration data were taken in a stationary test system in which the labelled particle was physically placed on radial increments of 1 cm from 0 to 6 cm, azimuthal increments of 22.5° from 0° to 337.5° and axial increments of 1.27 cm from -5.08 cm to +5.08 cm. From these 1232 positions the corresponding T, U and V voltage values were used to obtain the a_{ij} coefficients. Due to the stability of the monitoring system, and the long half-life of the Co-60 particle, calibrations were not required for each series of runs.

To process the raw analog records of the particle motion, analog-to-digital conversion of the continuous signals was done at each milli-second in time. This digital information enabled the instantaneous particle position to be evaluated from which values of particle velocity were determined in all three coordinate directions. From these values the detailed statistical structure of the particle velocity was determined which included: mean position, rms position, mean velocity, rms velocity and particle turbulent Reynolds number and drag coefficient. In addition, the particle autocovariance and power spectral density in all three directions were evaluated and ensembled over the runs of the series.

The particle results were then corrected for bias due to noise which is statistically uncorrelated to the true particle behavior. The noise was determined, with the particle stationary in the calibration facility, from a series of data records which were processed in the same manner as the particle data. Since the true particle behavior and the noise are statistically independent, the noise can be simply subtracted from the observed particle data results to improve the accuracy of the particle turbulent behavior results. Such results are reported in Appendix B.

LIST OF REFERENCES

Ahmadi, G. and V. Goldschmidt, "Analytical Prediction of Turbulent Dispersion of Finite Size Particles," Technical Report FMTR-70-3, Purdue University (1970).

Basset, A. B., "A Treatise on Hydrodynamics," Dover Publications, Inc., New York, 2, Ch. 22, p. 285 (1961).

Batchelor, G. K., A. M. Binnie and O. M. Phillips, "The Mean Velocity of Discrete Particles in Turbulent Flow in a Pipe," Proceedings of the Royal Physical Society-B, 68, pp. 1095-1104 (1955).

Binnie, A. M. and O. M. Phillips, "The Mean Velocity of Slightly Buoyant and Heavy Particles in Turbulent Flow in a Pipe," Journal of Fluid Mechanics, 4, pp. 87-96 (1958).

Boussinesque, J., "Theorie Analytique de la Chaleur," 2, p. 224, Gauthier Villars, Paris (1903).

Burchill, W. E., "Statistical Properties of Velocity and Temperature in Isothermal and Nonisothermal Turbulent Pipe Flow," PhD Thesis, University of Illinois (1970).

Chao, B. T., "Turbulent Transport Behavior of Small Particles in Dilute Suspension," Osterreichisches Ingenieur-Archiv, 18, pp. 7-21 (1964).

Corrsin, S. and J. L. Lumley, "On the Equation of Motion for a Particle in Turbulent Fluid," Applied Scientific Research, Sec. A, 6, pp. 114-119 (1956).

Friedlander, S. K., "Behavior of Suspended Particles in a Turbulent Fluid," American Institute of Chemical Engineering Journal, 3, pp. 381-385 (1957).

Hinze, J. O., Turbulence, McGraw-Hill Co., Inc., New York, p. 357 (1959).

Howard, N. M., "Experimental Measurements of Particle Motion in a Turbulent Pipe Flow," PhD Thesis, University of Illinois (1974).

Howard, N. M., B. G. Jones and C. C. Meek, "Experimental Measurement of Particle Dispersion in Turbulent Flow," 3rd Biennial Symposium on Turbulence in Liquids, Rolla, Missouri (1973).

Jones, B. G., "An Experimental Study of the Motion of Small Particles in a Turbulent Fluid Field Using Digital Techniques For Statistical Data Processing," PhD Thesis, University of Illinois (1966).

Jones, B. G., et al., "Transport Processes of Particles in Dilute Suspensions in Turbulent Water Flow-Phase I," University of Illinois Water Resources Center, Report No. 40 (1971).

Jones, B. G., et al., "Transport Processes of Particles in Dilute Suspensions in Turbulent Water Flow-Phase II, University of Illinois Water Resources Center, Report No. 58 (1972).

Jones, B. G., R. J. Ostensen and C. C. Meek, "Linearized Non Stoksian Drag in

Kada, H. and T. J. Hanratty, "Effects of Solids on Turbulence in a Fluid," A.I.Ch.E. Journal, 6, No. 4, pp. 624-630 (1960).

Kennedy, D. A., "Some Measurements of the Dispersion of Spheres in a Turbulent Flow," PhD Thesis, The Johns Hopkins University (1965).

Laufer, J., "The Structure of Turbulence in Fully Developed Pipe Flow," NACA Report 1174, (1954).

Lumley, J. L., "Some Problems Connected With the Motion of Small Particles in Turbulent Fluid," PhD Thesis, The Johns Hopkins University (1957).

Meek, C. C., "Statistical Characterization of Dilute Particulate Suspensions in Turbulent Fluid Fields," PhD Thesis, University of Illinois (1972).

Meek, C. C. and B. G. Jones, "Studies of the Behavior of Heavy Particles in a Turbulent Fluid Flow," J. of Atmos. Sci., Vol. 30, No. 2, pp. 239-244 (1973).

Oseen, C. S., Hydrodynamik, p. 132, Leipzig (1927).

Peskin, R. L., "Stochastic Estimation Applications to Turbulent Diffusion," Stochastic Hydraulics, Proc. of the Int. Symp. on Stochastic Hydraulics, University of Pittsburgh Press, Pittsburgh, pp. 251-257 (1971).

Sabot, J., J. Renault and G. Compte-Bellot, "Space-Time Correlations of the Transverse Velocity Fluctuation in Pipe Flow," Physics of Fluids, Vol. 16, No. 9, pp. 1403-1405 (1973).

Shirazi, M. A., "On the Motion of Small Particles in a Turbulent Field," PhD Thesis, University of Illinois (1967).

Snyder, W. H., "Some Measurements of Particle Velocity Autocorrelation Functions in a Turbulent Flow," PhD Thesis, The Pennsylvania State University (1969).

Soo, S. L., "Statistical Properties of Momentum Transfer in Two Phase Flow," Chemical Engineering Science, 5, p. 57 (1956).

Soo, S. L., Fluid Dynamics of Multiphase Systems, Blaisdell Publishing Co., Waltham, Massachusetts, pp. 28-29 (1967).

Taylor, G. I., "Diffusion by Continuous Movements," Proc. London Math Society, 151, pp. 196-211 (1921).

Tchen, C. M., "Mean Value and Correlation Problems Connected With the Motion of Small Particles Suspended in a Turbulent Fluid," Martinus Nijhoff, The Hague, Ch. 4, p. 72 (1947).

Torobin, L. B. and W. H. Gauvin, "Fundamental Aspects of Solid-Gas Flow," Canadian Journal of Chemical Engineering, Part I, 37, pp. 129-141, Part II, 37, pp. 167-176, Part III, 37, pp. 224-236 (1959), Part IV, 38, pp. 142-153, Part V, 38, pp. 189-200 (1960), Part VI, 39, pp. 113-120 (1961).

Wandel, C. F., and Kofoed-Hansen, O., "On the Eulerian-Lagrangian Transform in the Statistical Theory of Turbulence," J. of Geophy. Res., 67, p. 3089 (1962).